POLITECNICO DI TORINO

Master's Degree in Electrical Engineering

Master's Degree Thesis

Magnetic and Structural Optimization of Internal Permanent Magnet Motors

Supervisors:

Simone FERRARI
Gustavo GARBELINI DE MENEZES

Candidate:

Fabio GREC

ACADEMIC YEAR 2026-2027

Abstract

Interior Permanent Magnet (IPM) machines are widely adopted in traction applications due to their high efficiency, good power density, and wide operating speed range. To improve power density, a common strategy is to increase the rotating speed, leading to mechanical issues and compromising structural integrity. In this context, this thesis focuses on the optimization of an IPM motor, implementing a multi-physical design optimization, that accounts for both magnetic and structural objectives.

The study starts from a reference motor, which is used as design baseline. An initial optimization was carried out by considering only the rotor design variables, with the aim of obtaining a new motor configuration while keeping the original stator. Then a second optimization was launched considering stator and rotor design variables, in order to obtain a result which satisfies the electromagnetic and structural target. Since the motor selected from the Pareto Front did not fulfill all the electromagnetic and structural targets, a scaling of the initial motor was done, followed by a comparison of the scaled motor variables with the *Variables and Parameters* settings of the second optimization. This was done to understand whether all the rages were set correctly.

After the scaling process, other three optimizations were executed, exploiting the results of the scaling process to improve the optimization convergence with slightly different boundaries conditions and design objectives. The former considers just a radial scaling, while the others include the full results of the scaling process and adopt as third objective torque ripple, for design consistency, or power factor, for improved field-weakening capability. These choices were done to highlight the fact that there may be multiple possibilities to achieve the desired result, rather than just one.

At the end, selected motors from each design stage are compared, both in terms of performance and structural metrics.

The optimization procedures were conducted using the SyR-e environment, which combines finite element analysis (FEA) with multi-objective optimization algorithms, to which some implementations and modifications were made and described in the second chapter.

Overall, this work highlights the importance of a combined electromagnetic and mechanical design approach for the development of high-speed IPM machines, giving also a general framework for the optimization process.

Contents

List of Figures

List of Tables

Chapter 1

Introduction

The global automotive sector is currently undergoing a profound transition driven by increasingly stringent emission regulations, rising fuel costs, and the need to reduce greenhouse gas emissions. In this context, electric mobility has emerged as a key enabling technology for achieving long-term sustainability targets in the transportation sector.

According to recent international outlooks on electric mobility, the global electric vehicle (EV) market has experienced sustained growth over the last decade, with annual sales reaching several tens of millions of units worldwide. Projections indicate that this trend is expected to continue in the coming years, supported by technological advancements, large-scale investments from automotive manufacturers, and the expansion of charging infrastructures.

Fig.1.1 shows in terms of millions of vehicles the stock predictions of Battery Electrical Vehicles (BEV) and Plug-In Electrical Vehicles (PHEV), in particular the Passenger Light-Duty Vehicles (PLDV), Light Commercial Vehicles (LCV), busses and trucks.

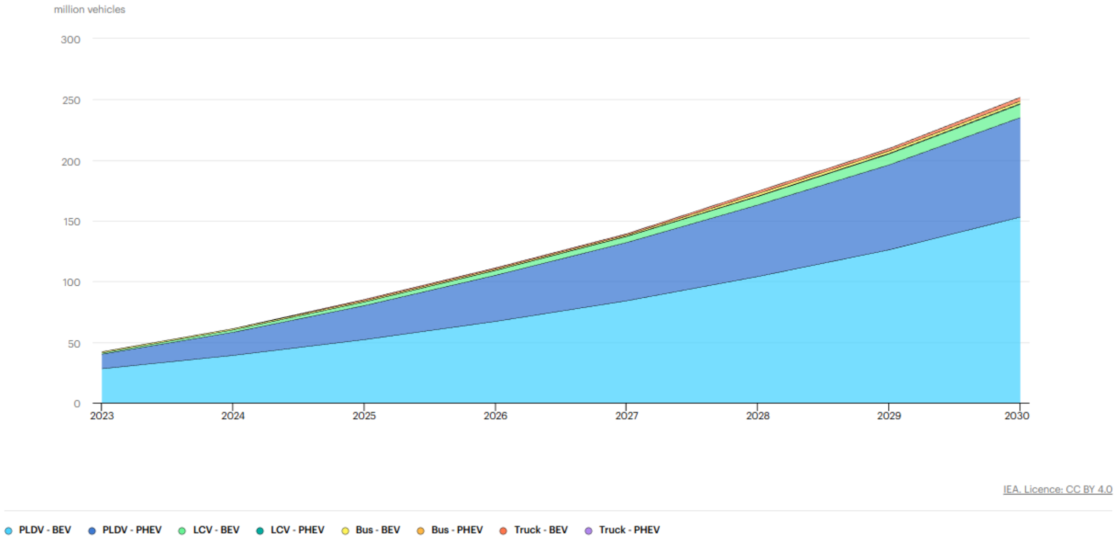

IEA. Licence: CC BY 4.0

Figure 1.1: Stock of electric vehicles in the Stated Policies Scenario, 2024-2030.[1]

As highlighted in the Outlook for Electric Mobility, electrified powertrains are progressively becoming the dominant solution for passenger vehicles, with battery electric vehicles (BEVs) and plug-in hybrid electric vehicles (PHEVs) accounting for an increasing share of global vehicle sales. This rapid market expansion places stringent requirements on traction systems in terms of efficiency, power density, reliability, and cost effectiveness, especially in high-performance and high-speed operating conditions. [1]

Within this framework, Interior Permanent Magnet (IPM) synchronous motors remain the state-of-the-art solution for automotive traction applications. Their widespread adoption is primarily motivated by their high torque density, excellent efficiency over a wide operating range, and inherent suitability for field-weakening operation, which enables extended constant-power speed regions. These characteristics make IPM motors particularly attractive for modern electric vehicles, where compactness, high efficiency, and robust high-speed performance are essential design targets.

However, the continuous push towards higher maximum speeds and increased power density introduces new challenges, particularly from a mechanical and structural standpoint. Elevated centrifugal forces acting on the rotor may lead to critical stress levels, especially in the presence of sharp geometrical features such as rotor slots and magnet cavities. As a result, the optimal design of IPM motors increasingly requires a multiphysics approach that simultaneously addresses electromagnetic performance and mechanical integrity.

The mentioned approach is called 'Multi-Objective Optimization Process' and the thesis aims to realize this process, which consist in varying the stator and rotor parameters in order to maximize electromagnetic performance, while ensuring mechanical integrity under centrifugal loading.

To better understand the work done, some notes will be presented on the IPM machines and the software used, including the updates and improvements done for the implementation of the multi-physics optimization.

1.1 Internal Permanent Magnet Synchronous Motor

The Internal Permanent Magnet (IPM) synchronous motor is one of the numerous types of synchronous motors used in traction applications, but the characteristics previously cited make this motor the best solution. Before understanding how it works, its structure will be presented.

1.1.1 Motor Structure

The synchronous motor is composed of two parts: the stator and the rotor. The first is the fixed part, and is generally the external one, while the second is the rotating part. Between stator and rotor there is the air gap, which allows the rotor to move. The figures below show their assembly.

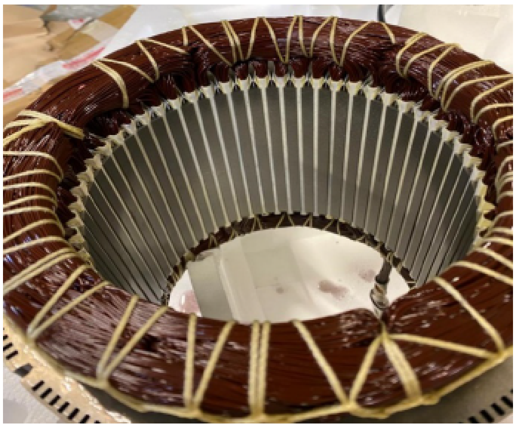

Figure 1.1.1: Stator assembly. [2]

Figure 1.1.2: Rotor assembly. [2]

On both stator and rotor there are some grooves called slots and barriers, respectively. The stator slots include the three-phase stator winding, which is responsible for the rotating magnetic field of the stator, while the barriers host the permanent magnets.

Unlike Surface-mounted Permanent Magnet (SPM) motors, in Interior Permanent Magnet (IPM) machines the magnets are embedded inside the rotor lamination stack rather than placed on its surface.

This design choice provides two major advantages. First, the magnets are better mechanically protected, which allows the motor to safely operate at high rotational speeds without the risk of magnet detachment due to centrifugal forces. This aspect is particularly important in traction applications, where wide speed ranges are required.

Second, the internal placement of the magnets gives the rotor a non-uniform magnetic structure, meaning that its magnetic permeability differs along different directions. As a result, the motor is able to produce not only torque due to the interaction between the stator field and the permanent magnets, but also an additional component known as reluctance torque. This aspect will be explained better in the next section.

The combination of permanent magnet torque and reluctance torque improves the overall torque capability of the machine and enhances its efficiency, especially over a wide operating range.

Based on the aforementioned barriers, IPM motors can be classified into several types, as:

- I-type
- V-type
- Triangle-type

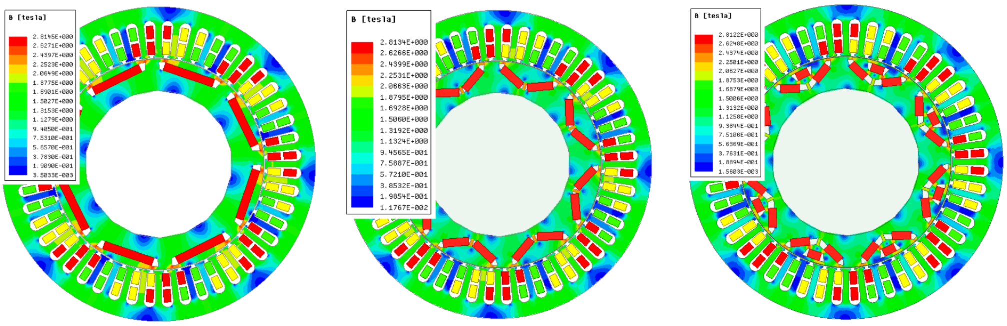

(a) (b) (c)

Figure 1.1.3: a) I-type, b) V-type and c) Triangle-type [3]

Regarding the magnet material, instead, they can be made of different materials, but the best and most employed one is an alloy of neodymium, iron and boron (NeFeB). Compared to the other materials they guarantee a strong air-gap magnetic flux due to high remanent flux density (B_r in the range of 1.0 - 1.4 T) and provide resistance to demagnetization because of their high coercivity (H_r typically over 800 kA/m).

Stator and rotor laminations are used for the realization of the two parts in order to reduce the losses and increase efficiency. Fig.1.1.4 shows stator and rotor laminations. For their complete realization, many of them are stacked and held together to form the actual rotor.

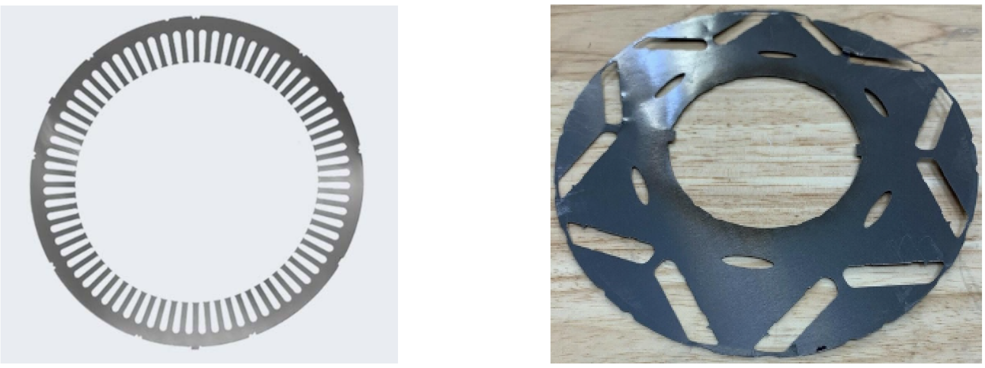

(a) Stator lamination. [4]

(b) Rotor lamination. [2]

Figure 1.1.4: a) Stator and b) rotor laminations

1.1.2 Operating Principles of an IPM Motor

The operating principle of an IPM machine is based on the interaction between the stator and rotor magnetic fields.

As already mentioned in the previous section, the stator slots contain the three-phase winding. Once a balanced AC current runs inside the winding, a rotating magnetic field is generated and its rotating speed depends on the frequency (f) with which the current is alimented and the number of pole pairs (p), as expressed below.

$$\omega_s = \frac{2\pi \cdot f}{p} \tag{1.1}$$

The speed at which the magnetic field rotates is called synchronous speed, while the means by which it is possible to supply the stator with an AC current is the power electronic converter, called inverted, which transforms the input DC current from the battery into AC. The rotor magnets, instead, produce a quasi-static magnetic field.

When the stator and rotor magnetic poles are not aligned, magnetic forces arise due to:

- attraction between opposite poles (north–south)
- repulsion between like poles (north–north or south–south).

These forces generate a tangential component in the air gap that produces a torque on the rotor. Because the stator poles are continuously rotating, the rotor poles are constantly subjected to these magnetic forces. The rotor accelerates until it reaches the same angular speed as the stator field. However, in general, the total torque produced by the motor is due to both the magnets and the anisotropy of the rotor. This last torque contribution is called reluctance torque, generated due to the rotor's tendency to align with the magnetic field for minimum magnetic reluctance (resistance to flux), leveraging magnetic saliency (uneven air gaps or magnetic properties).

The following equation shows the torque equation for an IPM machine:

$$T = \frac{3}{2} \cdot p \cdot [\lambda_{PM} \cdot i_q + (L_q - L_d) \cdot i_d \cdot i_q] = T_{mag} + T_{rel} \tag{1.2}$$

Where:

- p, represents the pole pairs
- λ_{PM} $[Wb]$, permanent magnet flux
- $L_q \neq L_d$ $[H]$, are the dq inductances

These last ones are inversely proportional to the reluctance since the inductance general expression is:

$$L = \frac{N^2}{\mathcal{R}} \tag{1.3}$$

With $\mathcal{R}$ $[H^{-1}]$ representing the reluctance, expressed as:

$$\mathcal{R} = \frac{l}{\mu \cdot S} \tag{1.4}$$

In the above equation:

- l $[m]$, is the length of the magnetic path
- $\mu = \mu_0 \cdot \mu_r$, is the permeability of the magnetic material, equal to the product of the permeability of the free space (μ_0) and the relative permeability (μ_r)
- A $[m^2]$, is the cross section area.

Once the synchronous speed is reached, the rotor poles remain at a nearly constant angular position with respect to the stator poles. This condition is referred to as magnetic locking, in which the rotor “follows” the rotating stator field without slipping.

Any deviation from this equilibrium position creates unbalanced magnetic forces that act to restore the alignment, thereby maintaining synchronous operation.

Section 1.2 will present the software used for the optimization process.

1.2 SyR-e

SyR-e (Synchronous Reluctance – evolution) [5] is an open-source software environment developed in MATLAB/Octave for the design and analysis of synchronous electrical machines. The tool enables the automated design of electric motors by combining finite element analysis (FEA) with multi-objective optimization techniques.

Through its main Graphical User Interface (GUI), SyR-e allows the user to define an electrical machine according to different design approaches. The motor geometry can be specified by manually setting the geometric parameters, generated via dedicated pre-design procedures, or obtained through automated design optimization processes. In all cases, the machine geometry is fully parameterized.

The electromagnetic model is generated within the FEMM [7] environment, which is seamlessly integrated into the SyR-e framework. A set of simulation routines operates in the background of the GUI, enabling the evaluation of the motor performance under different operating conditions.

Once the electromagnetic design is finalized, SyR-e allows the computation of flux and loss maps, which can then be exported to the MMM (Magnetic Model Manipulation) graphical interface. This secondary environment performs further model elaborations based on the computed maps and provides tools for drive-level simulations, including the implementation of control algorithms. Fig.1.2.1 below describes this process.

To start the design process, the main SyR-e GUI is launched via the appropriate command in MATLAB. The interface is organized into nine dedicated tabs, each corresponding to a specific design or analysis task, which are described in detail in the following sections. Upon startup, a default motor configuration is automatically loaded, providing a reference starting point for the design workflow.[6]

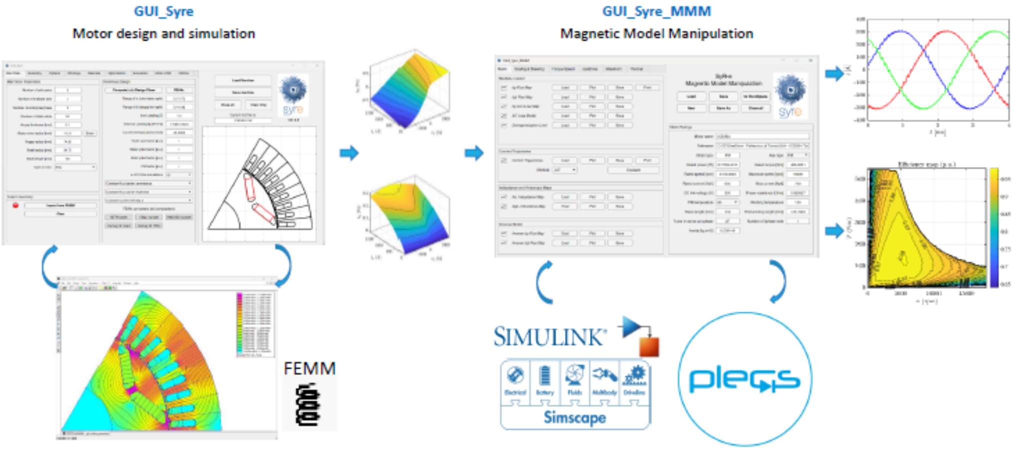

Figure 1.2.1: SyR-e data flow. [6]

1.2.1 Main tabs

As explained previously, in the main SyR-e GUI nine tabs are present, which are:

- *Main Data*
- *Stator*
- *Rotor*
- *Options*
- *Materials*
- *Optimizations*
- *Simulations*
- *Motor-CAD*
- *Utilities*

Main Data Tab

This tab is divided into three sections:

- *Main Motor Parameters*, where it is possible to set the principal parameters of a motor, select the type of motor and there is also the *Scale* button which, once selected, allows to modify the *Stator outer radius* and automatically all the other radial parameters will be scaled by the same factor.

- *Preliminary Design*, provides a design-plane approach in which key performance indicators, such as electromagnetic torque and power factor, are expressed as functions of two dimensionless design parameters by clicking on the *Compute (x,b) Design Plane* button ($x = \frac{D_r}{D}$ and $b = \frac{B_g}{B_{Fe,s}}$, where D_r is the rotor diameter, D is the stator diameter, B_g is the air gap peak flux density and $B_{Fe,s}$ is the back-iron iron peak flux density). Each point on this plane corresponds to a distinct motor configuration, allowing the designer to choose among different solutions according to the required performance targets and imposed constraints.

This methodology has been further refined through the introduction of the *FEAfix* button. This feature enables the analytical formulations underlying the design plane to be corrected and calibrated using a limited number of finite element simulations. The number of FEA evaluations used for this correction can be selected from the graphical user interface, providing a trade-off between computational effort and modeling accuracy.

- *Custom Geometry*, which allows to upload the custom geometry from FEMM inside the GUI. Once imported, the red led becomes green and the colored geometry will be displayed.

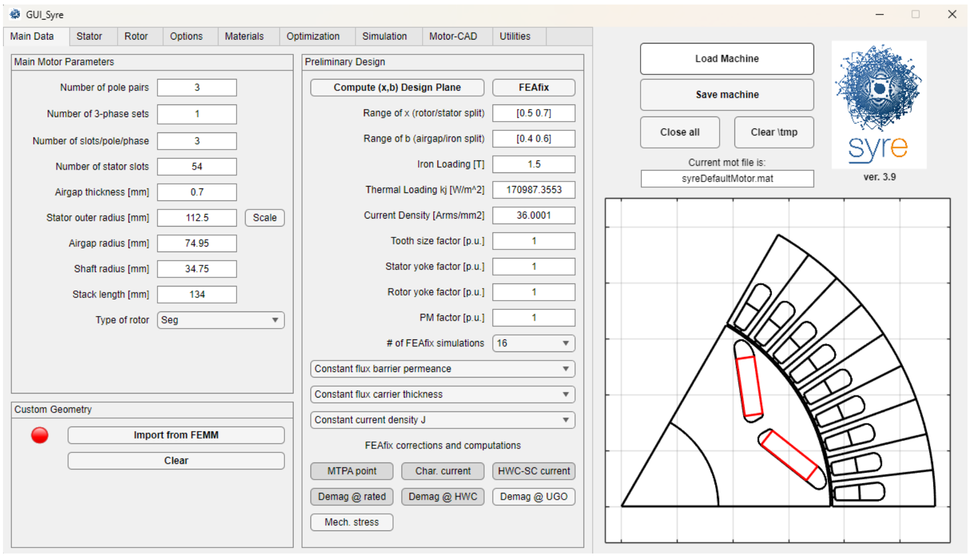

Number of pole pairs: 3
Number of 3-phase sets: 1
Number of slots/pole/phase: 3
Number of stator slots: 54
Airgap thickness [mm]: 0.7
Stator outer radius [mm]: 112.5
Airgap radius [mm]: 74.95
Shaft radius [mm]: 34.75
Stack length [mm]: 134
Type of rotor: Seg

Range of x (rotor/stator split): [0.5 0.7]
Range of b (airgap/iron split): [0.4 0.6]
Iron Loading [T]: 1.5
Thermal Loading kj [W/m^2]: 170987.3553
Current Density [Arms/mm2]: 36.0001
Tooth size factor [p.u.]: 1
Stator yoke factor [p.u.]: 1
Rotor yoke factor [p.u.]: 1
PM factor [p.u.]: 1
# of FEAfix simulations: 16
Constant flux barrier permeance
Constant flux carrier thickness
Constant current density J

Current mot file is: syreDefaultMotor.mat

Figure 1.2.2: SyR-e main tab. [6]

Stator Tab

The stator tab is organized as follows:

- *Stator Parameters*, where the stator lamination geometries can be modified.
- *Main Winding Data*, in which custom stator winding can be uploaded and where the number of simulated slots can be selected.
- *Slot Model*, which allows to change the type of conductor, but also its dimensions, quantity and insulation. Two buttons are then present at the end, which are *Draw slot model*, displays conductors inside the stator slot, and *Evaluate stator slot*, analyses the winding at the frequencies and temperatures written inside the *Frequency* and *Temperature vector*.

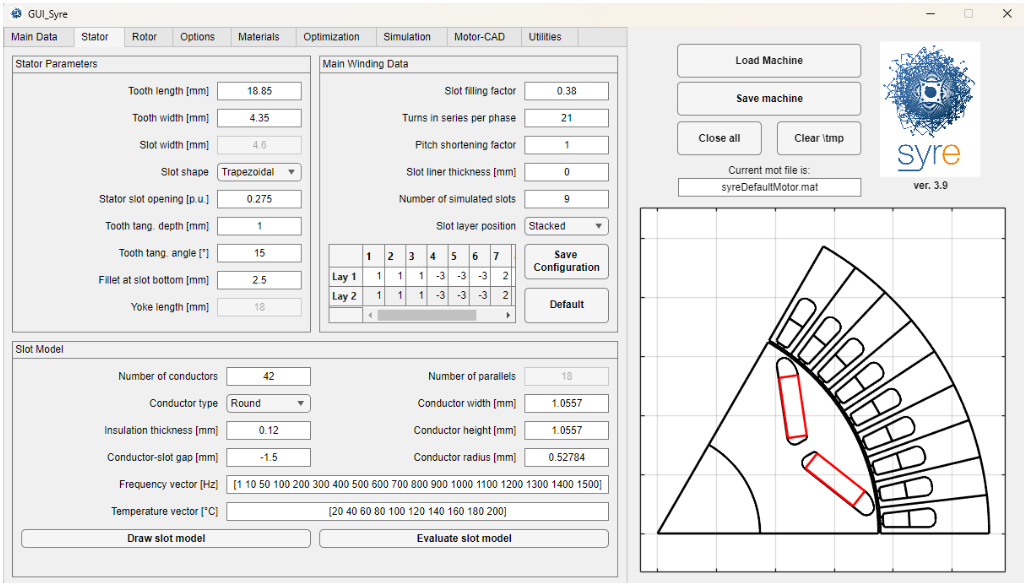

Stator Parameters

Tooth length [mm]	18.85
Tooth width [mm]	4.35
Slot width [mm]	4.6
Slot shape	Trapezoidal
Stator slot opening [p.u.]	0.275
Tooth tang. depth [mm]	1
Tooth tang. angle [°]	15
Fillet at slot bottom [mm]	2.5
Yoke length [mm]	18

Main Winding Data

Slot filling factor	0.38
Turns in series per phase	21
Pitch shortening factor	1
Slot liner thickness [mm]	0
Number of simulated slots	9
Slot layer position	Stacked

	1	2	3	4	5	6	7
Lay 1	1	1	1	-3	-3	-3	2
Lay 2	1	1	1	-3	-3	-3	2

Slot Model

Number of conductors	42	Number of parallels	18
Conductor type	Round	Conductor width [mm]	1.0557
Insulation thickness [mm]	0.12	Conductor height [mm]	1.0557
Conductor-slot gap [mm]	-1.5	Conductor radius [mm]	0.52784

Frequency vector [Hz] [1 10 50 100 200 300 400 500 600 700 800 900 1000 1100 1200 1300 1400 1500]

Temperature vector [°C] [20 40 60 80 100 120 140 160 180 200]

Current mot file is: syreDefaultMotor.mat

Figure 1.2.3: SyR-e stator tab. [6]

Rotor Tab

The rotor tab, as the stator, is divided in three sections:

- PMSM-SyR (Permanent Magnet Synchronous Motor-Synchronous Reluctance motor) Parameters
- EESM (Electrically Excited Synchronous Motor) Rotor Parameters
- IM (Induction motor) Rotor Parameters

The *PMSM-SyR* section will be active for all the motor types other than *EESM* and *IM*, in which cases the *EESM* and *IM* sections will be activated respectively.

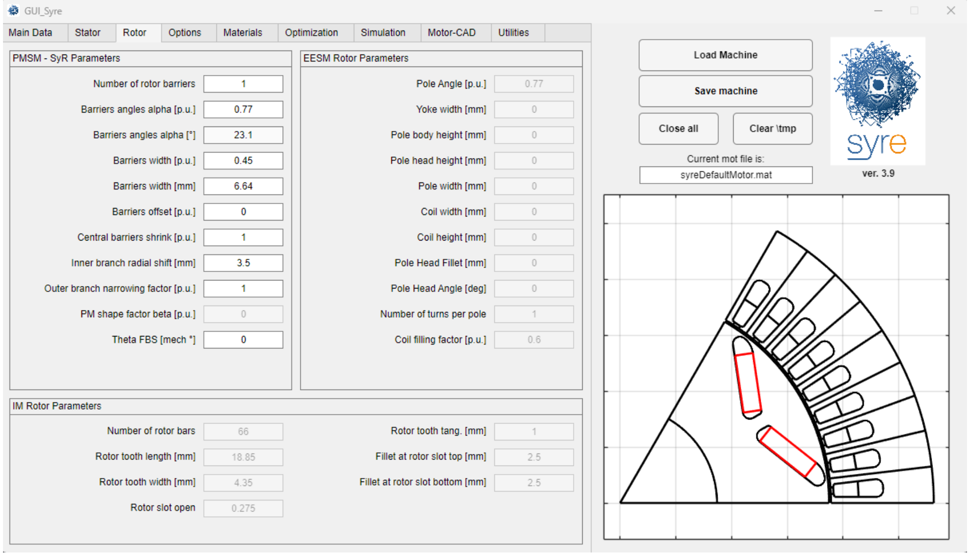

PMSM - SyR Parameters

Number of rotor barriers	1
Barriers angles alpha [p.u.]	0.77
Barriers angles alpha [°]	23.1
Barriers width [p.u.]	0.45
Barriers width [mm]	6.64
Barriers offset [p.u.]	0
Central barriers shrink [p.u.]	1
Inner branch radial shift [mm]	3.5
Outer branch narrowing factor [p.u.]	1
PM shape factor beta [p.u.]	0
Theta FBS [mech °]	0

EESM Rotor Parameters

Pole Angle [p.u.]	0.77
Yoke width [mm]	0
Pole body height [mm]	0
Pole head height [mm]	0
Pole width [mm]	0
Coil width [mm]	0
Coil height [mm]	0
Pole Head Fillet [mm]	0
Pole Head Angle [deg]	0
Number of turns per pole	1
Coil filling factor [p.u.]	0.6

IM Rotor Parameters

Number of rotor bars	66	Rotor tooth tang. [mm]	1
Rotor tooth length [mm]	18.85	Fillet at rotor slot top [mm]	2.5
Rotor tooth width [mm]	4.35	Fillet at rotor slot bottom [mm]	2.5
Rotor slot open	0.275		

Current mot file is: syreDefaultMotor.mat

Figure 1.2.4: SyR-e rotor tab. [6]

Options Tab

This tab presents:

- *Thermal Parameters*, where the rated current can be determined by specifying one of three alternative input quantities: the thermal loading $k_j [W/m^2]$, the rated losses $[W]$ or the RMS slot current density $J [A/mm^2]$. One of these parameters is selected as an input, while the remaining quantities are evaluated automatically by the software. The winding temperature and the rated current are estimated with a thermal mode, while the housing and target average winging temperatures have to be set.
- *Structural Parameters*, in which overspeed, minimum mechanical stress and the sleeve can be modified.
- *Rib Design*, that allows to modify the tangential and radial ribs as well as the fillets.

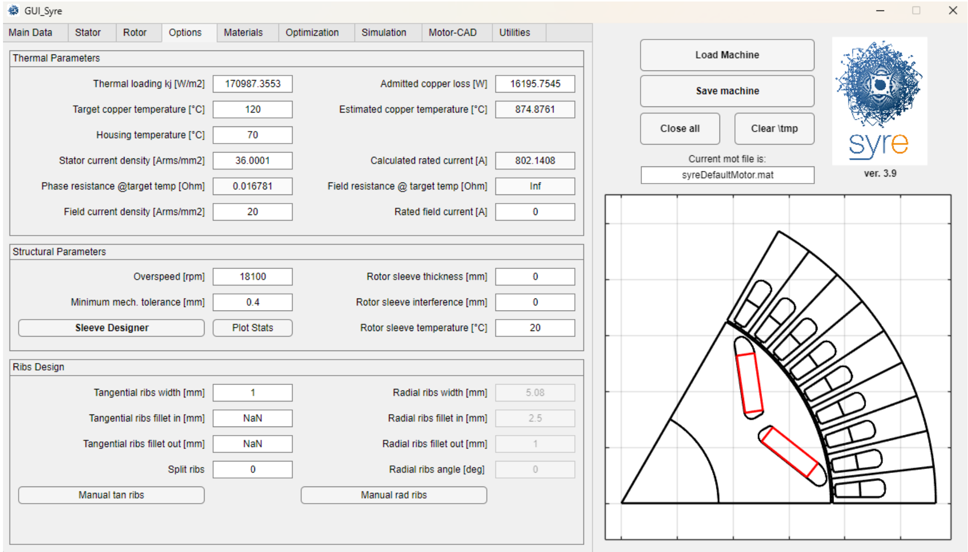

Thermal Parameters

Thermal loading kj [W/m2] 170987.3553
Admitted copper loss [W] 16195.7545
Target copper temperature [°C] 120
Estimated copper temperature [°C] 874.8761
Housing temperature [°C] 70
Stator current density [Arms/mm2] 36.0001
Calculated rated current [A] 802.1408
Phase resistance @target temp [Ohm] 0.016781
Field resistance @ target temp [Ohm] Inf
Field current density [Arms/mm2] 20
Rated field current [A] 0

Structural Parameters

Overspeed [rpm] 18100
Rotor sleeve thickness [mm] 0
Minimum mech. tolerance [mm] 0.4
Rotor sleeve interference [mm] 0
Rotor sleeve temperature [°C] 20

Ribs Design

Tangential ribs width [mm] 1
Radial ribs width [mm] 5.08
Tangential ribs fillet in [mm] NaN
Radial ribs fillet in [mm] 2.5
Tangential ribs fillet out [mm] NaN
Radial ribs fillet out [mm] 1
Split ribs 0
Radial ribs angle [deg] 0

Current mot file is: syreDefaultMotor.mat

Figure 1.2.5: SyR-e options tab. [6]

Materials Tab

The material of every part of the motor is selected from here and the weight is then automatically calculated accordingly also to their geometries. Other materials can be added and it is possible to look at their properties.

The *PM Design* button, at the bottom of the tab, allows to design the permanent magnets of PM-SyR and V-type motors targeting the characteristic current. [6]

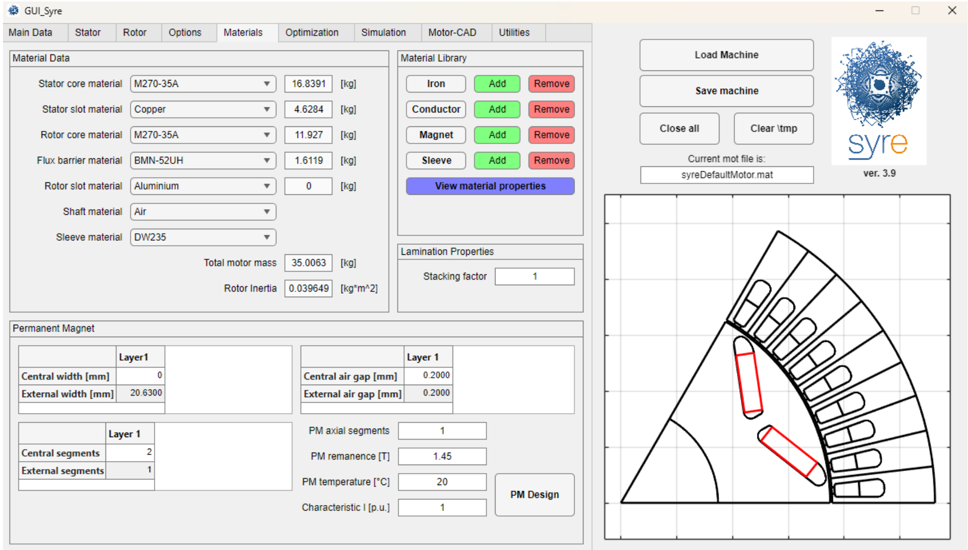

Stator core material: M270-35A, 16.8391 [kg]
Stator slot material: Copper, 4.6284 [kg]
Rotor core material: M270-35A, 11.927 [kg]
Flux barrier material: BMN-52UH, 1.6119 [kg]
Rotor slot material: Aluminium, 0 [kg]
Shaft material: Air
Sleeve material: DW235
Total motor mass: 35.0063 [kg]
Rotor Inertia: 0.039649 [kg*m^2]
Stacking factor: 1

	Layer1
Central width [mm]	0
External width [mm]	20.6300

	Layer 1
Central air gap [mm]	0.2000
External air gap [mm]	0.2000

	Layer 1
Central segments	2
External segments	1

PM axial segments: 1
PM remanence [T]: 1.45
PM temperature [°C]: 20
Characteristic I [p.u.]: 1
Current mot file is: syreDefaultMotor.mat

Figure 1.2.6: SyR-e material tab. [6]

Optimization tab

This tab has two sub-tabs *Evaluation options* and *Variables and Boundaries*. The first is then divided in:

- *Optimization options*, from where the optimization algorithm can be set, as well as the current overload in per unit, the population and generations size, the stator current setting, determines in which conditions the optimization will be executed (constant thermal loading k_j, constant current density J or constant phase current I), and the field by stator current density. It is also present the *Mechanical Stress Control* check, which returns the results of the structural analysis of the motors.

- *Objectives and Penalization limits*, includes the target of the optimization process. It is a process in which all the quantities are minimized. In particular, minimizing a negative target (*e.g* Torque or Power factor) is the same of maximizing a positive one but of opposite sign, while the positive target are minimized. Further ahead the optimization will be explained better.

- *Time stepping raw(evolution)* and *Time stepping fine(Pareto re-evaluation)*, define the rotor angular excursion and the number of rotor positions that will be used during the simulations.

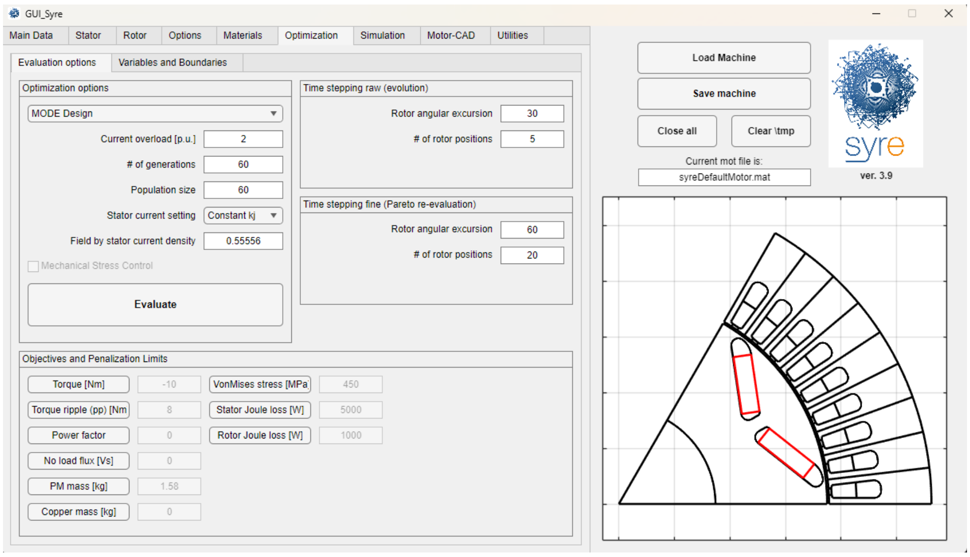

Optimization options

MODE Design
Current overload [p.u.] 2
# of generations 60
Population size 60
Stator current setting Constant kj
Field by stator current density 0.55556
☐ Mechanical Stress Control

Time stepping raw (evolution)

Rotor angular excursion 30
# of rotor positions 5

Time stepping fine (Pareto re-evaluation)

Rotor angular excursion 60
# of rotor positions 20

Objectives and Penalization Limits

Torque [Nm]	-10	VonMises stress [MPa]	450
Torque ripple (pp) [Nm	8	Stator Joule loss [W]	5000
Power factor	0	Rotor Joule loss [W]	1000
No load flux [Vs]	0		
PM mass [kg]	1.58		
Copper mass [kg]	0		

Current mot file is:
syreDefaultMotor.mat

Figure 1.2.7: SyR-e optimization tab - Evaluation options. [6]

The last, instead, presents all the adjustable variables. In particular, for every selected variable, a defined range has to be set.

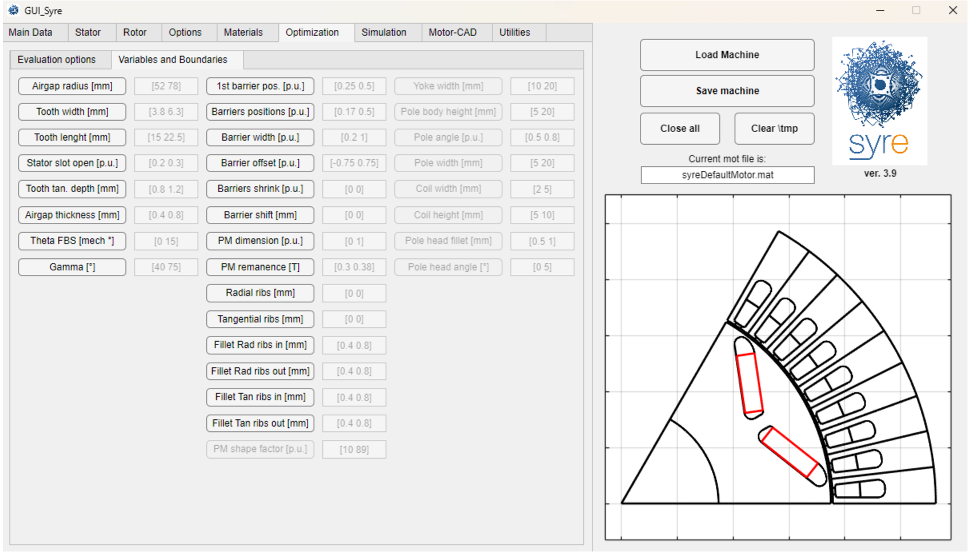

Airgap radius [mm]	[52 78]	1st barrier pos. [p.u.]	[0.25 0.5]	Yoke width [mm]	[10 20]
Tooth width [mm]	[3.8 6.3]	Barriers positions [p.u.]	[0.17 0.5]	Pole body height [mm]	[5 20]
Tooth lenght [mm]	[15 22.5]	Barrier width [p.u.]	[0.2 1]	Pole angle [p.u.]	[0.5 0.8]
Stator slot open [p.u.]	[0.2 0.3]	Barrier offset [p.u.]	[-0.75 0.75]	Pole width [mm]	[5 20]
Tooth tan. depth [mm]	[0.8 1.2]	Barriers shrink [p.u.]	[0 0]	Coil width [mm]	[2 5]
Airgap thickness [mm]	[0.4 0.8]	Barrier shift [mm]	[0 0]	Coil height [mm]	[5 10]
Theta FBS [mech °]	[0 15]	PM dimension [p.u.]	[0 1]	Pole head fillet [mm]	[0.5 1]
Gamma [°]	[40 75]	PM remanence [T]	[0.3 0.38]	Pole head angle [°]	[0 5]
		Radial ribs [mm]	[0 0]		
		Tangential ribs [mm]	[0 0]		
		Fillet Rad ribs in [mm]	[0.4 0.8]		
		Fillet Rad ribs out [mm]	[0.4 0.8]		
		Fillet Tan ribs in [mm]	[0.4 0.8]		
		Fillet Tan ribs out [mm]	[0.4 0.8]		
		PM shape factor [p.u.]	[10 89]		

Current mot file is:
syreDefaultMotor.mat

Figure 1.2.8: SyR-e optimization tab - Variables and Boundaries. [6]

Simulation Tab

In this tab it is possible to select the following simulations and the optimization variables, depending on the which simulation was set.

- Single Point
- Flux Map
- Characteristic Current
- Steady-State Short-Circuit Current

- HWC Short-Circuit Current (Hyper-Worst-Case)
- Demagnetization Curve
- Demagnetization Curve DQ
- Demagnetization Analysis
- Flux Density Analysis
- Current Offset
- Airgap Force
- Iron Loss – Single Point
- Iron Loss – Flux Map
- Structural Analysis

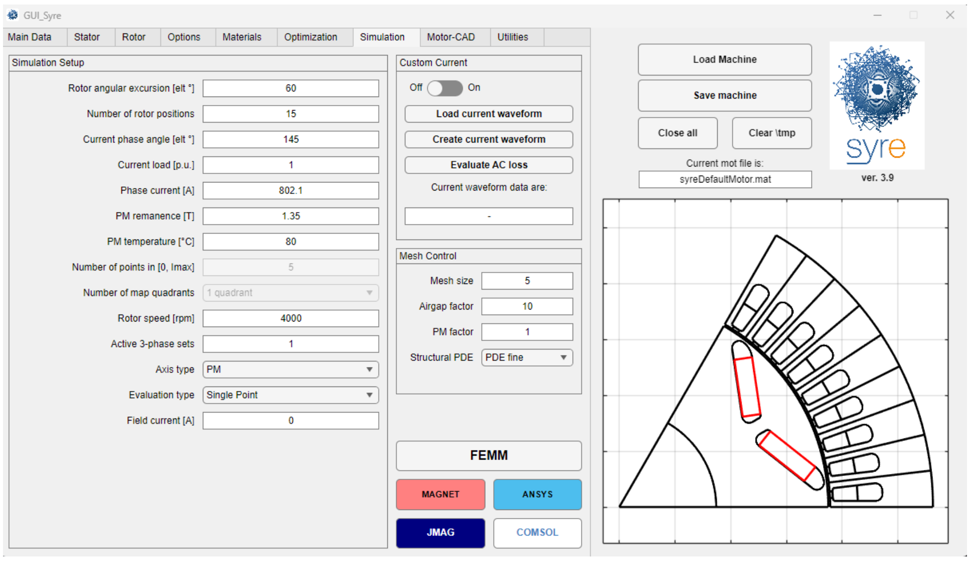

Rotor angular excursion [elt °] 60
Number of rotor positions 15
Current phase angle [elt °] 145
Current load [p.u.] 1
Phase current [A] 802.1
PM remanence [T] 1.35
PM temperature [°C] 80
Number of points in [0, Imax] 5
Number of map quadrants 1 quadrant
Rotor speed [rpm] 4000
Active 3-phase sets 1
Axis type PM
Evaluation type Single Point
Field current [A] 0

Current waveform data are: -

Mesh size 5
Airgap factor 10
PM factor 1
Structural PDE PDE fine

Current mot file is: syreDefaultMotor.mat

Figure 1.2.9: SyR-e simulation tab. [6]

Motor-CAD Tab

With the Motor-CAD tab is possible to export the model in Ansys Motor-CAD and perform electromagnetic and thermal simulations.

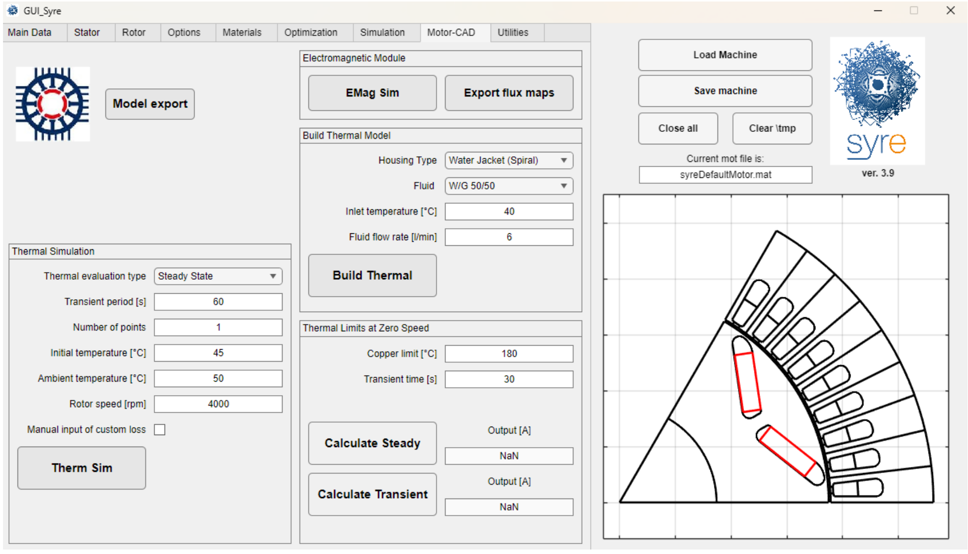

Housing Type: Water Jacket (Spiral)
Fluid: W/G 50/50
Inlet temperature [°C]: 40
Fluid flow rate [l/min]: 6
Thermal evaluation type: Steady State
Transient period [s]: 60
Number of points: 1
Initial temperature [°C]: 45
Ambient temperature [°C]: 50
Rotor speed [rpm]: 4000
Manual input of custom loss ☐
Copper limit [°C]: 180
Transient time [s]: 30
Output [A]: NaN
Output [A]: NaN
Current mot file is: syreDefaultMotor.mat
ver. 3.9

Figure 1.2.10: SyR-e Motor-CAD tab. [6]

Utilities Tab

The last tab contains:

- Section for the exportation to different commercial software
- Links for the manual and references
- Button to open SyR-e MMM and the *(x,b) Design Plane Explorer*
- Button to check the parallel pool

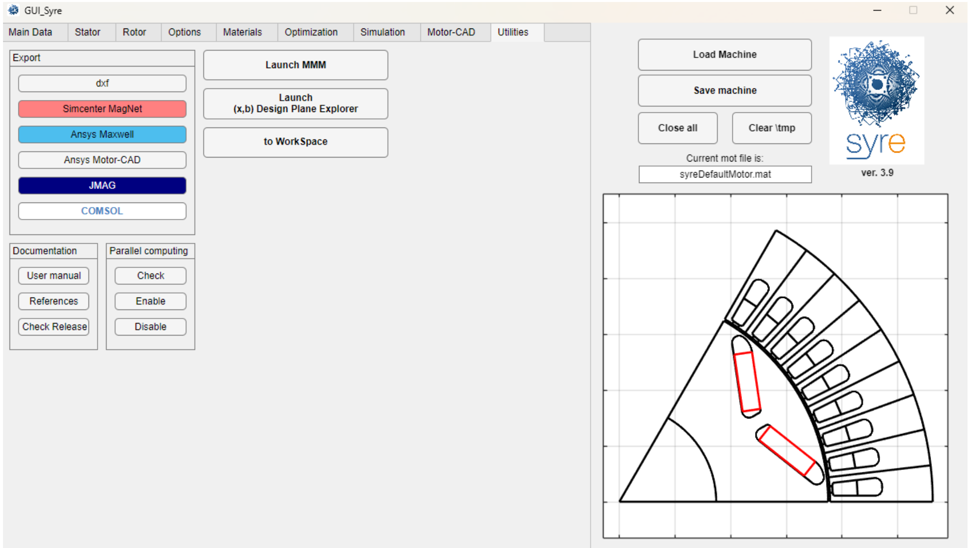

Current mot file is: syreDefaultMotor.mat
ver. 3.9

Figure 1.2.11: SyR-e utilities tab. [6]

1.2.2 SyR-e MMM

This GUI has the acronym MMM, which stands for Magnetic Model Manipulation. As the name suggests, this SyR-e interface is useful for the flux maps manipulations and can be launched through the button present inside the *Utilities* tab of SyR-e or with the command `GUI_Syre_MMM`.

This interface is composed of six tabs, which are

- *Main*
- *Scaling & Skewing*
- *Torque-Speed*
- *syreDrive*
- *Waveform*
- *Thermal*

and *Motor Ratings* tab always displayed on the right side of the GUI, as the following buttons:

- Load: loads a new model
- Save and Save as: used for saving the motor model
- to WorkSpace: load the model on Matlab WorkSpace
- New: creates a new motor model
- Close All: closes all the figures. [6]

Main Tab

The main tab is divided in four sections:

- *Model Loaded*, used to load the flux maps, obtained with the *Flux Map* simulation in SyR-e. The models that can be loaded are:
    - dq Flux Map
    - dqt Flux Map
    - dq Iron Loss Map
    - AC Loss Model
    - Demagnetization Limit

  Each model can be obtained from the *Simulation* tab in SyR-e and then uploaded with the *Load* button. The *Plot* button is used to display the results and save them. The *Print* button, instead, prints the results in .c format.

- *Control Trajectories*, which computes the Maximum Torque per Ampere (MTPA) and the Maximum Torque per Voltage (MTPV). Two methods of showing the results can be selected, Look Up Table (LUT) and Fit method. An *Evaluate* button in also present, in case some data from the *Motor Ratings* tab are modified. With this button the motor will be re-evaluated and the results displayed with the *Plot* button.

- *Inductance and Anisotropy Maps*, in which the incremental and apparent inductances cab be calculated.

- *Inverse Model*, where torque and current are computed in function of dq flux linkages.

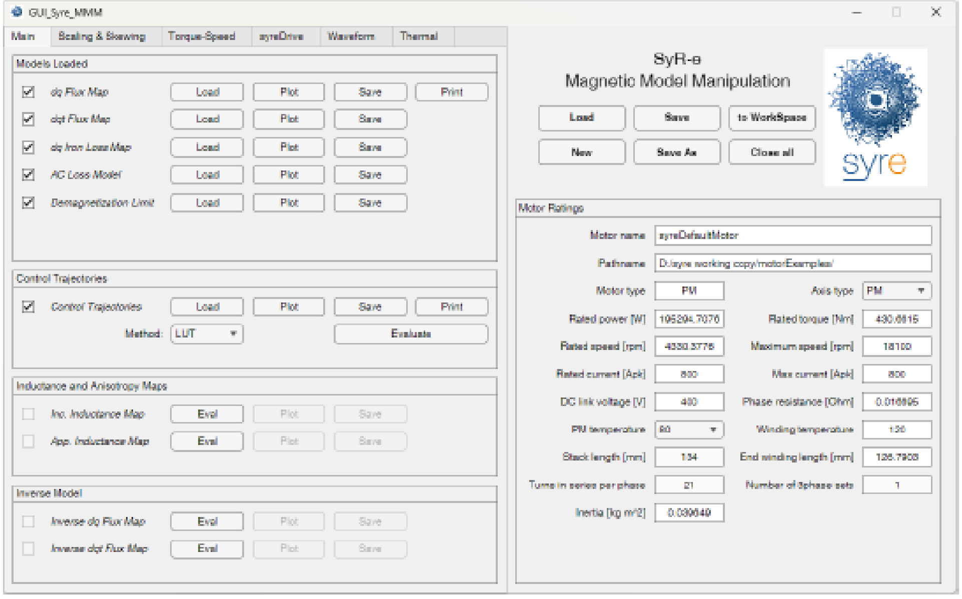

☑ dq Flux Map
☑ dqt Flux Map
☑ dq Iron Loss Map
☑ AC Loss Model
☑ Demagnetization Limit
☑ Control Trajectories
Method: LUT
☐ Inc. Inductance Map
☐ App. Inductance Map
☐ Inverse dq Flux Map
☐ Inverse dqt Flux Map

Motor name: syreDefaultMotor
Pathname: D:/syre working copy/motorExamples/
Motor type: PM
Axis type: PM
Rated power [W]: 105294.7076
Rated torque [Nm]: 430.6815
Rated speed [rpm]: 4330.3778
Maximum speed [rpm]: 18100
Rated current [Apk]: 800
Max current [Apk]: 800
DC link voltage [V]: 400
Phase resistance [Ohm]: 0.016895
PM temperature: 80
Winding temperature: 120
Stack length [mm]: 134
End winding length [mm]: 126.7908
Turns in series per phase: 21
Number of 3phase sets: 1
Inertia [kg m^2]: 0.039649

Figure 1.2.12: SyR-e MMM main tab. [6]

Scaling & Skewing Tab

This tab allows to do the homonymous functions, present in two different boxes, placed side by side.

The *Model Scaling* presents five parameters. Once one of them is modified, the *Scale Model* button becomes active and the motor scaling can be performed. The *(L,N_s) Scaling Plane* is then used to print the performance map function of the stack length L and number of turns N_s.

The *Model Skewing*, instead, presents four parameters to set the motor skewing and needs the dqt Flux Map for this purpose.

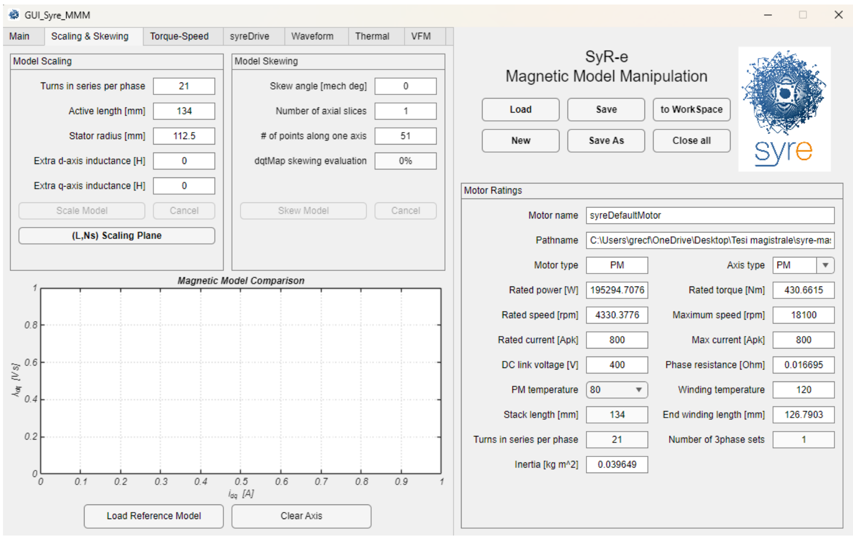

Model Scaling

Turns in series per phase 21
Active length [mm] 134
Stator radius [mm] 112.5
Extra d-axis inductance [H] 0
Extra q-axis inductance [H] 0

Model Skewing

Skew angle [mech deg] 0
Number of axial slices 1
# of points along one axis 51
dqtMap skewing evaluation 0%

Motor Ratings

Motor name syreDefaultMotor
Pathname C:\Users\grecf\OneDrive\Desktop\Tesi magistrale\syre-ma:
Motor type PM
Axis type PM
Rated power [W] 195294.7076
Rated torque [Nm] 430.6615
Rated speed [rpm] 4330.3776
Maximum speed [rpm] 18100
Rated current [Apk] 800
Max current [Apk] 800
DC link voltage [V] 400
Phase resistance [Ohm] 0.016695
PM temperature 80
Winding temperature 120
Stack length [mm] 134
End winding length [mm] 126.7903
Turns in series per phase 21
Number of 3phase sets 1
Inertia [kg m^2] 0.039649

Figure 1.2.13: SyR-e MMM scaling and skewing tab. [6]

Torque-Speed Tab

The following tab computes the torque-speed behavior in two ways, one more approximated and the other more accurate.

The first done in the *Operating Limits* section, setting the current value in per unit of the rated current present inside the *Motor Ratings* box. The *Evaluate* button shows the results of torque, power, power factor, current, voltage and flux linkage function of the speed and also the control trajectories.

The *Torque - Speed Performance Map & Efficiency Map*, instead, calculated the torque-speed behavior more accurately. From here also the efficiency map can be computed, selecting which losses have to be included in the calculation, and eventually a certain factor. Other parameters that have to be set are the map limits, the number of points in which are computed the results (trade-off between precision and time) and which control trajectory have to be used.

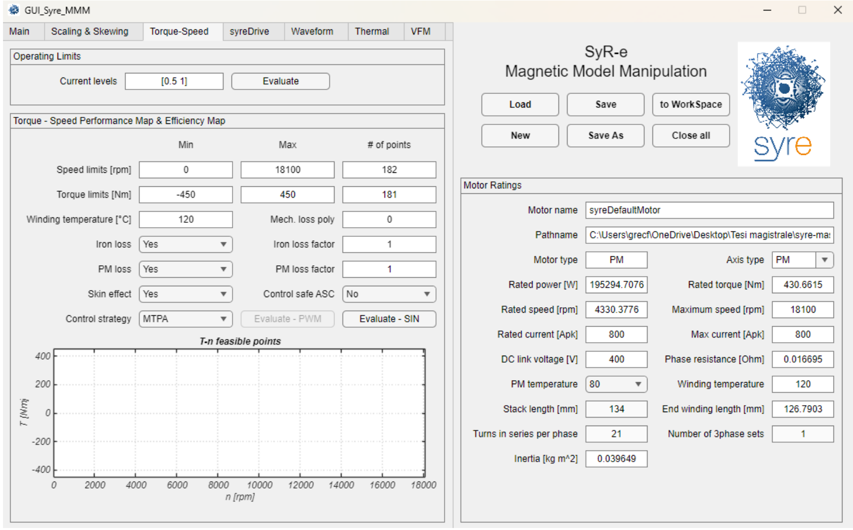

Operating Limits

Current levels [0.5 1]

Torque - Speed Performance Map & Efficiency Map

	Min	Max	# of points
Speed limits [rpm]	0	18100	182
Torque limits [Nm]	-450	450	181

Winding temperature [°C] 120
Mech. loss poly 0
Iron loss Yes
Iron loss factor 1
PM loss Yes
PM loss factor 1
Skin effect Yes
Control safe ASC No
Control strategy MTPA

Motor Ratings

Motor name syreDefaultMotor
Pathname C:\Users\grecf\OneDrive\Desktop\Tesi magistrale\syre-ma:
Motor type PM
Axis type PM
Rated power [W] 195294.7076
Rated torque [Nm] 430.6615
Rated speed [rpm] 4330.3776
Maximum speed [rpm] 18100
Rated current [Apk] 800
Max current [Apk] 800
DC link voltage [V] 400
Phase resistance [Ohm] 0.016695
PM temperature 80
Winding temperature 120
Stack length [mm] 134
End winding length [mm] 126.7903
Turns in series per phase 21
Number of 3phase sets 1
Inertia [kg m^2] 0.039649

Figure 1.2.14: SyR-e MMM Torque tab. [6]

syreDrive Tab

In this tab it is possible to export the motor model into Matlab/Simulink and PLECS for the evaluation of the dynamic model of the motor. It is divided in three sections:

- *Model Setup*, in which type, model, flux maps model, control type and strategy, iron and AC losses model of the motor can be set up.
- *Converter Data*, which sets the main parameters of the converter.
- *Sensorless Control*, where a sensorless control can be imposed.

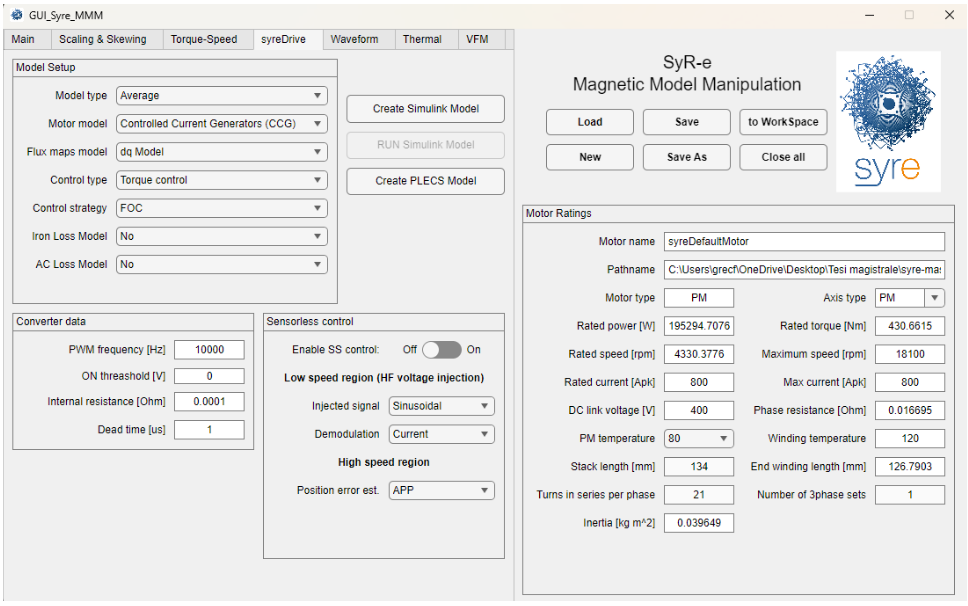

Model Setup

Model type: Average
Motor model: Controlled Current Generators (CCG)
Flux maps model: dq Model
Control type: Torque control
Control strategy: FOC
Iron Loss Model: No
AC Loss Model: No

Converter data

PWM frequency [Hz]: 10000
ON threashold [V]: 0
Internal resistance [Ohm]: 0.0001
Dead time [us]: 1

Sensorless control

Enable SS control: Off ○ On

Low speed region (HF voltage injection)

Injected signal: Sinusoidal
Demodulation: Current

High speed region

Position error est.: APP

Motor Ratings

Motor name: syreDefaultMotor
Pathname: C:\Users\grecf\OneDrive\Desktop\Tesi magistrale\syre-ma
Motor type: PM
Axis type: PM
Rated power [W]: 195294.7076
Rated torque [Nm]: 430.6615
Rated speed [rpm]: 4330.3776
Maximum speed [rpm]: 18100
Rated current [Apk]: 800
Max current [Apk]: 800
DC link voltage [V]: 400
Phase resistance [Ohm]: 0.016695
PM temperature: 80
Winding temperature: 120
Stack length [mm]: 134
End winding length [mm]: 126.7903
Turns in series per phase: 21
Number of 3phase sets: 1
Inertia [kg m^2]: 0.039649

Figure 1.2.15: SyR-e MMM syreDrive tab. [6]

Waveforms Tab

In this case it is possible to perform different evaluations, present inside the *Evaluations* box:

- *Single Point* evaluation, which needs dqt flux map
- *Constant Current Curve* evaluation
- *Steady-State Short-Circuit* evaluation, where steady-state dq current and torque function of the rotor speed are computed, with the motor terminals closed in short-circuit [6]
- *Transient Short-Circuit* evaluation from the selected pre-fault conditions

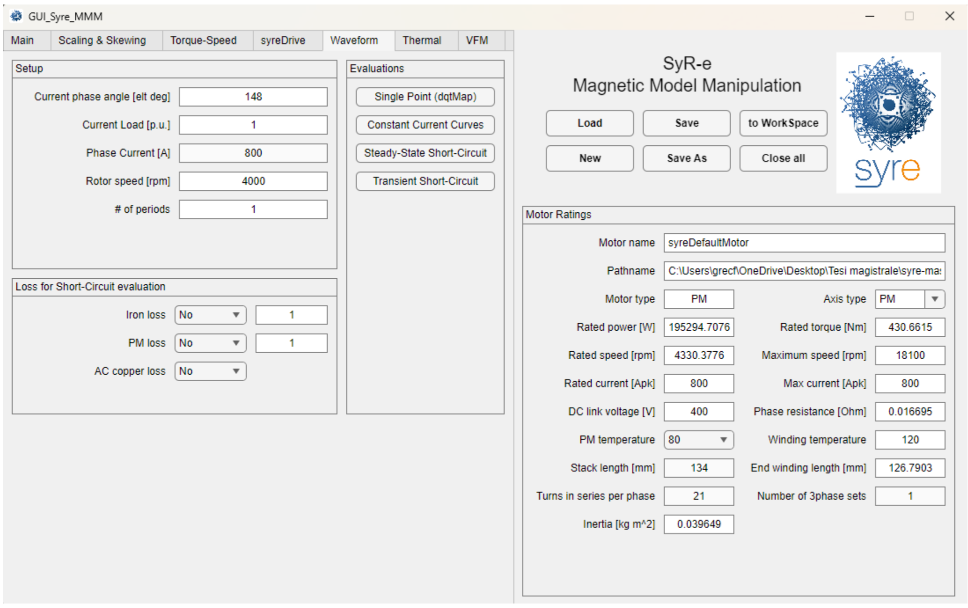

Setup
Current phase angle [elt deg] 148
Current Load [p.u.] 1
Phase Current [A] 800
Rotor speed [rpm] 4000
# of periods 1

Loss for Short-Circuit evaluation
Iron loss No 1
PM loss No 1
AC copper loss No

Motor Ratings
Motor name syreDefaultMotor
Pathname C:\Users\grecf\OneDrive\Desktop\Tesi magistrale\syre-ma
Motor type PM
Axis type PM
Rated power [W] 195294.7076
Rated torque [Nm] 430.6615
Rated speed [rpm] 4330.3776
Maximum speed [rpm] 18100
Rated current [Apk] 800
Max current [Apk] 800
DC link voltage [V] 400
Phase resistance [Ohm] 0.016695
PM temperature 80
Winding temperature 120
Stack length [mm] 134
End winding length [mm] 126.7903
Turns in series per phase 21
Number of 3phase sets 1
Inertia [kg m^2] 0.039649

Figure 1.2.16: SyR-e MMM waveforms tab. [6]

Thermal Tab

A thermal evaluation of the motor is performed in this tab, imposing the copper temperature and the limits of the torque-speed plane.

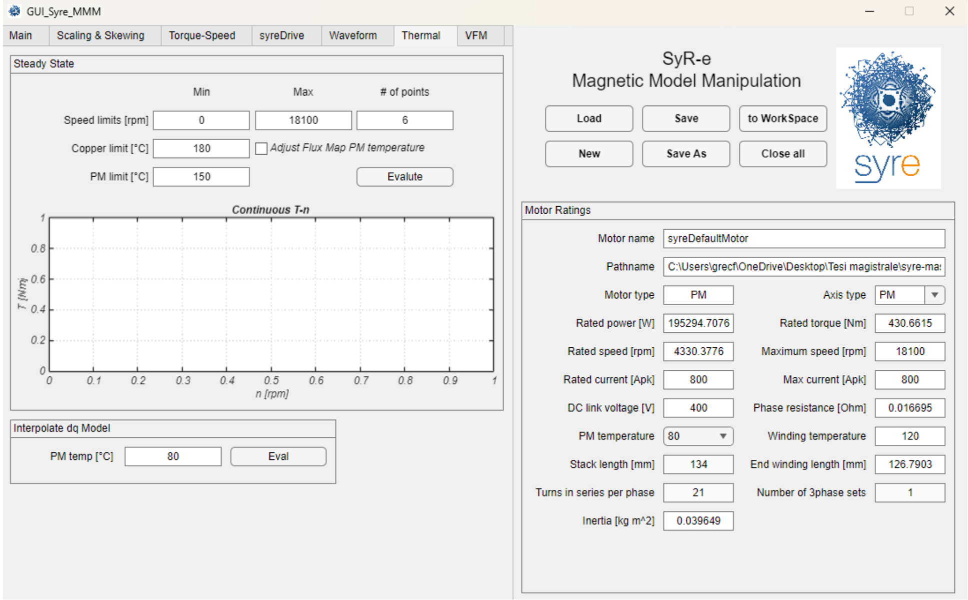

Steady State

	Min	Max	# of points
Speed limits [rpm]	0	18100	6
Copper limit [°C]	180	☐ Adjust Flux Map PM temperature	
PM limit [°C]	150		

Interpolate dq Model
PM temp [°C] 80

Motor Ratings
Motor name syreDefaultMotor
Pathname C:\Users\grecf\OneDrive\Desktop\Tesi magistrale\syre-ma
Motor type PM
Axis type PM
Rated power [W] 195294.7076
Rated torque [Nm] 430.6615
Rated speed [rpm] 4330.3776
Maximum speed [rpm] 18100
Rated current [Apk] 800
Max current [Apk] 800
DC link voltage [V] 400
Phase resistance [Ohm] 0.016695
PM temperature 80
Winding temperature 120
Stack length [mm] 134
End winding length [mm] 126.7903
Turns in series per phase 21
Number of 3phase sets 1
Inertia [kg m^2] 0.039649

Figure 1.2.17: SyR-e MMM thermal tab.

Chapter 2

SyR-e Updates and Improvements

For the realization of the electromagnetic and structural optimization, some changes in the SyR-e interface and code were made. The following sections will first show the implementation of the *Von Mises stress* objective and then some improvements done inside the optimization code.

2.1 Implementation of Multi-Physic Optimization

In SyR-e the optimization process is performed inside the *Optimization tab* and, as showed previously in Fig.1.2.7, the *Objectives and Penalization Limits* are eight:

- Torque
- Torque ripple
- Power Factor
- No load flux
- PM mass
- Copper mass
- Stator Joule loss
- Rotor Joule loss

For all of these buttons, which correspond to the desired optimization target, once selected, it is possible to set a penalization limit. In particular, if the desired torque value of the motor from the optimization process is 200 Nm, the torque button must be selected and set to that value. Once the *Evaluate* button is pressed, the optimization starts evaluating the initial motor population, which size is the same of the *Population size*. For every motor a finite element analysis (FEA) in FEMM is performed, from which all the electromagnetic properties are extrapolated and motors with a torque value lower than the target are penalized.

From the *Optimization options* box is also possible to perform a structural evaluation, which allows to verify the structural integrity of the motor by clicking on the

Mechanical Stress Control box. In this case, the penalization for the weakest motor is not provided and, compared to the other objectives, the stress target cannot be set since the structural evaluation is not an objective of the optimization process.

In order to give designers the possibility to set the mechanical penalization limit on their own and to obtain better results, the *Von Mises stress [MPa]* button was added among the *Objectives and Penalization Limits*, as shown in the following figure.

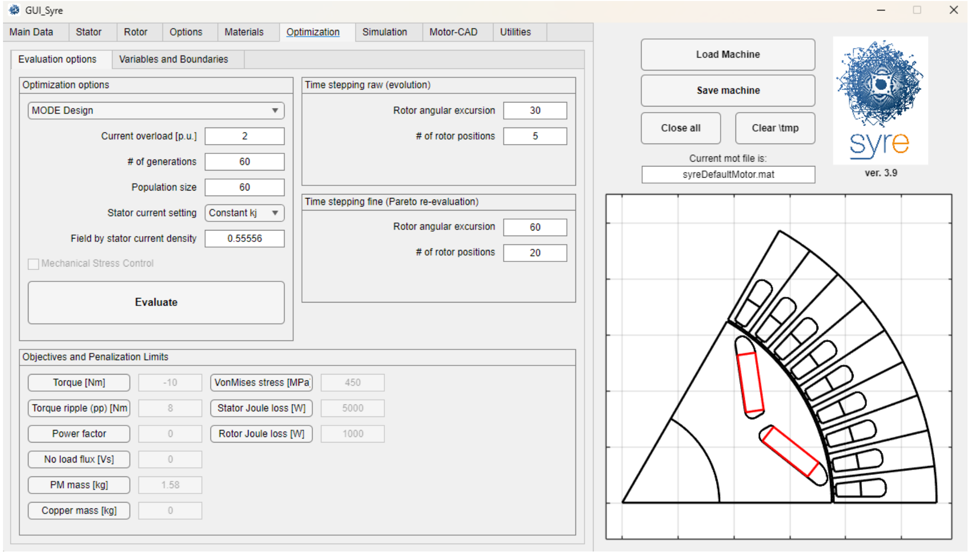

MODE Design
Current overload [p.u.] 2
# of generations 60
Population size 60
Stator current setting Constant kj
Field by stator current density 0.55556
☐ Mechanical Stress Control

Time stepping raw (evolution)
Rotor angular excursion 30
# of rotor positions 5

Time stepping fine (Pareto re-evaluation)
Rotor angular excursion 60
# of rotor positions 20

Torque [Nm] -10
Torque ripple (pp) [Nm 8
Power factor 0
No load flux [Vs] 0
PM mass [kg] 1.58
Copper mass [kg] 0
VonMises stress [MPa 450
Stator Joule loss [W] 5000
Rotor Joule loss [W] 1000

Current mot file is:
syreDefaultMotor.mat

Figure 2.1.1: SyR-e MMM new Optimization tab. [6]

It can also be noticed that the *Mechanical Stress Control* box is disabled and will be removed in the next version, while the remaining options are the same.

The tool used for the implementation was the MATLAB App Designer, which is a development environment provided by MATLAB for creating graphical user interfaces (GUIs). It allows users to develop interactive applications by combining a graphical layout editor with MATLAB code. Using the layout editor, the user can build the interface by placing elements such as buttons, sliders, tables, and plots, while the program logic and data processing are implemented through MATLAB scripts and callback functions. Fig.2.1.2 shows the design view of the *Optimization* tab.

For the implementation of the structural objective, a *State Button* and an *Edit Field (Numeric)* were selected from the *Component Library*. Then a callback function was associated for both elements. In particular, to the *Von Mises stress [MPa]* button was associated the `VonMisesstressMPaButtonValueChanged` function, while for the other element the `MaxExpMechStressValueChanged` function, present inside the *Code View* from line 5706 to 5720, as reported in the following.

```
5706 % Value changed function: VonMisesstressMPaButton
5707 function VonMisesstressMPaButtonValueChanged(app, event)
5708     value = app.VonMisesstressMPaButton.Value;
5709     app.dataSet.VonMisesstressOptCheck = value;
5710     GUI_APP_SetParameters(app);
```

```matlab
end

% Value changed function: MaxExpMechStress
function MaxExpMechStressValueChanged(app, event)
    value = app.MaxExpMechStress.Value;
    value = eval(value);
    if value<0
        value = abs(value);
    end
    app.dataSet.MaxExpMechStress = value;
    GUI_APP_SetParameters(app);
end
```

Thanks to the callback functions it is possible to extract the values from the two elements, which are 0 (disable) or 1 (enable) for the button and the numerical value for the edit field, and pass them to the MATLAB function `GUI_APP_SetParameters`, a dedicated function used to enable or disable the buttons for each graphical interface. The MATLAB code used for the activation of the *Von Mises stress [MPa]* button and the deactivation of the *Mechanical Stress Control* box is also reported below.

```matlab
set(app.VonMisesstressMPaButton,'Value',dataSet.
   VonMisesstressOptCheck);
if dataSet.VonMisesstressOptCheck
    set(app.MaxExpMechStress,'Enable','on');
else
    set(app.MaxExpMechStress,'Enable','off');
end

set(app.MechStressOptCheck,'Value',0,'Enable','off');
```

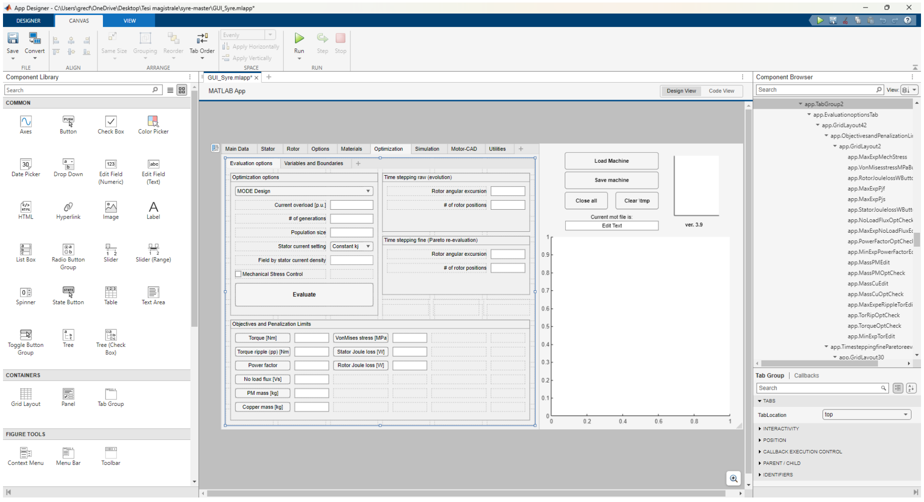

Figure 2.1.2: Design view of the optimization tab

2.2 Code Modifications

Taking into account the previous implementation, some changes inside the other MATLAB functions were made to make the structural simulation work as the other objectives.

Once the *Evaluate* button is pressed, the `eval_OptimizationProblem` function runs. Inside the function, all the data from the GUI are collected, thanks to the `data0` function, and organized into five matrices which are:

- `bounds`, containing the boundaries of each selected variable from the *Variables and Boundaries* sub-tab of the *Optimization* tab
- `objs`, including all the optimization *Objectives and Penalization Limits* and their flag, 0 (disabled) or 1 (enabled)
- `geo`, where are collected all the parameters that define the motor geometry
- `per`, in which are present the main performance target, the custom current, the multi-objective optimization algorithm (MOOA) tresholds and the number of simulated rotor positions
- `mat`, collects the material properties for every part of the motor

Since the *Von Mises stress [MPa]* button was implemented, inside the `objs` matrix was added the structural objective and flag (line 672).

```
664 %% OBJECTIVES
665 objs = [
666     per.min_exp_torque  dataIn.TorqueOptCheck          0
667     per.max_exp_ripple  dataIn.TorRipOptCheck          0
668     per.max_Cu_mass     dataIn.MassCuOptCheck          0
669     per.max_PM_mass     dataIn.MassPMOptCheck          0
670     per.min_pf          dataIn.PowerFactorOptCheck
       0.1
671     per.max_fdq0        dataIn.NoLoadFluxOptCheck      0
672     per.max_mechstress  dataIn.VonMisesstressOptCheck  0
673     per.max_exp_Pjs     dataIn.StatorJouleLossOptCheck 0
674     per.max_exp_Pjf     dataIn.FieldJouleLossOptCheck  0
675     ];
```

After that, other variables regarding the optimization are saved and then the optimization algorithm runs. The function assigned to this task is `MODE`, which stands for Multi-Objective Differential Evolution.

The optimization evaluation starts with the creation of the *Parent population*, in which all the variables selected from the optimization sub-tub are taken randomly from their range.

Then, for every motor, a FE analysis in FEMM is performed thanks to the `FEMMfitness` function, previously defined inside `eval_OptimizationProblem` and renamed `costFunction` in `MODE`.

Within `FEMMfitness`, some modifications were made in order to perform the structural analysis.

As shown previously, the mechanical objective is the seventh element and cannot be obtained with the same FEMM simulation from which all the electromagnetic properties are obtained. For this reason, the following code was added in between the *No-load flux* and *Stator Joule loss* evaluations.

```
% Structural properties
%if temp1<=length(geo.OBJnames) && strcmp(geo.OBJnames{temp1},'MechStress')
if per.objs_check(7)

    [geo,~,mat] = interpretRQ(RQ,geo,mat);
    % Set up info for solving structural model
    simSetup0.evalSpeed = geo.nmax;
    simSetup0.meshSize  = 'PDE fine';
    simSetup0.meshShaft = 0;
    simSetup0.flagFull  = 0;
    simSetup0.shaftBC   = 1;
    geo.custom = 0;
    warning('off')
    filemot = [pathname filename];
    [~, filename, ~] = fileparts(filemot);

    % Geometry/points generation
    [geo,mat] = draw_motor_in_FEMM(geo,mat,pathname,filename);
    simSetup0.pathname  = pathname;
    simSetup0.filename  = [filename '.mat'];

    % Convertion FEMM - PDE
    [out.structModel] = femm2pde(geo,mat,simSetup0);
    %Solving the PDE model
    [out.sVonMises,R,out.structModel] = calcVonMisesStress(out.structModel);
    % Deformation, clearance and stress calculations
    [outMech] = eval_maxStress(out.structModel,out.sVonMises,R,geo,mat);

     if (strcmp(geo.RotType,'Circular')||strcmp(geo.RotType,'Seg'))
         cost(7) = max([outMech.Rad_sigmaTotPrc outMech.Tan_sigmaTotPrc])/1e6;
    % Deformation magnitude
    %      OUT.MaxDef              = outMech.MaxDef;
    %      % Air-gap clearance
    %      OUT.agclear             = outMech.agclear;
```

```
512     %     % Maximum stress values
513     %     OUT.MaxStress         = outMech.MaxStress/1e6;
514     %     OUT.TanRibsStress     = (max(outMech.sigmaTanMax))/1e6;
515     %     OUT.RadRibsStress     = (max(outMech.sigmaRadMax))/1e6;
516     %     % Percentile stress values
517     %     %OUT.MaxStress_prc     = out.Stress.sigmaTotPrc/1e6;
518     %     OUT.TanRibsStress_prc = outMech.Tan_sigmaTotPrc/1e6;
519     %     OUT.RadRibsStress_prc = outMech.Rad_sigmaTotPrc/1e6;
520      else
521          cost(7) = outMech.MaxStress/1e6;
522     %     OUT.MaxDef            = outMech.MaxDef;
523     %     OUT.agclear           = outMech.agclear;
524     %     OUT.MaxStress         = outMech.MaxStress/1e6;
525     %     % OUT.MaxStress_prc     = out.Stress.sigmaTotPrc/1e6;
526      end
527 
528     %temp1=temp1+1;
529 end
```

The results of the analysis are obtained from the function `eval_maxStress` in line 504 of the code reported above, which returns the 99th percentile of the radial and tangential stress inside `outMech` matrix.

Von Mises equivalent stress is, in fact, able to predict the yielding of materials under multiaxial loading conditions using results from simple uniaxial tensile and is computed on each element of the twodimensional mesh, but it reaches its peak values in the rib regions [8], which are evidenced in Fig.2.2.1.

The average stress over the 99th percentile is used instead of the maximum value to avoid overestimating the maximum stress due to isolated peaks, which may arise from mesh discretization or local geometric features. Then, the maximum value between the radial and tangential percentile stress is considered, as shown in line 507. As can be noticed, the result is saved inside a vector called `cost`, within which are reported the results of all the objectives selected from the tab, which are then subjected to verification. If the results do not respect the penalization limit, they will be subject to a penalization.

```
558 % penalize weak solutions
559     for ii = 1:length(cost)
560         if ~isnan(cost(ii))
561             if ii ~= 7 && cost(ii)>per.objs(ii,1) && per.objs(ii,3)==0
562                 if per.objs(ii,1)>0
```

```
                    cost(ii)=cost(ii)*10;  % minimization problem
                else
                    cost(ii)=cost(ii)*0.1; % maximization problem
                end

            elseif ii == 5 && ((cost(ii)<per.objs(ii,1)-per.objs(ii,3)) || (cost(ii)>per.objs(ii,1)+per.objs(ii,3))) %&& per.objs(ii,3)
                if per.objs(ii,1)>0
                    cost(ii)=cost(ii)*10;  % minimization problem
                else
                    cost(ii)=cost(ii)*0.1; % maximization problem
                end

            elseif ii == 7 % Mechanical penalization.
                if cost(ii)>per.objs(ii,1) %&& per.objs(ii,3)==0
                    cost(ii)=cost(ii)*10;
                end
            end
        end
    end
```

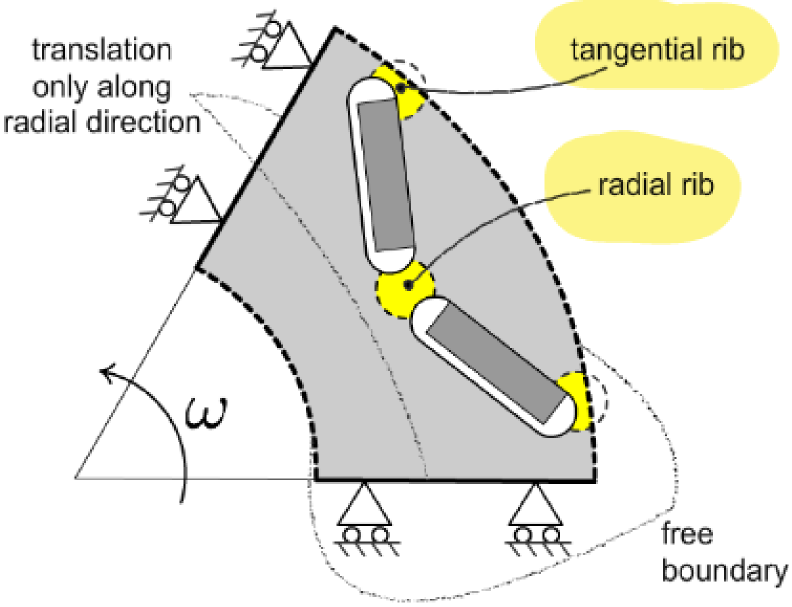

Figure 2.2.1: Tangential and radial rib regions. [8]

Chapter 3

Multi-Objective Optimization and IPM Motor Scaling

Considering the modifications and implementations mentioned in the previous chapter, it is now possible to perform multiphysics optimizations, taking into account both the electromagnetic and structural aspects. The objective, in this case, is to optimize one of the versions of the Tesla Model 3 motor, whose geometry and specifications are reported below.

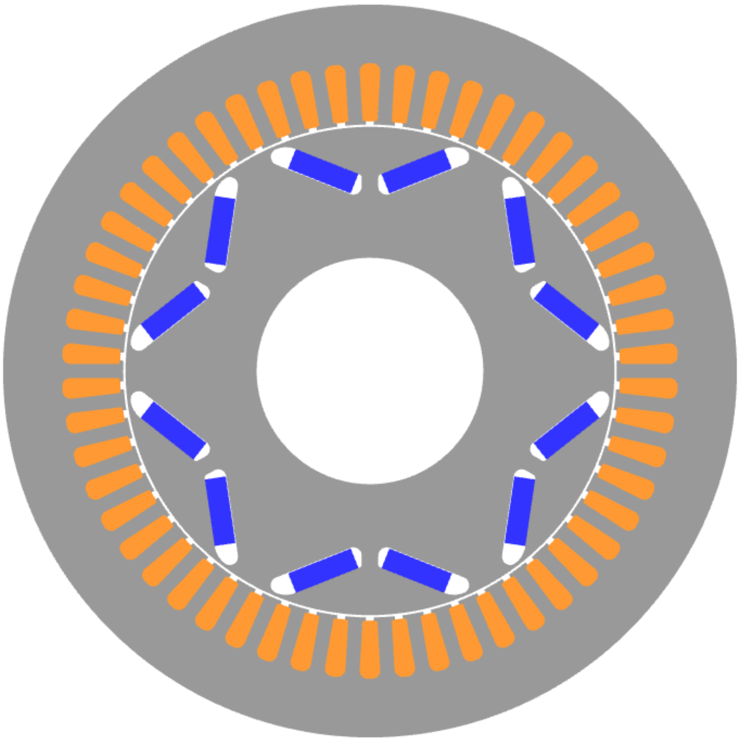

Figure 3.1: Initial motor geometry

Regarding the optimization of the motor, the goal is to increase its maximum speed by a factor of 1.4, while keeping the same inverter used for the original motor. Tab.3.2 shows the specifications that the final motor should meet.

Peak torque [Nm]	430
Peak power [kW]	187
Power at max speed [kW]	137
Base speed [rpm]	4150
Maximum speed [rpm]	18100
Peak current density [Arms/mm^2]	36
Peak phase current [Apk]	800
DC-link voltage [V$_{DC}$]	400
Turns in series per phase	21
Thermal loading [kW/m^2]	171
Stator outer diameter [mm]	225
Rotor outer diameter [mm]	149.9
Air-gap length [mm]	0.7
Stack length [mm]	134

Table 3.1: Initial motor specifications

Increasing the maximum operating speed while keeping the rated power constant leads to a reduction of the required torque. As a consequence, the motor size can be reduced, resulting in a more compact and lightweight design. For this reason, increasing the maximum speed represents a key objective with respect to the reference machine. The inverter operating limits, instead, will remain the same.

Peak torque [Nm]	$\geq$307
Peak power [kW]	$\geq$187
Power at max speed [kW]	$\geq$137
Base speed [rpm]	$\geq$5810
Maximum speed [rpm]	$\geq$25340
Peak current density [Arms/mm^2]	$\leq$36
Peak phase current [Apk]	$\leq$800
DC-link voltage [V$_{DC}$]	$\leq$400
Scaling factor	1.4

Table 3.2: Optimization target

The entire optimization process is summarized in Fig.3.2 and starts from the aforementioned motor considering only the rotor optimization. The best motor among all the ones resulting from the optimization, is then submitted to a second optimization. In this case, since the objective is to have a smaller motor, both stator and rotor are considered for the optimization.

Since the final motor does not respect all the target, a scaling of the initial motor was done, followed by a comparison of the scaled motor variables and the *Variables and Parameters* ranges set for the second optimization. This was done to understand whether all the rages were set correctly.

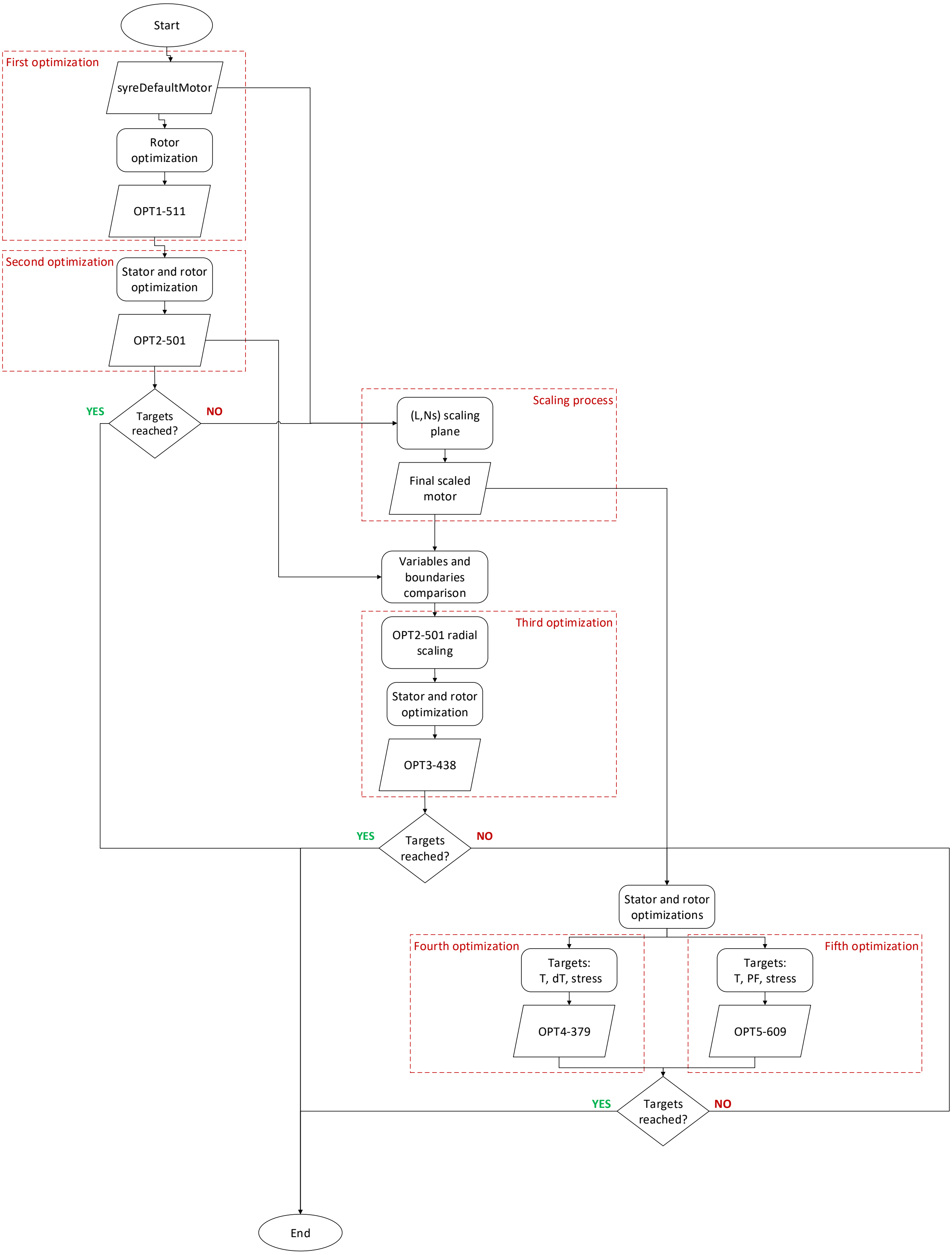

Figure 3.2: Optimization process

After the scaling process, three other optimizations were launched. The first starts from the resulting motor of the first optimization, submitted to a scale of radial dimensions. The last ones start both from the motor resulting from the scaling process, but with different choice of the *Objectives and Penalization Limits*.

This choice was made to highlight the fact that there may be multiple possibilities to achieve the desired result, rather than just one.

In the following, all the optimization results will be presented in detail.

3.1 First Optimization: Rotor-Only Optimization

As already mentioned before, the first optimization starts from the initial motor, called *syreDefaultMotor* inside SyR-e, but with the overspeed set equal to the maximum speed of Tab.3.2. The current density value, already set to 36 $Arms/mm^2$, and the other stator and rotor variables are the same.

The optimization settings, instead, were set as follows and also reported in Fig.3.1.1:

- *Optimization options*:
  - Current overload set to 1 p.u. since the maximum current wanted is 800 A, which corresponds to 36 $Arms/mm^2$
  - Number of generations and initial population set to 60, which is a good trade-off between accuracy and computation time
  - Stator current setting set to *Constant J*, which determines the optimization conditions
- *Objectives and Penalization limits*:
  - Torque, set to the desired value of 307 Nm
  - Torque ripple, set to 15 Nm in order to not penalize only the motors with very low ripple value
  - Von Mises stress, set to 450 MPa, which is the maximum value for the M270-35A alloy, used for the stator and rotor cores

Inside the *Variables and Boundaries* tab, in addition to the rotor variables, also the current angle *Gamma [°]* was selected. In this way, also the current angle for the MTPA will be found during the optimization process. The other variable ranges, instead, were selected by giving the software the ability to consider the largest operating ranges that could generate feasible motors, in such a way that an error would not be generated during the motor drawing in FEMM. The choice of selecting only the rotor variables was made in order to obtain a new motor configuration while preserving the original stator, as a result of the increased maximum speed requirement.

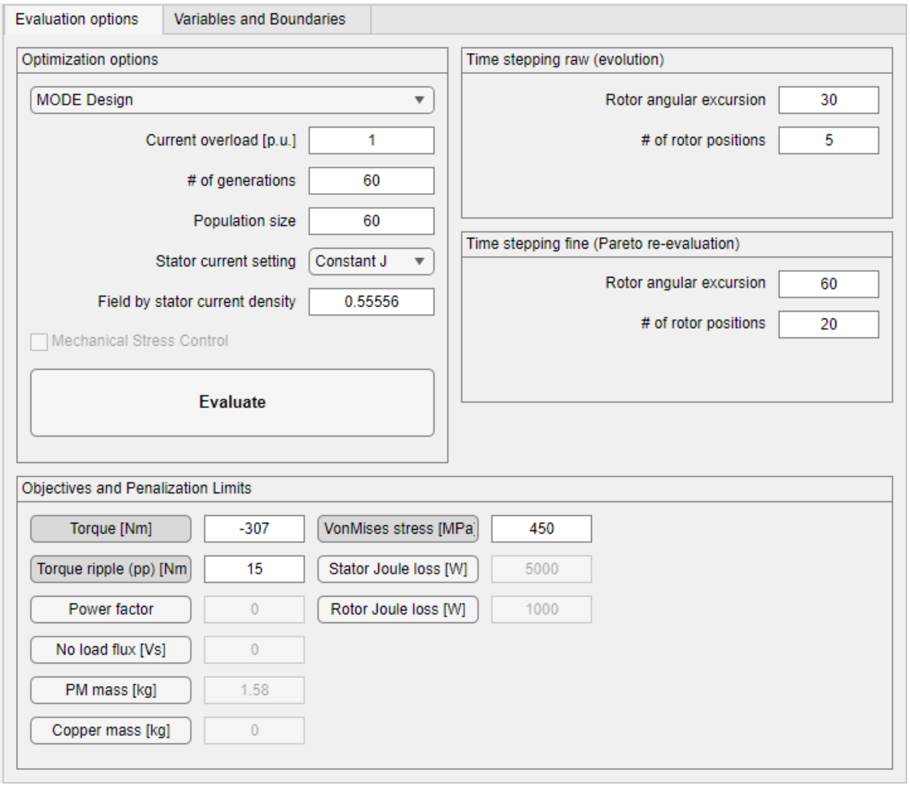

Optimization options

MODE Design

Current overload [p.u.]	1
# of generations	60
Population size	60
Stator current setting	Constant J
Field by stator current density	0.55556

☐ Mechanical Stress Control

Time stepping raw (evolution)

Rotor angular excursion	30
# of rotor positions	5

Time stepping fine (Pareto re-evaluation)

Rotor angular excursion	60
# of rotor positions	20

Objectives and Penalization Limits

Torque [Nm]	-307	VonMises stress [MPa	450
Torque ripple (pp) [Nm	15	Stator Joule loss [W]	5000
Power factor	0	Rotor Joule loss [W]	1000
No load flux [Vs]	0		
PM mass [kg]	1.58		
Copper mass [kg]	0		

(a) Evaluation options tab of the first optimization

Airgap radius [mm]	[52 78]	1st barrier pos. [p.u.]	[0.65 0.8]	Yoke width [mm]	[10 20]
Tooth width [mm]	[3.8 6.3]	Barriers positions [p.u.]	[0.17 0.5]	Pole body height [mm]	[5 20]
Tooth lenght [mm]	[15 22.5]	Barrier width [p.u.]	[0.32 0.5]	Pole angle [p.u.]	[0.5 0.8]
Stator slot open [p.u.]	[0.2 0.3]	Barrier offset [p.u.]	[-0.65 0.65]	Pole width [mm]	[5 20]
Tooth tan. depth [mm]	[0.8 1.2]	Barriers shrink [p.u.]	[0 0]	Coil width [mm]	[2 5]
Airgap thickness [mm]	[0.4 0.8]	Barrier shift [mm]	[-2 6]	Coil height [mm]	[5 10]
Theta FBS [mech °]	[0 15]	PM dimension [p.u.]	[0 1]	Pole head fillet [mm]	[0.5 1]
Gamma [°]	[40 75]	PM remanence [T]	[0.3 0.38]	Pole head angle [°]	[0 5]
		Radial ribs [mm]	[0 12]		
		Tangential ribs [mm]	[0.5 3]		
		Fillet Rad ribs in [mm]	[0.4 2]		
		Fillet Rad ribs out [mm]	[0.4 2]		
		Fillet Tan ribs in [mm]	[0.4 2]		
		Fillet Tan ribs out [mm]	[0.4 2]		
		PM shape factor [p.u.]	[10 89]		

(b) Variables and boundaries tab of the first optimization

Figure 3.1.1: Settings of the first optimization

The optimization was then launched with the *Evaluate* button and after performing the electromagnetic and structural analysis of the initial population, the 60 generations are evaluated. Each of them is generated considering the differential evolution (DE) algorithm, described in [9].

Then for every generation the Pareto Front is generated, based on the *dominance* concept. A solution is *nondominated* when there is no other solution having better values for all the cost functions or objectives. The optimization process adopts the approach proposed in the NSGA-II algorithm for nondominated and crowing distance sorting [10][11]. Therefore, for each generation, the *nondominated* solutions are saved inside a matrix.

Every motor inside the matrix is then re-evaluated, but in this case the number of rotor positions are 20 instead of 5, in order to filter off any overestimated solutions [10], and reported inside the chart with a cross. The *nondominated* solutions of the matrix are considered and represented inside the chart with a red circle.

After that, the bar charts of torque, torque ripple and Von Mises stress are generated with the objective on the y-axis and the motors on the x-axis, sorted by torque in a descending order. The same in done also for all the variables selected.

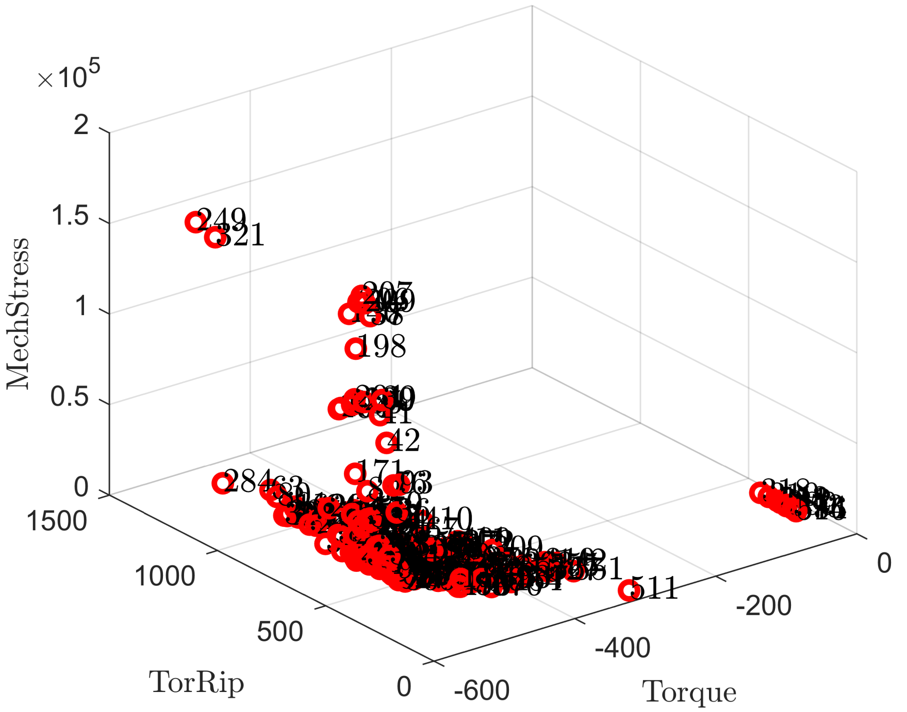

Figure 3.1.2: Final Pareto front of the first optimization

From the Pareto front represented in Fig.3.1.2, it can be noticed that only the motor 511 respects the torque and torque ripple target. All the other motors, instead, are penalized and it is evident by looking at the torque and torque ripple values, which are less than and greater than ten times the target, respectively. The penalization criterion was reported in the previous chapter. In terms of mechanical stress, instead, none of the motors respects the target limit of 450 MPa, also motor 511. In order to better understand the values of the selected motor, compared to the others, two 2D charts are reported below, which are post-processing results. Therefore, none of them can be obtained from the SyR-e optimization.

For each chart only the motors which stand in the range of ±20% of the target torque were considered. The reason for considering only the motors within that range is that the desired motor must have a torque value very close to the target, so that the speed and power can also be close to the desired values. In particular, the motors with the torque value higher than the target are reported in green, while the others in red. The target values are also reported with a green dotted line.

As can be noticed from Fig.3.1.3, only motor 511 evidenced with a red circle, then called OPT1-511, respects both target since the torque and torque ripple values are higher than and lower than the target, respectively. In the last two figures, instead, it can be seen that none of the motors respects the structural target.

Fig.3.1.5 shows the design of the selected motor, while Tab.3.1.1 reports the values that the selected objectives and variables assume. From the figure it can be noticed that the outer radial and tangential fillets are very sharp, therefore a critical value of the Von Mises stress is expected in those areas.

Fig.3.1.6, instead, shows the toque and power characteristics function of the speed. Since the stator and rotor dimensions are the same of *syreDefaultMotor*, the base speed is close to the one of Tab.3.1. A structural analysis of the motor was also performed considering the rotor speed at the maximum value of 25340 rpm. The results, reported in Fig.3.1.7, confirm that in the inner and outer radial fillets areas, the Von Mises stress exceeds the limit. For this reason, all the fillets were modified. The tangentials were automatically imposed by the software, while the radial ones were set both to a value of 1.8.

Peak torque [Nm]	318
Torque ripple [Nm]	14.8
Von Mises stress [MPa]	512
Barrier angles [p.u.]	0.71
Barrier width [p.u.]	0.32
Barrier offset [Arms/mm^2]	0.03
Barrier shift [mm]	-2
Radial ribs [mm]	11.35
Tangential ribs [mm]	2.35
Fillet Rad. ribs in [mm]	1.1
Fillet Rad. ribs out [mm]	1.6
Fillet Tan. ribs in [mm]	0.4
Fillet Tan. ribs out [mm]	0.71
Gamma [°]	56

Table 3.1.1: OPT1-511 motor objective and variable values

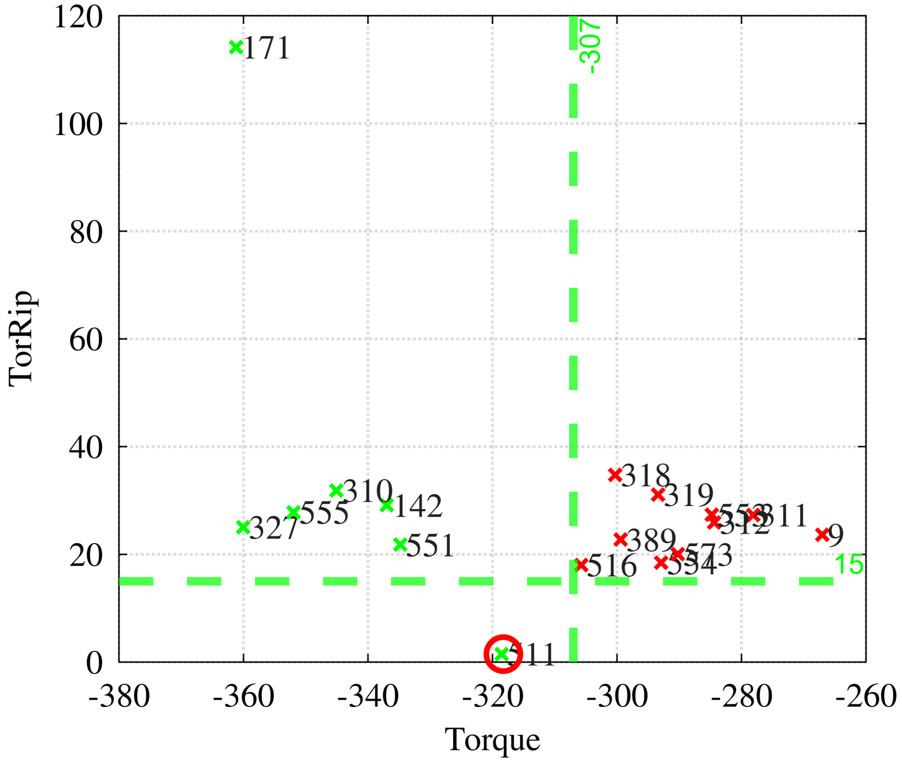

Figure 3.1.3: Torque-Torque ripple chart

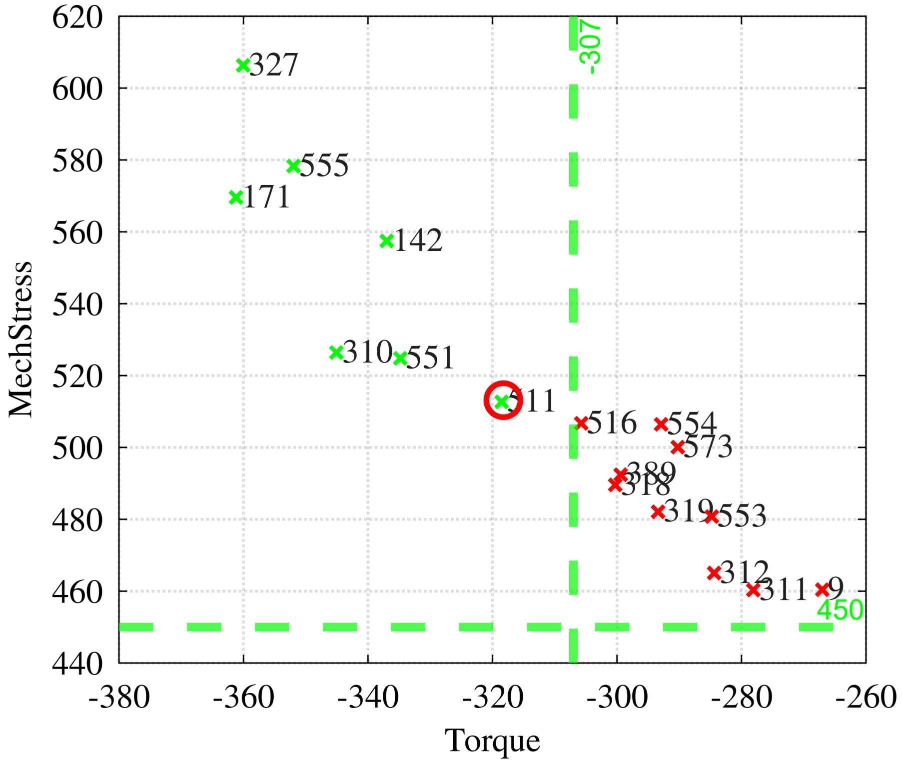

Figure 3.1.4: Torque-stress ripple chart

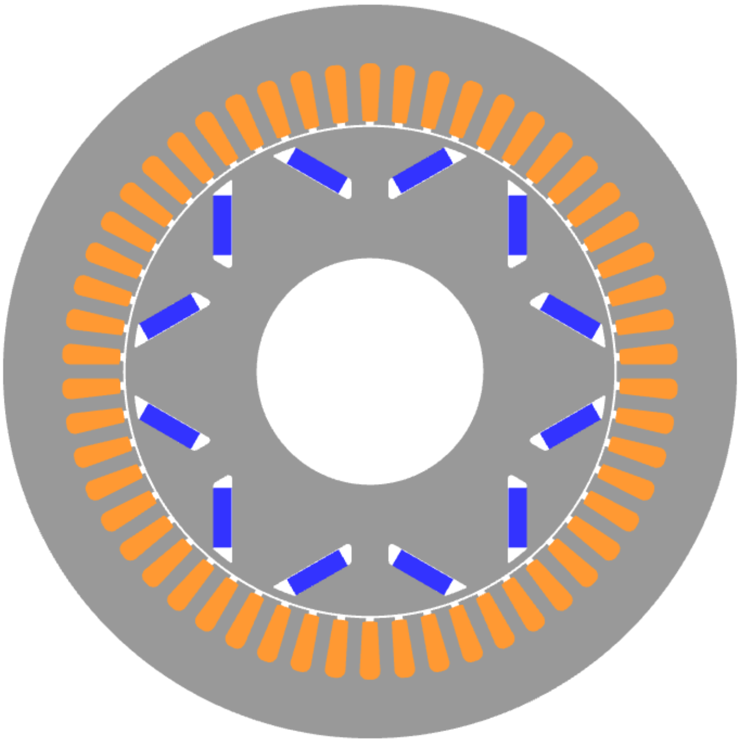

Figure 3.1.5: OPT1-511 motor design

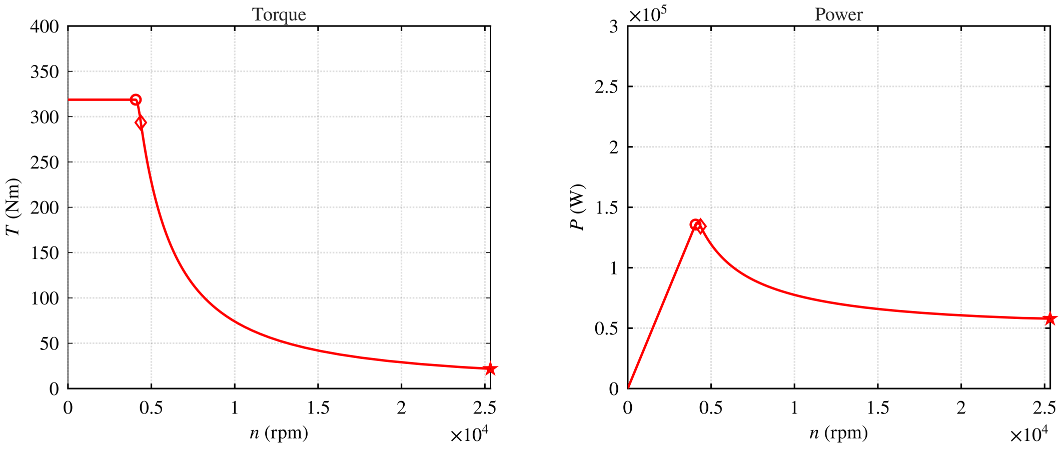

(a)

(b)

Figure 3.1.6: OPT1-511 motor torque-speed (a) and power-speed (b) characteristics.

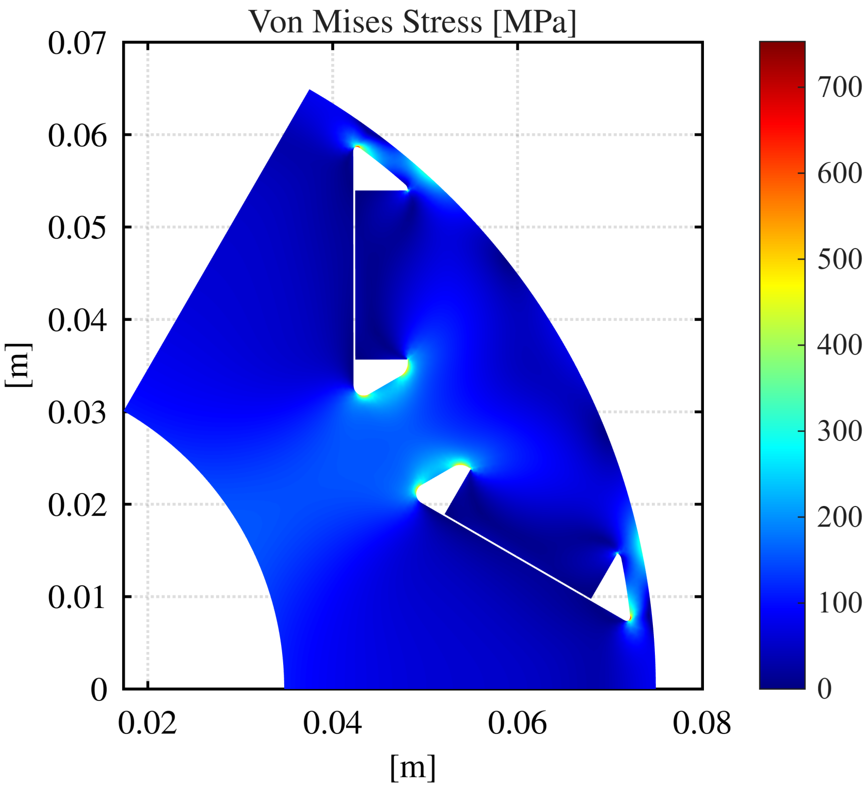

(a) Von Mises stress

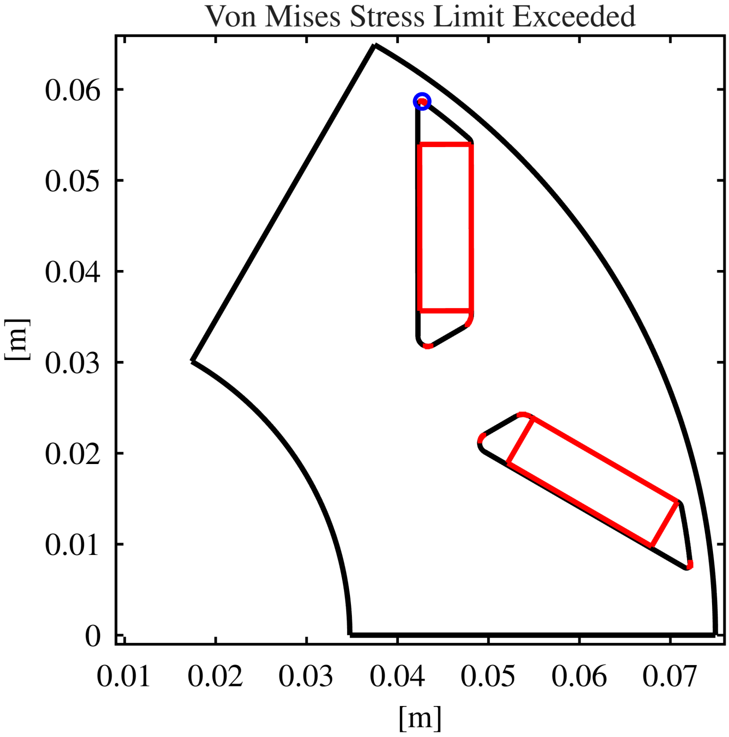

(b) Exceeded stress areas

Figure 3.1.7: OPT1-511 motor structural analysis

3.2 Second Optimization: Stator and Rotor Optimization

The second optimization is based on the 511 motor, whose fillets have been modified.

For this optimization the settings of the *Evaluation options* sub-tab are the same of the first optimization. In this case the *Variables and Boundaries* are different since both stator and rotor are considered. As can be noticed in the figure below, the airgap radius, tooth width and tooth length are now selected, while all the rotor fillets are not considered.

Airgap radius [mm]	[62 75]	1st barrier pos. [p.u.]	[0.65 0.8]	Yoke width [mm]	[10 20]
Tooth width [mm]	[2 5]	Barriers positions [p.u.]	[0.17 0.5]	Pole body height [mm]	[5 20]
Tooth lenght [mm]	[8 25]	Barrier width [p.u.]	[0.32 0.5]	Pole angle [p.u.]	[0.5 0.8]
Stator slot open [p.u.]	[0.2 0.3]	Barrier offset [p.u.]	[-0.65 0.65]	Pole width [mm]	[5 20]
Tooth tan. depth [mm]	[0.8 1.2]	Barriers shrink [p.u.]	[0 0]	Coil width [mm]	[2 5]
Airgap thickness [mm]	[0.4 0.8]	Barrier shift [mm]	[-2 6]	Coil height [mm]	[5 10]
Theta FBS [mech °]	[0 15]	PM dimension [p.u.]	[0 1]	Pole head fillet [mm]	[0.5 1]
Gamma [°]	[40 75]	PM remanence [T]	[0.3 0.38]	Pole head angle [°]	[0 5]
		Radial ribs [mm]	[0 12]		
		Tangential ribs [mm]	[0.5 3]		
		Fillet Rad ribs in [mm]	[0.4 2]		
		Fillet Rad ribs out [mm]	[0.4 2]		
		Fillet Tan ribs in [mm]	[0.4 2]		
		Fillet Tan ribs out [mm]	[0.4 2]		
		PM shape factor [p.u.]	[10 89]		

Figure 3.2.1: Variables and boundaries of the second optimization

The final Pareto front is reported in Fig.3.2.2. From this last figure it can be noticed that a lot of motors respect two out of three target imposed in the *Objectives and Penalization Limits*, as can be seen for the motors located on the left which satisfy the torque and stress target, or for the ones located on the right side close to the Torque-axis, which respect the torque ripple and stress limits. None of the motors, instead, satisfies all the three targets.

In this case, more than in the first optimization, can be useful to explore the 2D charts in the neighborhood of the torque target to understand which is the best motor that can be selected, since there is a great density of motors in that area.

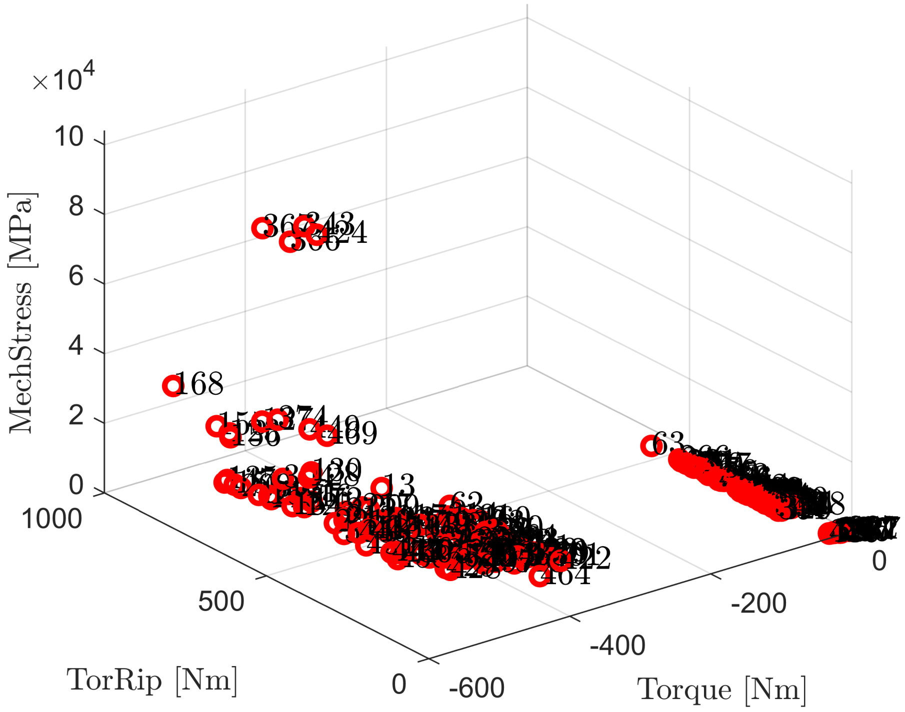

Figure 3.2.2: Final Pareto front of the second optimization

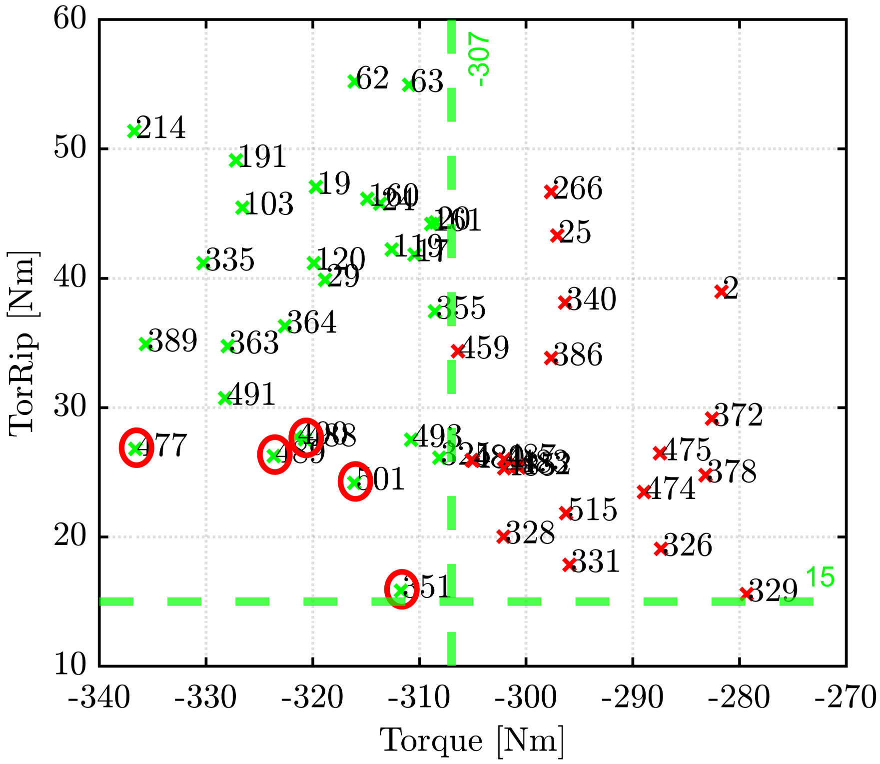

Figure 3.2.3: Torque-torque ripple chart

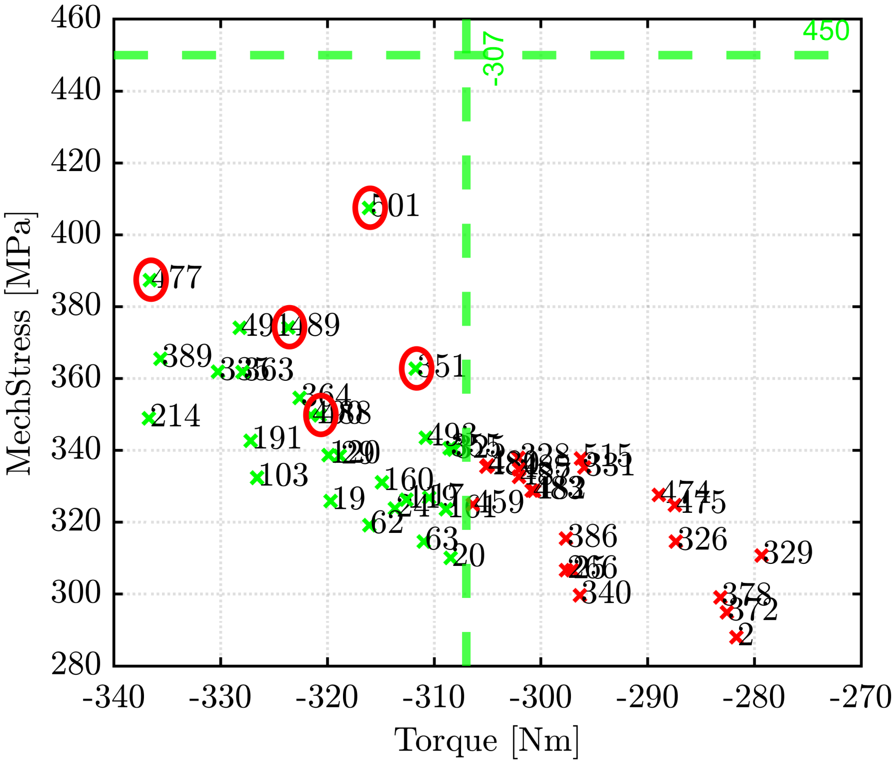

Figure 3.2.4: Torque-stress chart

As can be noticed, the figures have five red circles which show the motors selected, that are:

	T [Nm]	dT [Nm]	stress [MPa]
OPT2-351	311.74	15.84	362.71
OPT2-477	336.61	26.79	387.41
OPT2-488	320.71	27.55	349.77
OPT2-489	323.65	26.26	374.19
OPT2-501	316.09	24.18	407.42

Table 3.2.1: Selected motor of the second optimization

The selection was made considering the motors with $T > 307\ Nm$ and torque ripple as close to 15 Nm as possible. The choice of OPT2-488, which has a bit lower torque and higher torque ripple values than OPT2-489, is related to its stress value.

The bar charts of the objectives and variables are also reported, in which the green dot lines represent the target values and the upper and lower limits of the variables, respectively.

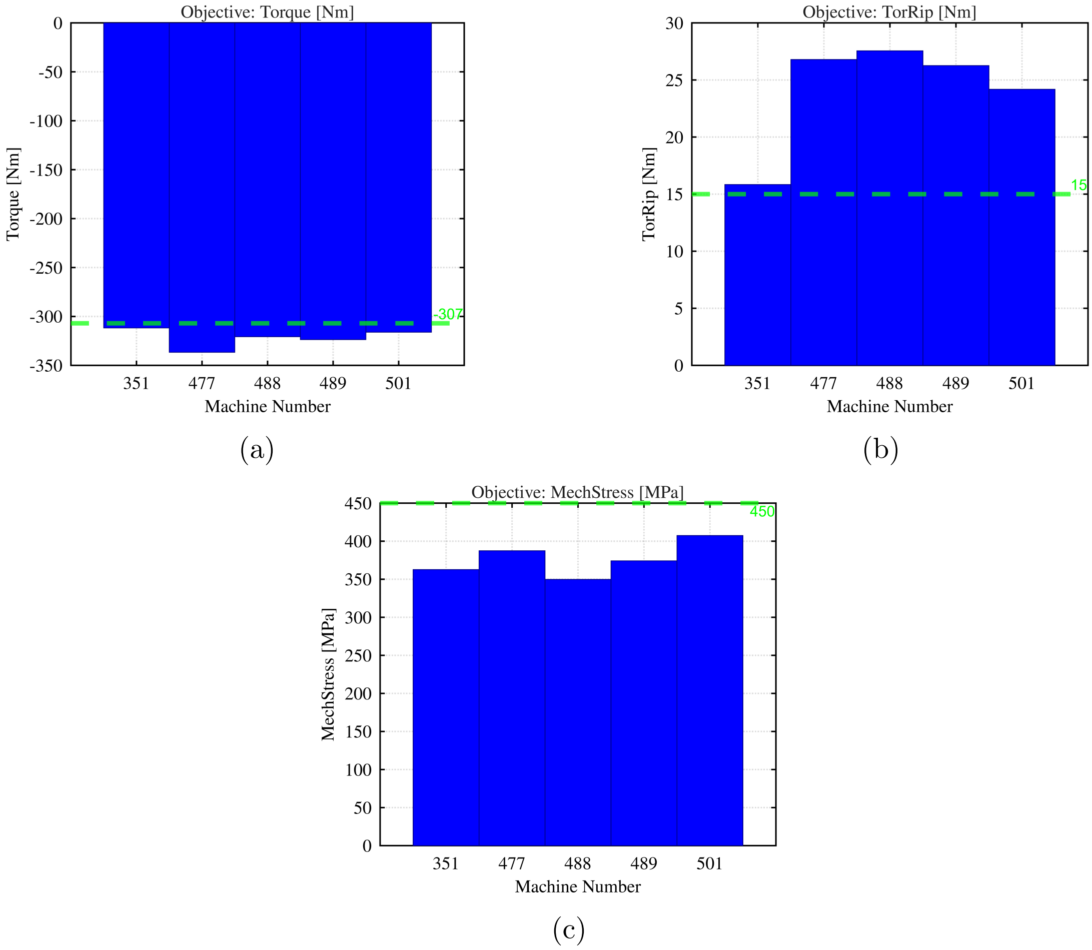

(a)

(b)

(c)

Figure 3.2.5: Bar charts of the target of the second optimization

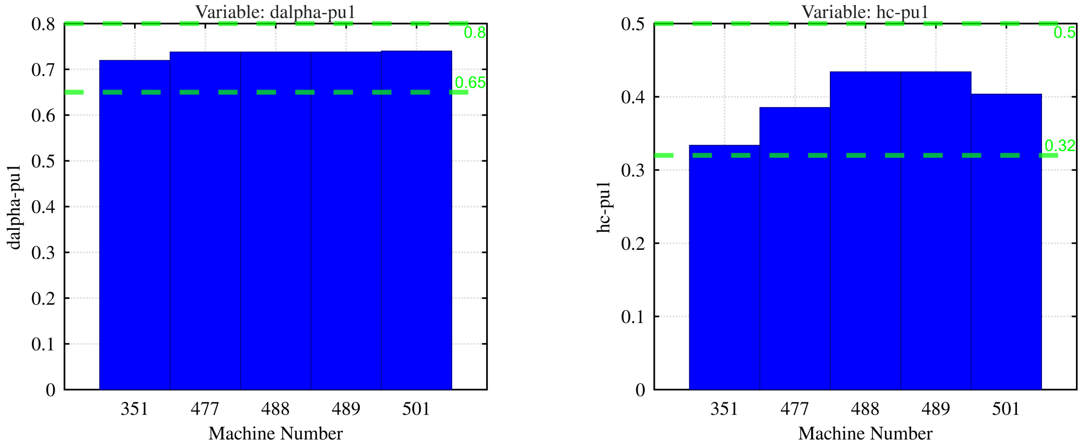

(a) Barrier angles (b) Barrier width

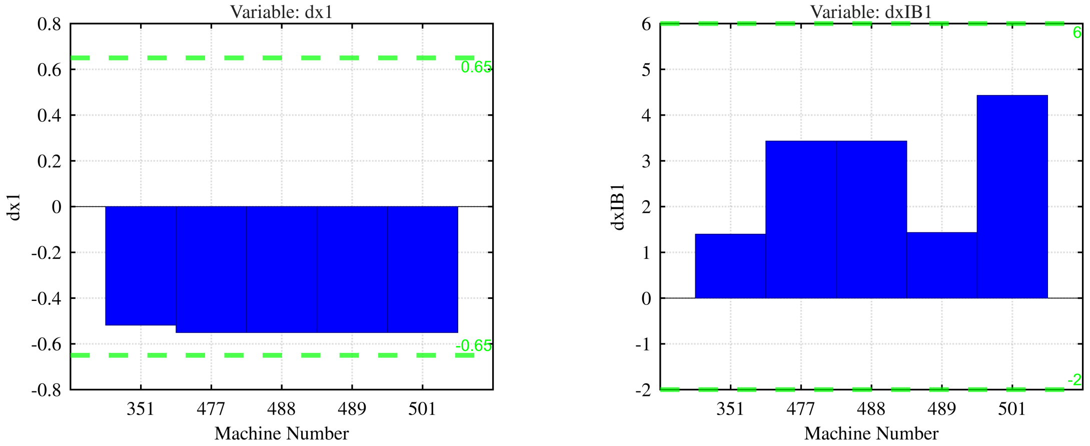

(c) Barrier offset (d) Barrier shift

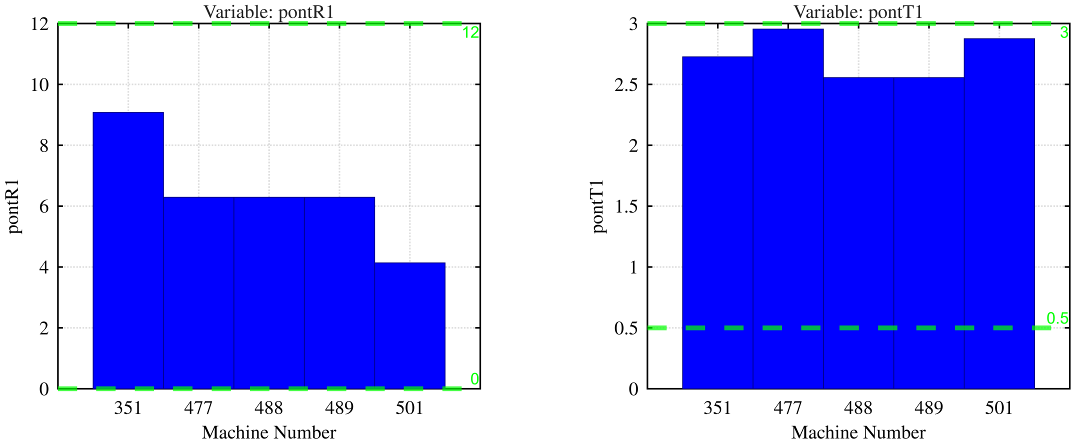

(e) Radial ribs (f) Tangential ribs

Figure 3.2.6: Bar charts of the variables of the second optimization

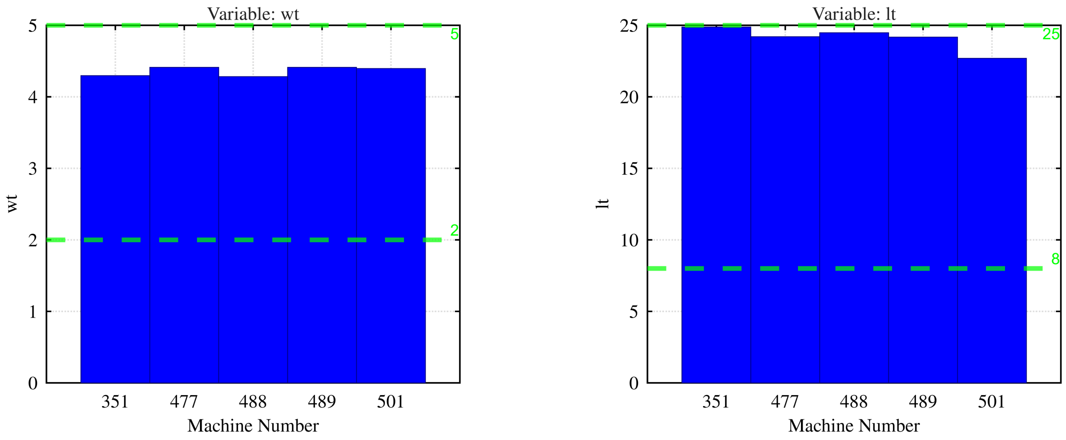

(a) Tooth width (b) Tooth length

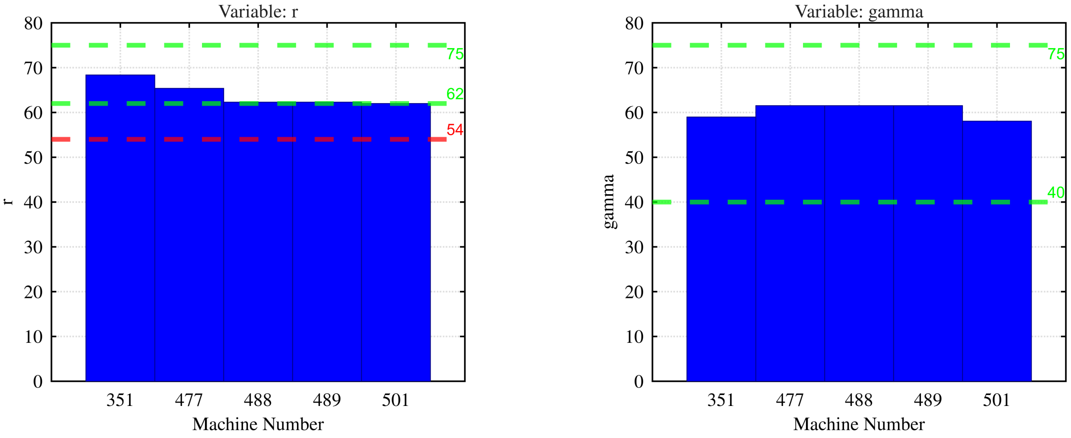

(c) Airgap radius (d) Gamma

Figure 3.2.7: Bar charts of the variables of the second optimization

From these charts it is possible to observe that for the barrier angles and offset, tooth width and length and for gamma, the values are very similar, while for the other variables there is a higher variance. The red dot line present inside the airgap radius bar chart, which represent the outer rotor radius, will be explained during the scaling procedure.

For every motor, then, the torque and power charts function of the speed and the stress analysis were reported in the following, considering the parameters of the table below to be the same for all the selected motors.

Maximum speed [rpm]	25340
Peak current density [Arms/mm^2]	36
DC-link voltage [V$_{DC}$]	400
Turns in series per phase	21
Stator outer diameter [mm]	225
Air-gap length [mm]	0.7
Stack length [mm]	134

Table 3.2.2: Constant parameters among the selected motors

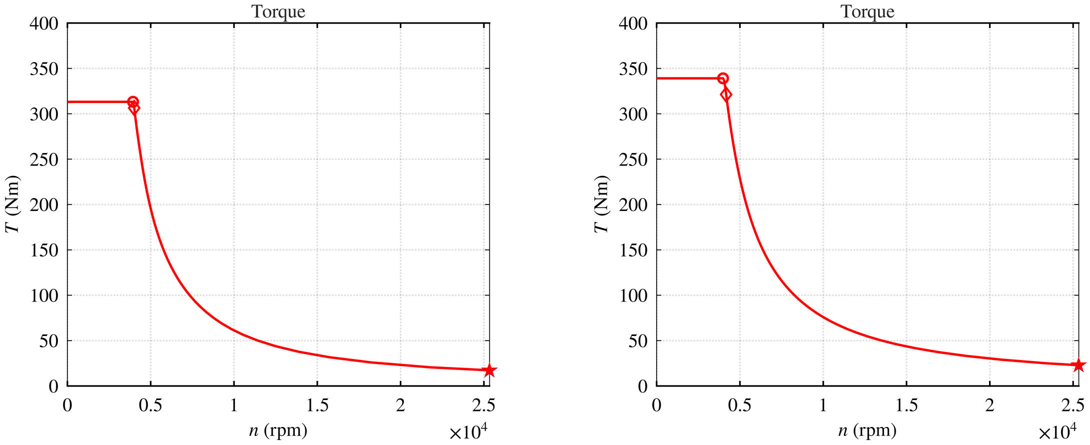

(a) OPT2-351 - $I_{max} = 1011.4A$ (b) OPT2-477 - $I_{max} = 887.1A$

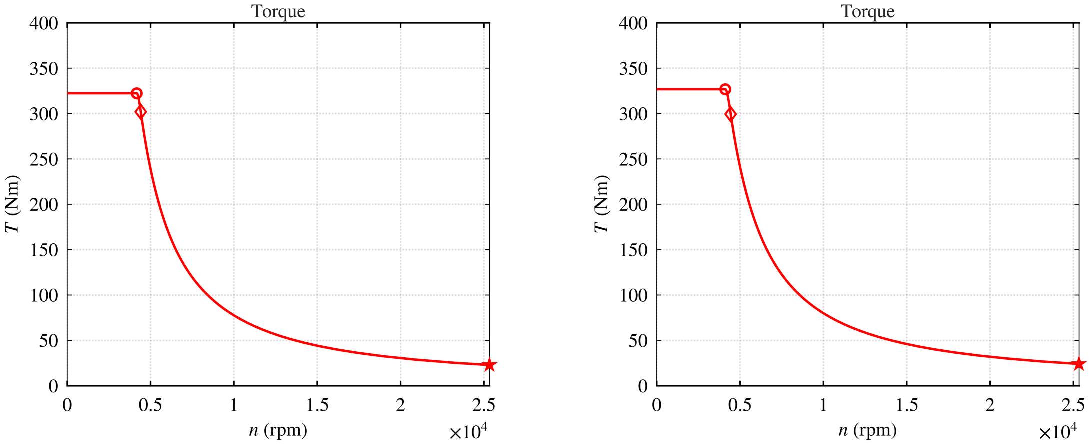

(c) OPT2-488 - $I_{max} = 857.0A$ (d) OPT2-489 - $I_{max} = 817.6A$

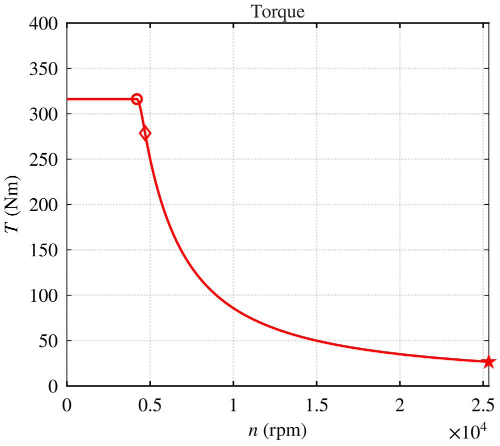

(e) OPT2-501 - $I_{max} = 743.1A$

Figure 3.2.8: Torque-speed characteristic of the second optimization

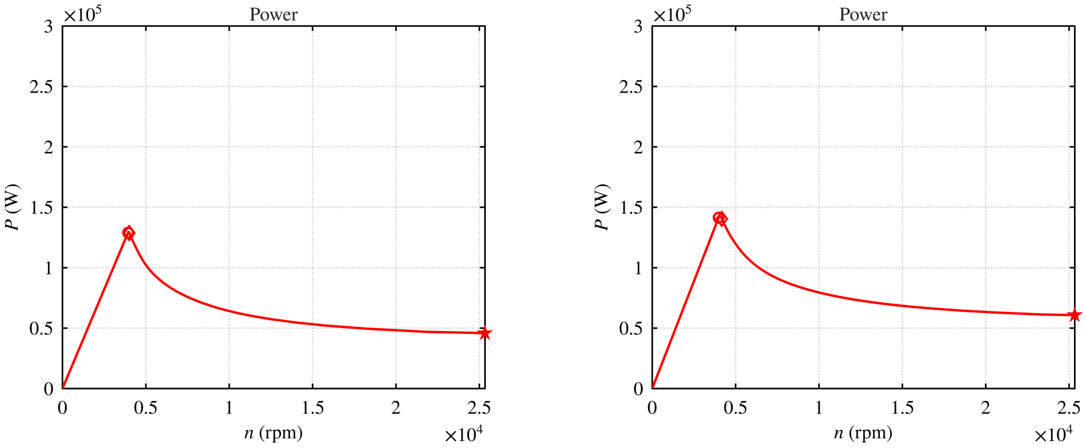

(a) OPT2-351 - $I_{max} = 1011.4A$ (b) OPT2-477 - $I_{max} = 887.1A$

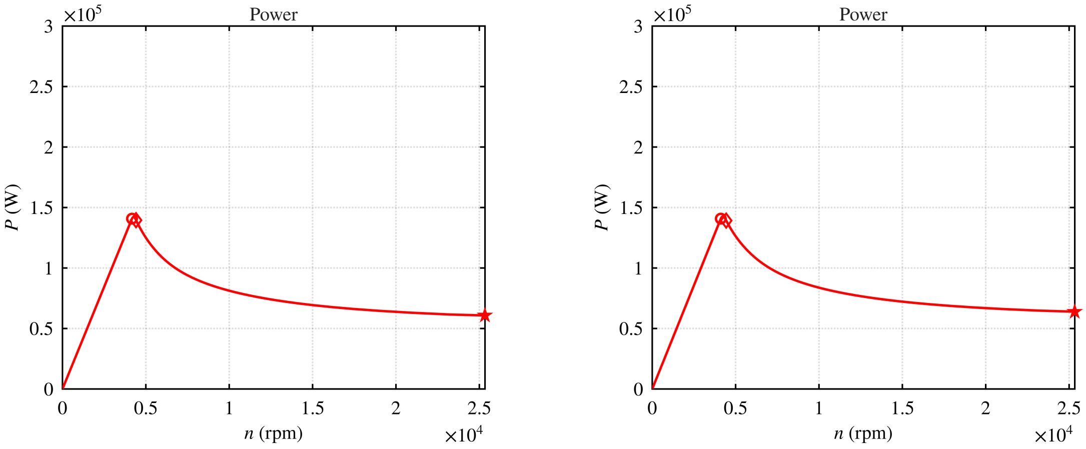

(c) OPT2-488 - $I_{max} = 857.0A$ (d) OPT2-489 - $I_{max} = 817.6A$

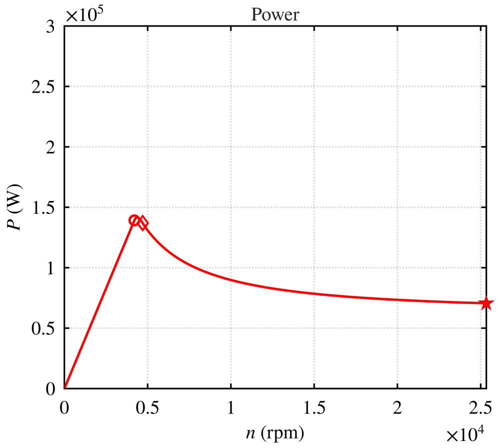

(e) OPT2-501 - $I_{max} = 743.1A$

Figure 3.2.9: Power-speed characteristic of the second optimization

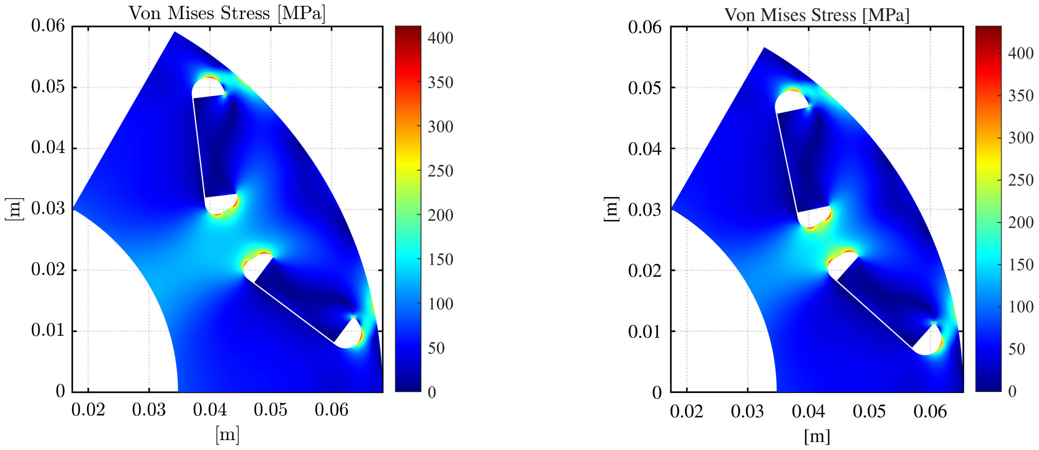

(a) OPT2-351

(b) OPT2-477

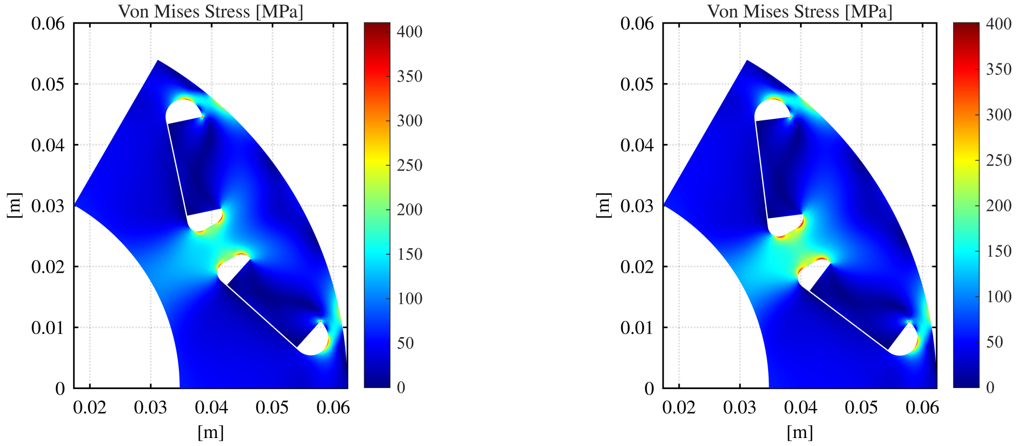

(c) OPT2-488

(d) OPT2-489

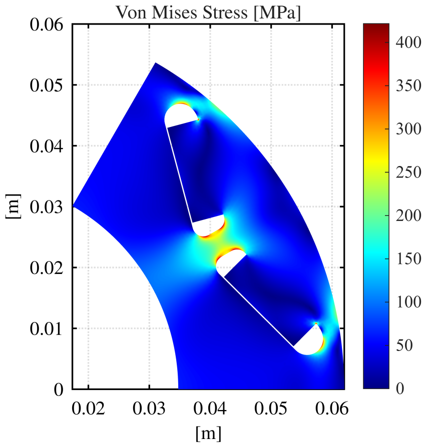

(e) OPT2-501

Figure 3.2.10: Von Mises stress charts of the second optimization

The torque and power characteristics function of the speed are realized with SyR-e MMM from the *Torque-Speed* tab. In particular, inside the *Operating Limits* box [1] was inserted as current levels, which is represented with the red line. Those are the $p.u.$ of the current density, meaning that the current level stands for a current density of $J = 36Arms/mm^2$.

Considering the charts of Fig.3.2.8, it can be seen that for every motor, the target torque $T = 307Nm$ is reached, but the base speeds are too small compared to the target of 5810 rpm. The maximum current values, representing the current density, are also reported in the description of the figures and it can be seen that only the current value of motor OPT2-501 respects the target limit of 800 A. For these reasons, this motor can be considered the best among those selected.

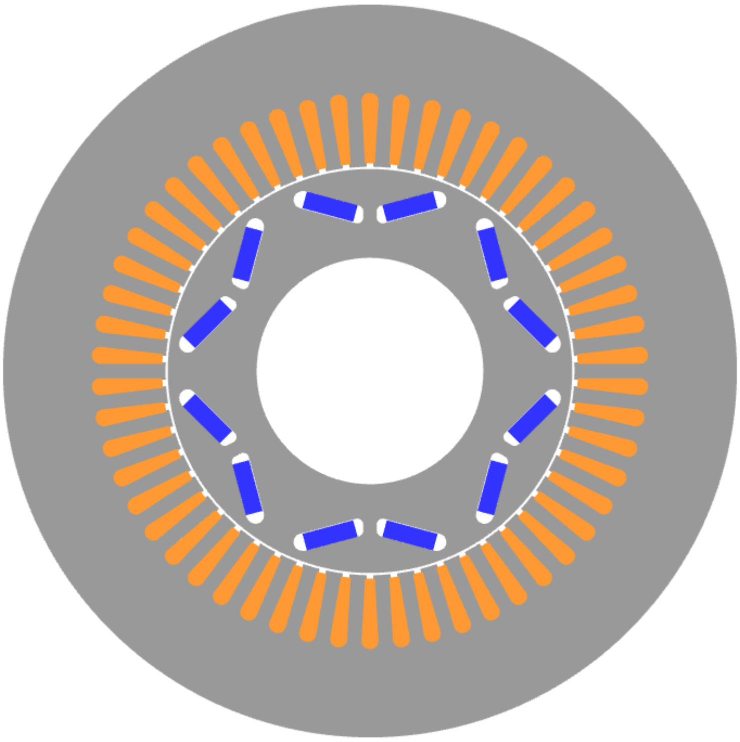

Figure 3.2.11: OPT2-501 motor design

Fig.3.2.9, instead, shows the power-speed charts of the selected motors. The red and blue lines consideration that was made before is valid also in this case. None of the motors reaches the target power of 187 kW since the base speeds are too low. Therefore, none of the motors can satisfy all the target requirements reported in Tab.3.2, even if the structural simulations show that all the motors are structurally reliable. In addition, it can be noticed that the peak powers at maximum speed have a very low value compared to that of the aforementioned table, meaning that some problems regarding the field-weakening occur. Possible causes can be attributed to excessively thick ribs and a rotor that is too big.

For this reason, a scaling of the *syreDefaultMotor* will be executed in order to understand whether these variables were correctly set from the *Variables and Boundaries* tab.

3.3 Scaling Study of the Reference Machine

The scaling procedure was performed in SyR-e MMM, using the *Scaling & Skewing* tab, in particular the *Motor Scaling* box. Before interacting with the scaling tools, some changes have been made to the *Motor Ratings* box on the right side of the SyR-e MMM screen. The maximum speed was set at 25340 *rpm*, the rated and maximum currents were set at 800 *A*, while the DC link voltage was set at 400 *V*.

The *Motor Scaling* box was then used, from which the stator radius of *syreDefaultMotor* was divided by the scaling factor, obtaining 80.3571 *mm*. The *Scale Model* button was then pressed, to allow the software to automatically scale all the radial dimensions of the motor, including the airgap thickness which was reduced from 0.7 *mm* to 0.5 *mm*. At the end of this process, which generally takes less than two minutes, the *(L,N_S) Scaling Plane* button was pressed, from which a box containing the minimum and maximum axial length and number of turns, DC link voltage and peak phase current opens. All variables were kept as the software suggests and then the *Ok* button was clicked, showing two scaling planes. In one, the torque, base speed and thermal loading k_j are represented, while in the other the torque, power factor and current density J are represented.

In order to be able to consider all the target parameters in one single graph, the thermal loading curves were replaced with the current density ones, thanks to a manipulation of the scaling plane performed with the *Command Window* of MATLAB. Fig.3.3.1 shows the new scaling plane, in which the torque, base speed and current density targets are reported. From this graph, the torque and base speed targets were highlighted and it can be seen that the first increases from the bottom left to the top right, while the second increases from the top right to the bottom left. Therefore, only the area above the torque curve and below the speed curve can satisfy both targets. Moreover, knowing that the number of turns N_s must be a multiple of three, for the constructive aspects of the winding, the point (187.4, 15) represents the most compact solution within the aforementioned area and was called *scale_1*. It can be seen that compared to the *syreDefaultMotor* stack length, *scale_1* is longer.

Thereafter, in order to extract the *scale_1* motor, the following modifications were made inside the *Model Scaling* box:

- Stator outer radius, from 112.5 *mm* to 80.3571 *mm*
- Number of turns, from 21 to 15
- Stack length, from 134 *mm* to 187.4 *mm*.

Once the *Scale Model* button was pressed again and the motor scaling was completed, the model was saved using the *Save As* button. After waiting for the model to be saved and loaded, the *Evaluate* button inside the *Control Trajectories* box was clicked in order to update the *Motor Ratings* data, reported in Tab.3.3.1.

From here, it can be noticed that almost all of the electromagnetic targets were satisfied, except for the base speed and the current density. The last is very high considering the target of 36 $Arms/mm^2$. In this case, the fact that the base speed is not reached does not represent a critical point since the peak power is higher than

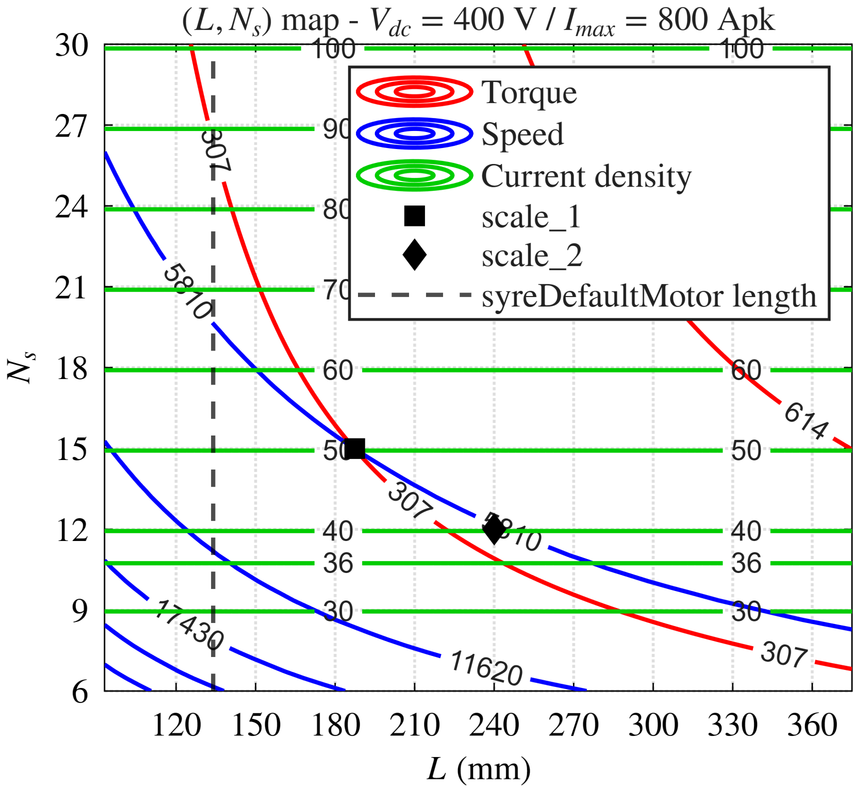

Figure 3.3.1: Scaled motor T, n, J scaling plane

the target. Another point that must be highlighted is the air-gap length, which was automatically reduced during the scaling, as said previously. Therefore, all the electromagnetic data present in the scaling planes and in Tab.3.3.1 are slightly higher than those that would be obtained considering the desired air gap of 0.7 *mm*.

As said previously, since the current density of the *scale_1* motor is too high compared to the target one, a longer motor has to be chosen from the aforementioned area. Taking into account the winding constraint and the air gap thickness considerations made before, the point (240, 12) was chosen as the new scaled motor.

From this point, it can be seen that the base speed is very close to the desired value, while the torque has a bit of margin to the target. In this way, once the air gap thickness is set at the desired value, the same current density will produce a lower torque, which means that the target torque curve will slightly shift to the right, approaching the selected point.

As for the previous scaled motor, the stack length and number of turns inside the *Model Scaling* box were updated and the motor was saved. Then the *Evaluate* button inside the *Main* tab was clicked, updating the data of the *Motor Rating* box, reported in the following table.

	1^{st} scale	2^{nd} scale
Peak torque [Nm]	307	332
Peak power [kW]	192.9	213.4
Base speed [rpm]	5796	6131
Maximum speed [rpm]	25340	
Peak current density [Arms/mm^2]	50	40.25
Peak phase current [Apk]	800	
DC-link voltage [V$_{DC}$]	400	
Turns in series per phase	15	12
Thermal loading [kW/m^2]	179.5	108.0
Stator outer diameter [mm]	160.7	
Rotor outer diameter [mm]	107.1	
Air-gap length [mm]	0.5	
Stack length [mm]	187.4	240

Table 3.3.1: Scaled motors specifications

Taking into account the *scale_2* motor, some structural modifications were made. In particular, from its *Main Data* tab, the final scaled motor was obtained by rounding the following radial dimensions:

- the stator outer radius was set to 80 *mm*, instead of 80.3571 *mm*
- the airgap radius was rounded from 53.5357 *mm* to 54 *mm*
- the shaft radius rounded to 25 *mm* from a previous value of 24.82 *mm*
- the airgap thickness imposed to the desired value of 0.7 *mm*

From this motor, named *scale_2_adj*, the torque and power characteristics were evaluated with SyR-e MMM by setting [0.894 0.964 1] as current levels. In Fig.3.3.2 the blue curves are relative to the lowest current level, representing the target current density. The red curves are relative to the second current level, found by trial and error, with the purpose of understanding the current density needed to reach the desired torque. The green curves, relative to the highest current level, are relative to the current density of *scale_2* motor, obtained from the scaling plane.

Tab.3.3.2, summarizes all the *scale_2_adj* motor specifications. As expected, the peak torque of the blue curve, representing the target current density, is lower than the theoretical value predicted in Fig.3.3.1 since the air-gap thickness was increased to 0.7 *mm*. The current density of the red curve generates peak torque and power higher than the targets and also the base speed reaches a maximum value higher than the target. From what can be seen, therefore, despite a slight increase in current density, all the initial targets are respected.

From the table, moreover, it can be noticed that the rotor outer radius, representing the airgap radius of the *Variables and Boundaries* sub-tub of SyR-e, is 54 *mm*. Looking now at Fig.3.2.7 of the Section 3.2, it can be noticed that this value in not included inside the two limits represented with the green dot lines. This is the reason why the motors resulting from the second optimization do not reach the target base speed. The rotors of these motors were too big, therefore, the range of this variable must be changed so that this value is included. Another aspect that must be considered observing Fig.3.3.2, compared to all the motors of Fig.3.2.9, is the peak power at maximum speed and the field-weakening, definitely better for the final scaled motor. This is a further confirmation of the fact that the airgap radius range was not set correctly.

Moreover, considering the length and outer diameter, it can be observed that compared to the *syreDefaultMotor*, the *scale_2_adj* motor presents a length 50% bigger than the diameter. Compared to the default motor, in which the length was 60% smaller than the radial dimension, a more longilineal and less compact motor was obtained. Therefore, since the result from the second scaling procedure respects most of the targets, it can be a good starting motor for further optimizations.

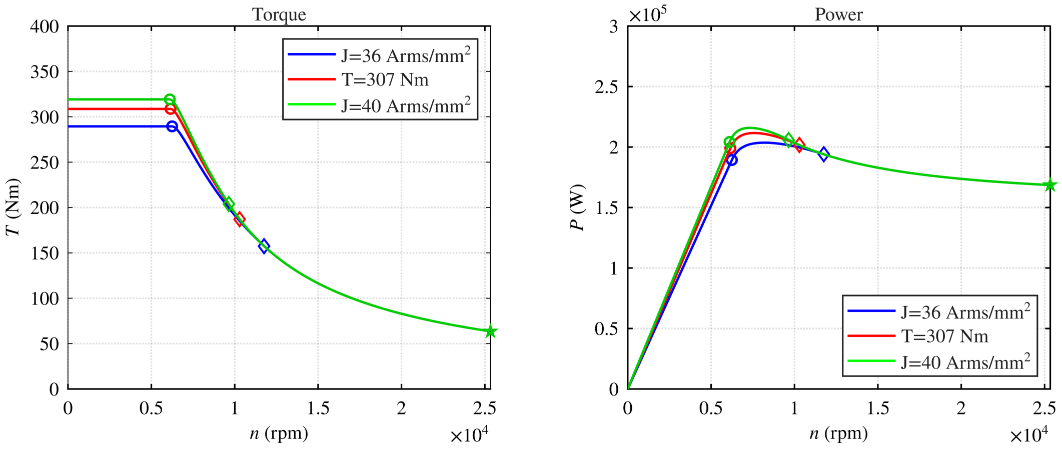

(a) (b)

Figure 3.3.2: scale_2_adj motor torque-speed (a) and power-speed (b) characteristics.

	J=40 Arms/mm^2	T=307 Nm	J=36 Arms/mm^2
Peak torque [Nm]	319	308	289.5
Peak power [kW]	215.5	211	203.5
Power at max speed [kW]	168.5	168.5	168.5
Base speed [rpm]	6109	6155	6242
Maximum speed [rpm]	25340		
Peak current density [Arms/mm^2]	40.25	38.8	36
Peak phase current [Apk]	820.1	785.6	728.9
DC-link voltage [V$_{DC}$]	400		
Turns in series per phase	12		
Thermal loading [kW/m^2]	112	102.8	88.5
Stator outer diameter [mm]	160		
Rotor outer diameter [mm]	108		
Air-gap length [mm]	0.7		
Stack length [mm]	240		

Table 3.3.2: scale_2_adj motor specifications

3.4 Final Optimizations: Stator and Rotor Optimization on Scaled Designs

The last optimization processes start all from a scaled motor design and involve all the same stator and rotor variables. The only differences among the following optimizations are the starting motor and the choice of the *Objectives and Penalization Limits*. The figure below shows the *Variables and Boundaries* sub-tab common to all of the following procedures.

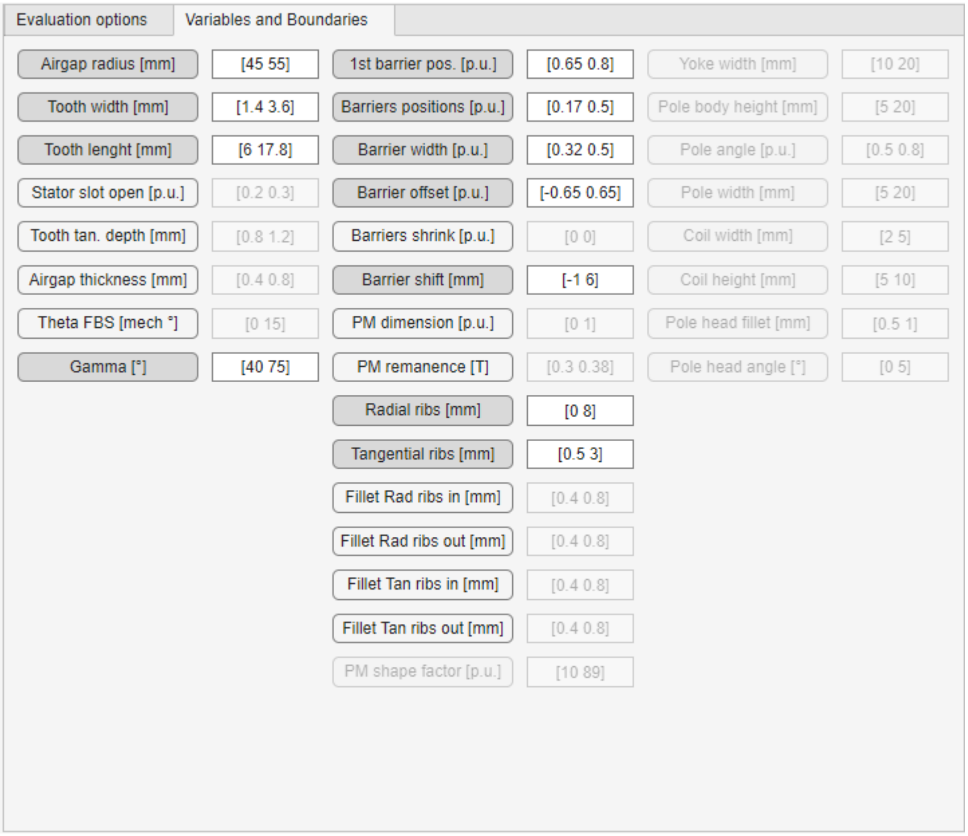

Airgap radius [mm] [45 55]
Tooth width [mm] [1.4 3.6]
Tooth lenght [mm] [6 17.8]
Stator slot open [p.u.] [0.2 0.3]
Tooth tan. depth [mm] [0.8 1.2]
Airgap thickness [mm] [0.4 0.8]
Theta FBS [mech °] [0 15]
Gamma [°] [40 75]

1st barrier pos. [p.u.] [0.65 0.8]
Barriers positions [p.u.] [0.17 0.5]
Barrier width [p.u.] [0.32 0.5]
Barrier offset [p.u.] [-0.65 0.65]
Barriers shrink [p.u.] [0 0]
Barrier shift [mm] [-1 6]
PM dimension [p.u.] [0 1]
PM remanence [T] [0.3 0.38]
Radial ribs [mm] [0 8]
Tangential ribs [mm] [0.5 3]
Fillet Rad ribs in [mm] [0.4 0.8]
Fillet Rad ribs out [mm] [0.4 0.8]
Fillet Tan ribs in [mm] [0.4 0.8]
Fillet Tan ribs out [mm] [0.4 0.8]
PM shape factor [p.u.] [10 89]

Yoke width [mm] [10 20]
Pole body height [mm] [5 20]
Pole angle [p.u.] [0.5 0.8]
Pole width [mm] [5 20]
Coil width [mm] [2 5]
Coil height [mm] [5 10]
Pole head fillet [mm] [0.5 1]
Pole head angle [°] [0 5]

Figure 3.4.1: Variables and boundaries sub-tab of the third optimizations

The stator boundaries are those of the second optimization, but scaled by a factor of 1.4. The rotor ones are the same except for the maximum limit of the radial ribs width and the minimum limit of the barrier shift which were 12 mm and –2 mm, respectively.

3.4.1 Third optimization: Reduced Diameter

Since the second optimization, whose baseline motor had too big rotor dimensions, produced poor results and knowing that the stator variables have to reduced by the scaling factor for the aforementioned reasons, OPT2-501 motor, scaled with the button *Scale* present inside the *Main Data* tab, can be used as the initial motor of the third optimization.

Therefore, by pressing the *Scale* button, imposing the stator outer radius to 80 *mm* and adjusting the airgap thickness, airgap radius and shaft radius, keeping the same length and imposing the correct overspeed inside the *Options* tab, the initial optimization motor is the one represented in Fig.3.4.2.

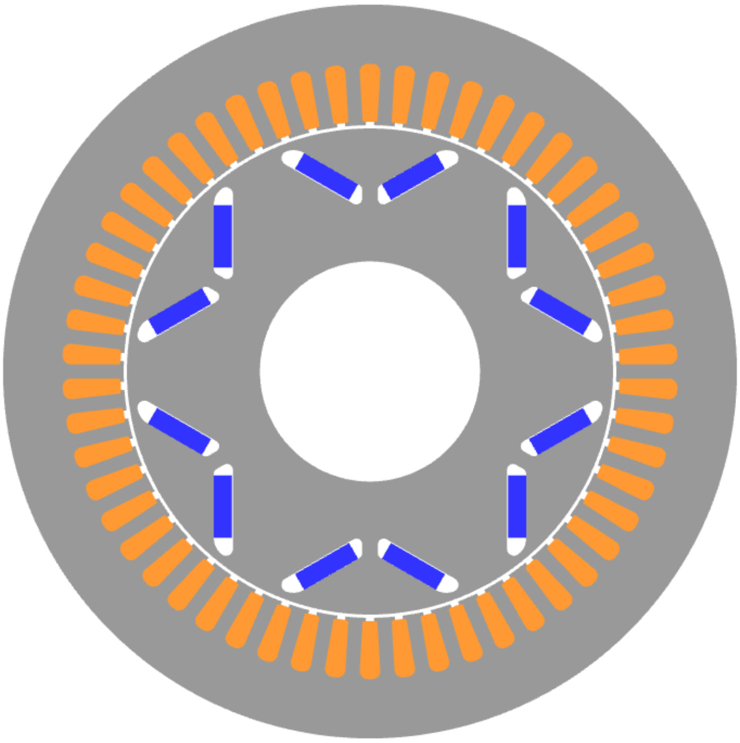

Figure 3.4.2: Initial motor of the third optimization

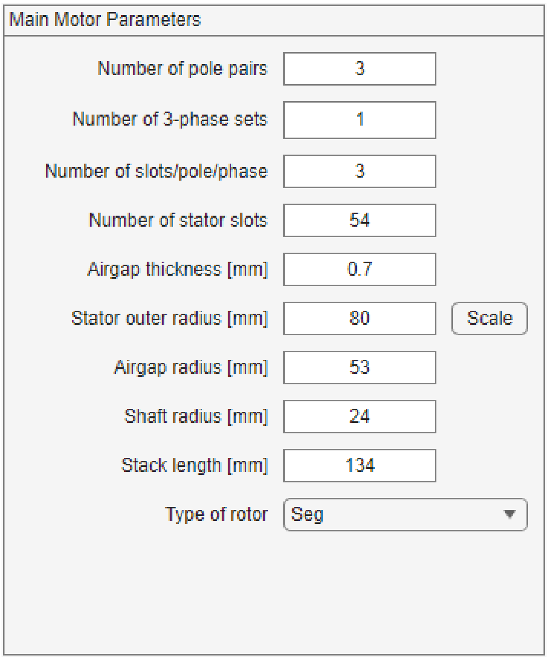

Main Motor Parameters

Number of pole pairs	3
Number of 3-phase sets	1
Number of slots/pole/phase	3
Number of stator slots	54
Airgap thickness [mm]	0.7
Stator outer radius [mm]	80
Airgap radius [mm]	53
Shaft radius [mm]	24
Stack length [mm]	134
Type of rotor	Seg

Figure 3.4.3: Main motor parameters of the third optimization

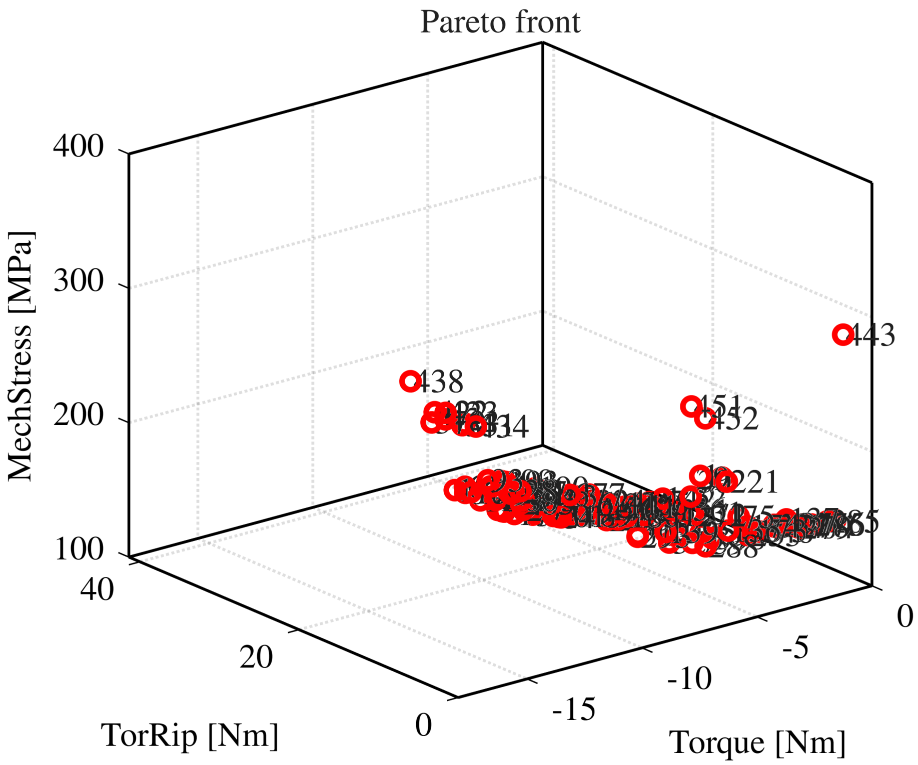

Figure 3.4.4: Pareto front of the third optimization

The *Evaluation options* sub-tab from the *Optimization* tab, instead, was set as for the first optimization. At the end of the process, the Pareto front was evaluated generating the result of Fig.3.4.4.

As can be observed from the torque values on the axis, none of the solutions reached the target torque. This is due to the initial motor, which has the same radial dimensions as *scale_2_adj* motor (rotor radius = 80 mm), but the length of the default one. Since the torque is proportional to the motor length and diameter, which was reduced, the torque will be lower than that of *syreDefaultMotor*. In fact, the maximum torque value of the initial motor is slightly higher than 141 Nm, considering the target current density, as shown in Fig.3.4.5.

Therefore, the fact that the optimization did not have any motor that reaches the torque target value is because the optimization algorithm did not have enough generations to converge towards the target. For this reason, the following optimizations will have as baseline motor the result of the scaling process.

Fig.3.4.6 represents the penalized bar chart of the Pareto front, in particular the motors with the highest torque. The torque value for all the machines is reduced by ten times due to the penalization algorithm, already explained in the previous chapter. From this it becomes clearer that none of the motors can generate the target torque, therefore the most performing motor is the 438, which is the one producing the highest peak torque. Then also the bar charts of the torque ripple and Von Mises stress are reported, highlighting that both penalization limits are respected.

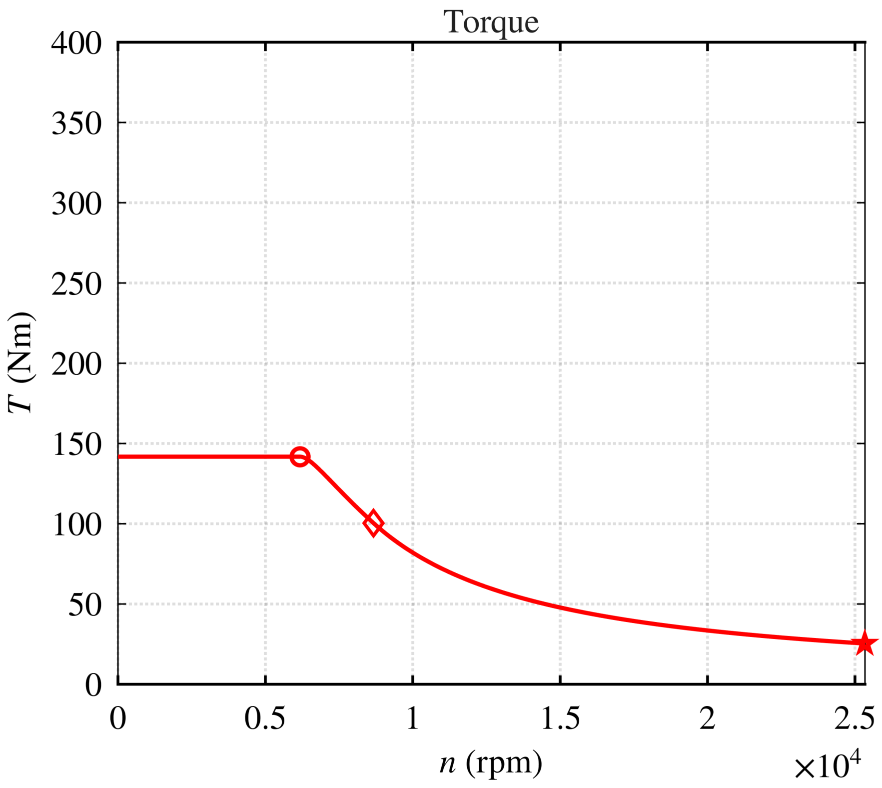

Figure 3.4.5: Torque-speed characteristic of the baseline motor of the third optimization

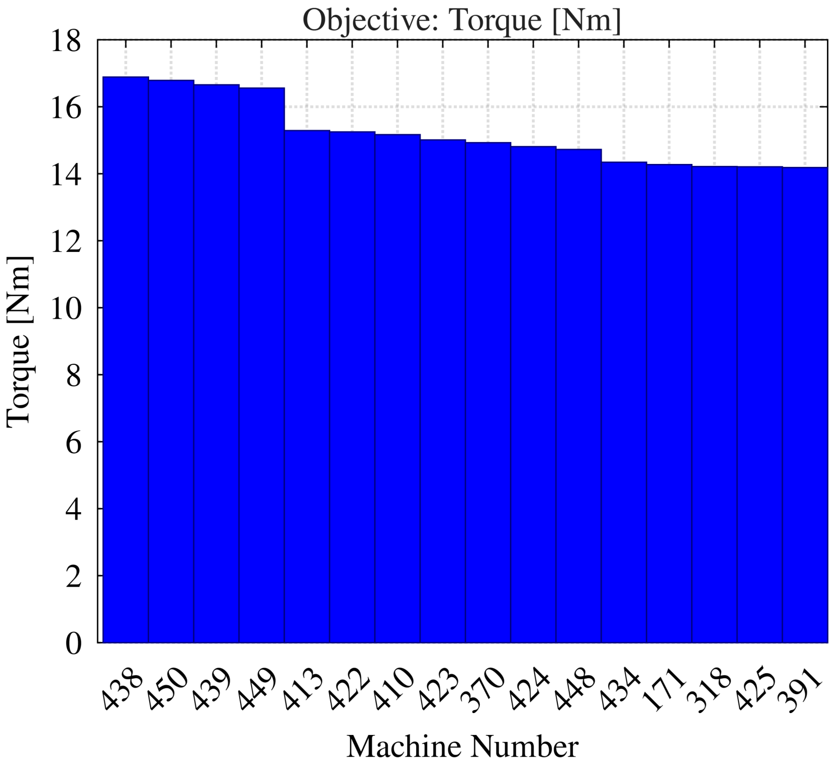

Figure 3.4.6: Torque bar chart of the Pareto front of the third optimization

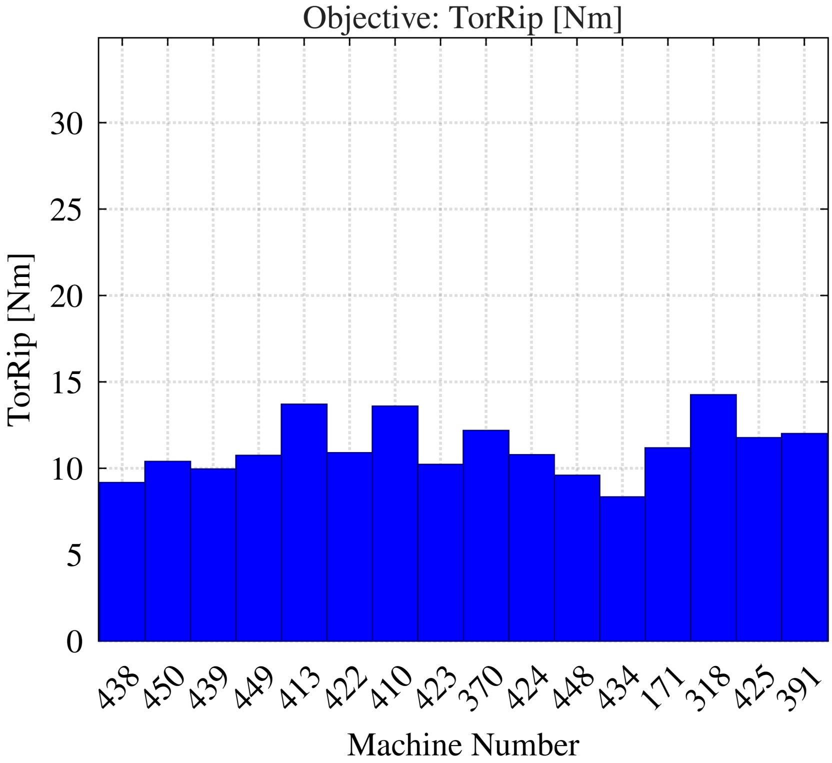

Figure 3.4.7: Torque ripple bar chart of the Pareto front of the third optimization

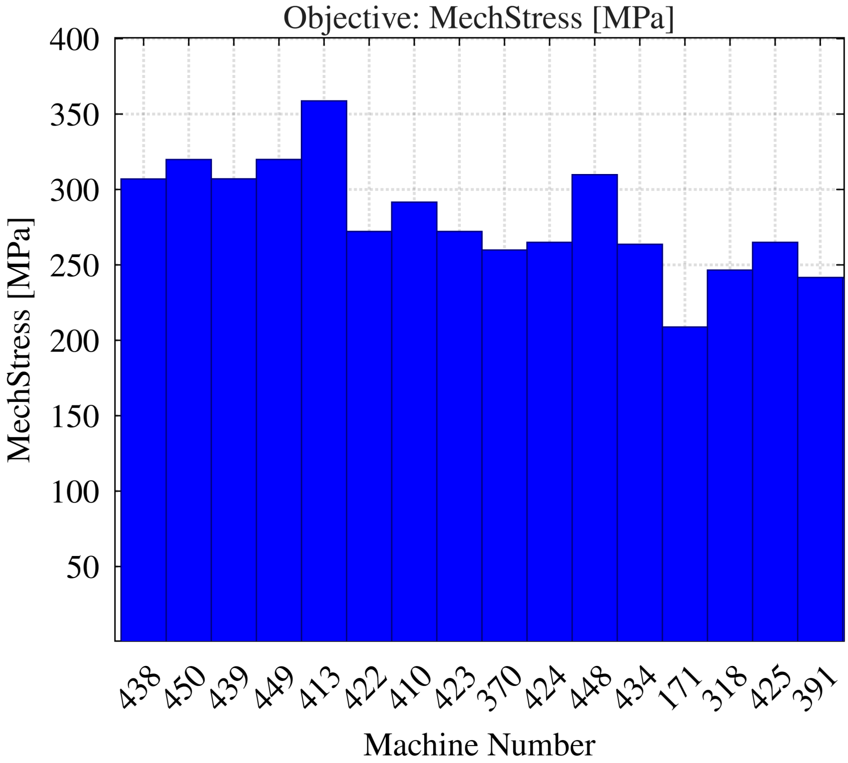

Figure 3.4.8: Von Mises stress bar chart of the Pareto front of the third optimization

The motor design and specifications are reported below. From the last one it is also possible to notice that the peak torque has a low value also due to the peak phase current, much lower compared to the target value.

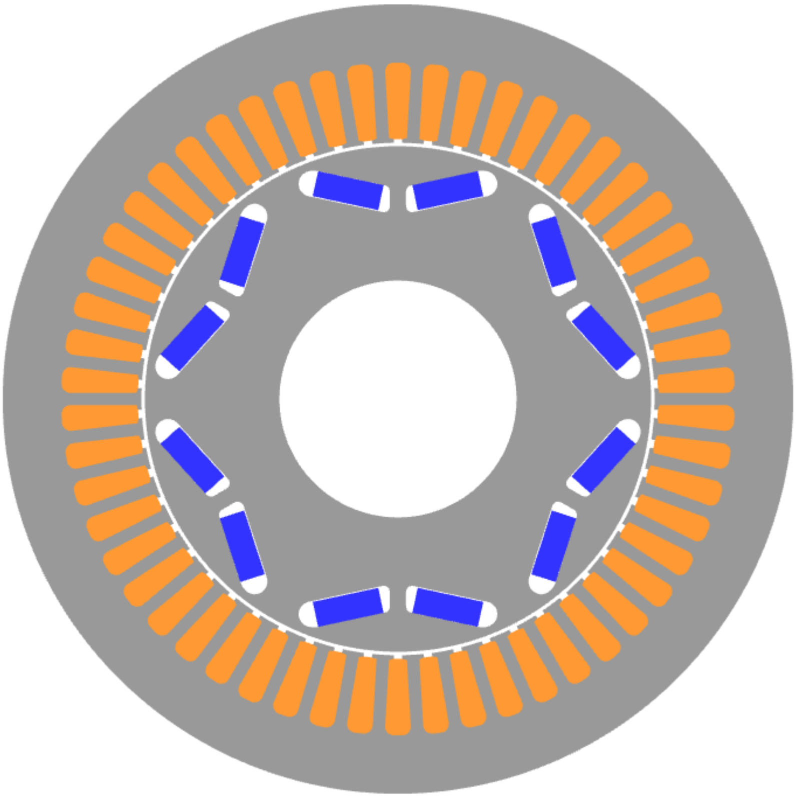

Figure 3.4.9: OPT3-438 motor design

Peak torque [Nm]	169
Peak power [kW]	127.8
Power at max speed [kW]	88.7
Base speed [rpm]	7000
Maximum speed [rpm]	25340
Peak current density [Arms/mm^2]	36
Peak phase current [Apk]	567
DC-link voltage [V$_{DC}$]	400
Turns in series per phase	21
Thermal loading [kW/m^2]	149.6
Stator outer diameter [mm]	160
Rotor outer diameter [mm]	102.46
Air-gap length [mm]	0.7
Stack length [mm]	134

Table 3.4.1: OPT3-438 motor specifications

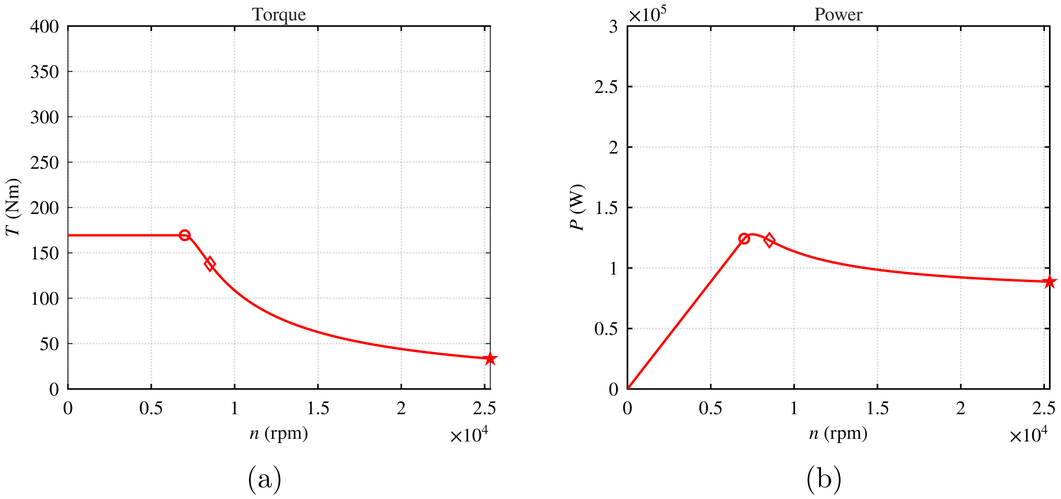

Figure 3.4.10: OPT3-438 motor torque-speed (a) and power-speed (b) characteristics.

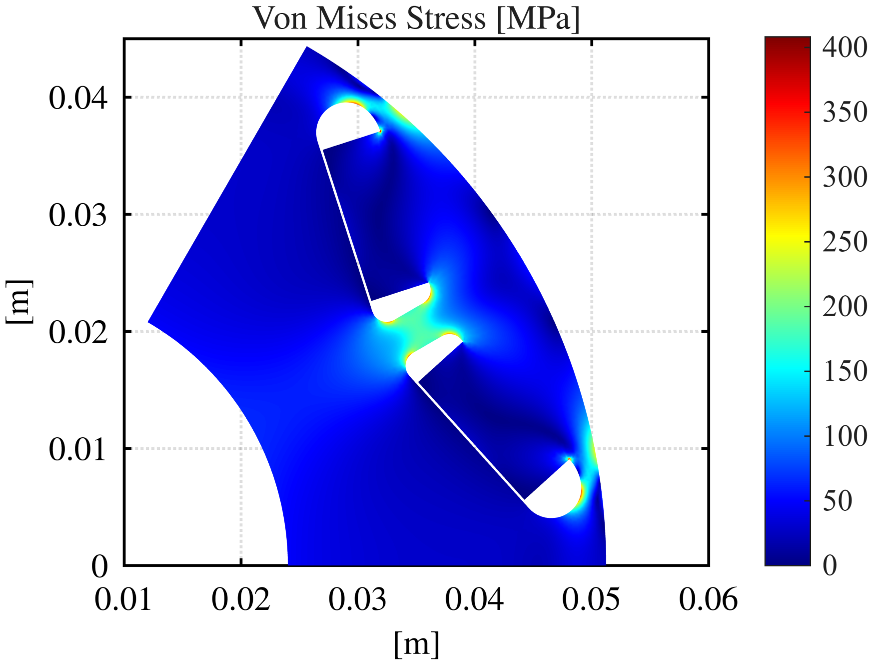

Figure 3.4.11: OPT3-438 motor Von Mises stress chart

From the previous figures, showing the torque, power and stress analysis it is clear that even if the base speed exceeds the target value, the power does not reach the desired value because of the low peak phase current value. From the Von Mises stress analysis, instead, it can be observed that the motor is structurally valid, since the maximum stress value is slightly above 400 MPa. This value seems to be not consistent with the value represented in Fig.3.4.8, but it has to be remembered that this last value represents the average stress over the 99th percentile, not the maximum value.

Therefore, considering that for this optimization the main problem was the initial motor, two other optimizations were performed having as baseline motor the *scale_2_adj*.

3.4.2 Fourth optimization: Ripple-Oriented Optimization

The fourth optimization, as just mentioned, used the final scaled motor as baseline. Compared to the fifth optimization, this one has as selected *Objective and Penalization Limits* the same of the first optimization, represented in Fig.3.1.1. The results of the process are presented in Fig.3.4.12.

Then, also the 2D post-processing graphs are reported to better understand which motor can be the best solution.

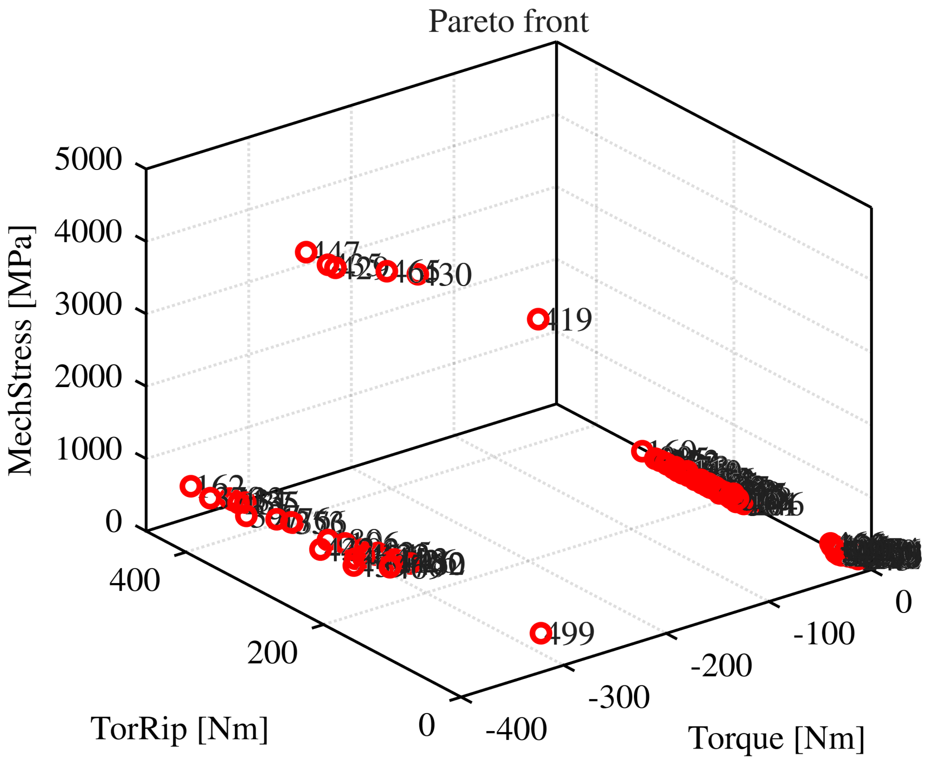

Figure 3.4.12: Pareto front of the fourth optimization

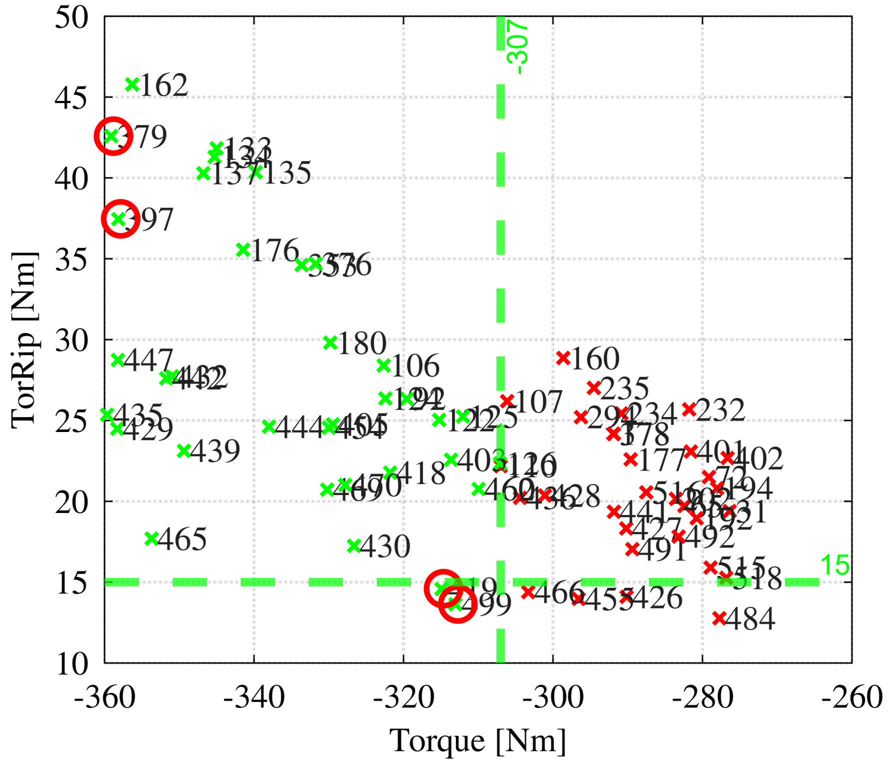

Figure 3.4.13: Torque-torque ripple chart

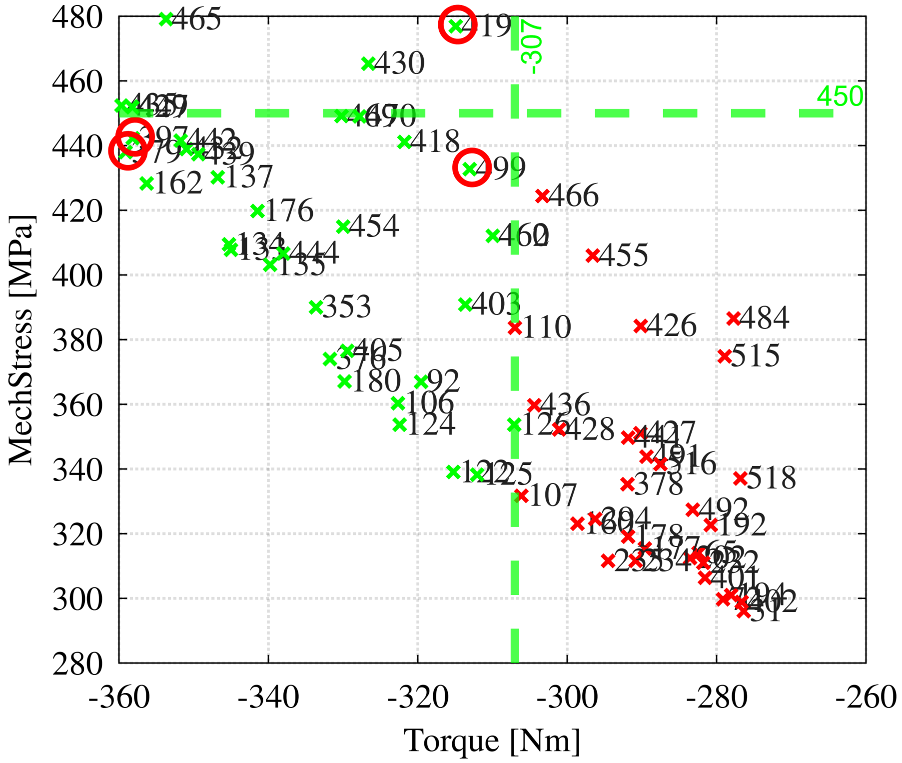

Figure 3.4.14: Torque-stress chart

As can be noticed, the figures have four red circles, which show the motors selected, that are:

	T [Nm]	dT [Nm]	stress [MPa]
OPT4-379	359.12	42.57	437.93
OPT4-397	358.16	37.46	442.25
OPT4-419	313.03	13.64	476.94
OPT4-499	314.93	14.58	432.76

Table 3.4.2: Selected motor of the fourth optimization

Motors OPT4-419 and OPT4-499 were selected because both respect the target limits, while OPT4-379 and OPT4-397 were selected because they can produce the highest torque at the target current density, respecting the stress limit. It must be remembered that the baseline motor has a length of 240 *mm* and a stator outer diameter of 160 *mm* and that in the automotive field it is fundamental to have a motor that is the most compact possible. In order to reduce the length of the motor, the motor that generates the highest torque should be selected. In this way, since the torque is proportional to the length, this last parameter can be reduced until the torque of the selected motor reaches the target value. For this reason, the motor OPT4-379 was chosen as the best option among all the solutions.

The following torque and power characteristics, together with Tab.3.4.3, show that all electromagnetic targets of Tab.3.2, while Fig.3.4.15 shows the motor design.

Peak torque [Nm]	360
Peak power [kW]	246.5
Power at max speed [kW]	189
Base speed [rpm]	6239
Maximum speed [rpm]	25340
Peak current density [Arms/mm^2]	36
Peak phase current [Apk]	947.7
DC-link voltage [V$_{DC}$]	400
Turns in series per phase	12
Thermal loading [kW/m^2]	117
Stator outer diameter [mm]	160
Rotor outer diameter [mm]	98.5
Air-gap length [mm]	0.7
Stack length [mm]	240

Table 3.4.3: OPT4-379 motor specifications

From the table it is possible to observe that all electromagnetic targets are respected, except for the peak phase current, which value exceeds the target of 800 *A*. This aspect will be considered during the shortening process presented in the next section.

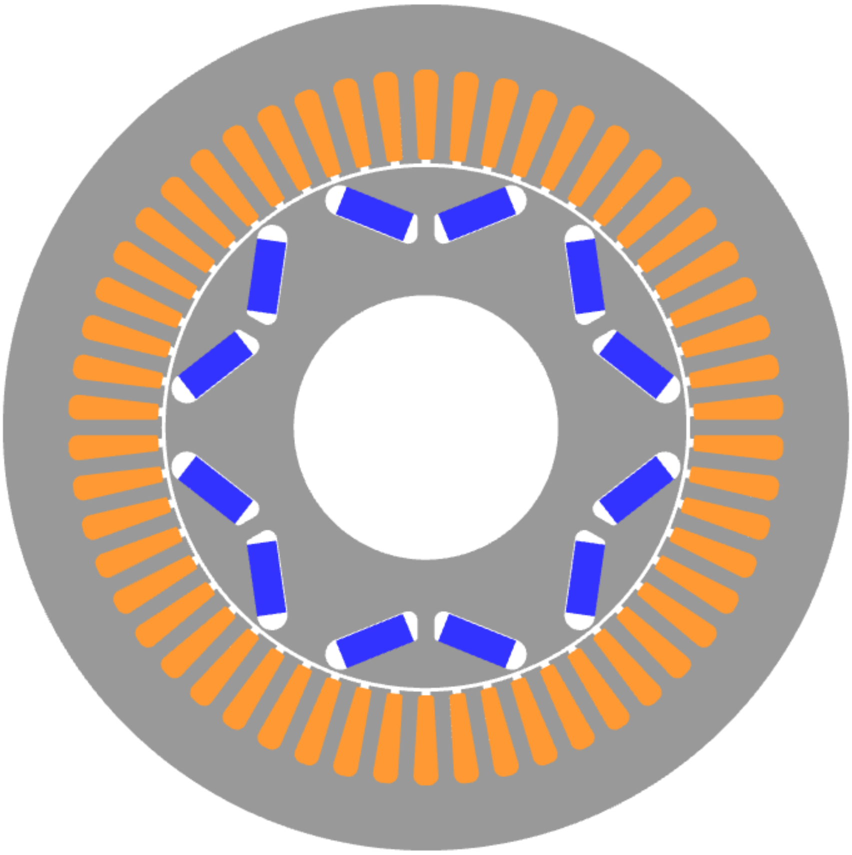

Figure 3.4.15: OPT4-379 motor design

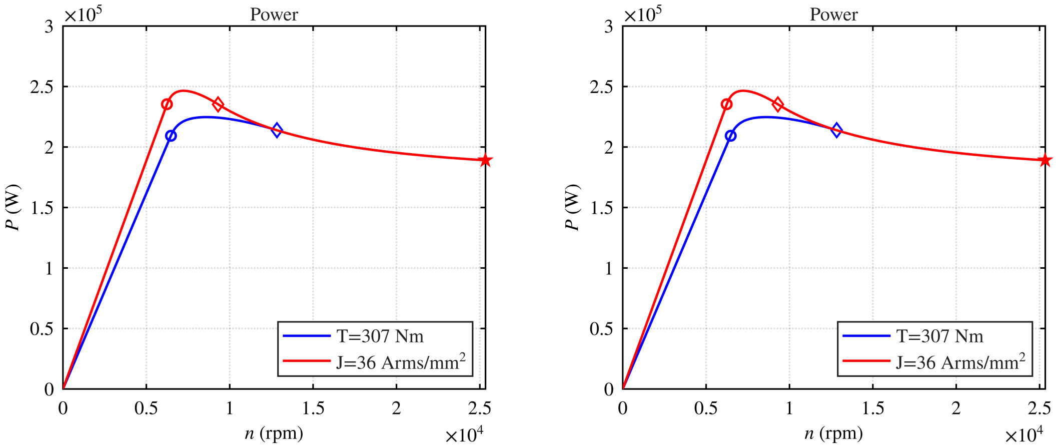

(a) (b)

Figure 3.4.16: OPT4-379 motor torque-speed (a) and power-speed (b) characteristics.

Unlike the torque and power characteristics of the second optimization, in this case the current levels were set at [0.83 1]. The first value is related to the current density that allows to match the torque target. As for the *scale_2_adj* motor, this value was reached by trial and error. The second value of the current levels, instead, represents the target of the current density.

Fig.3.4.17, instead, shows the structural analysis performed on the selected motor, from which it can be seen that the maximum stress exceeds the limit in the area indicated in Fig.3.4.18. Since the structural analysis is performed in SyR-e following a linear, and therefore not faithful, model, and knowing that there may be isolated peaks due to the mesh, the following motor should be re-evaluated more specifically from a structural point of view.

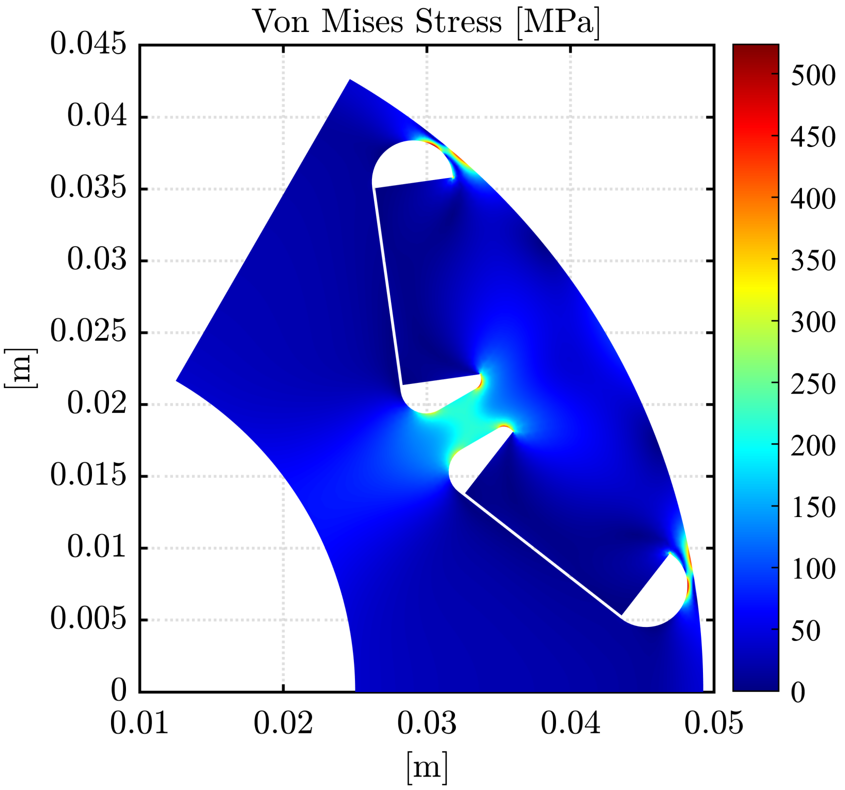

Figure 3.4.17: Von Mises stress graph of motor OPT4-379

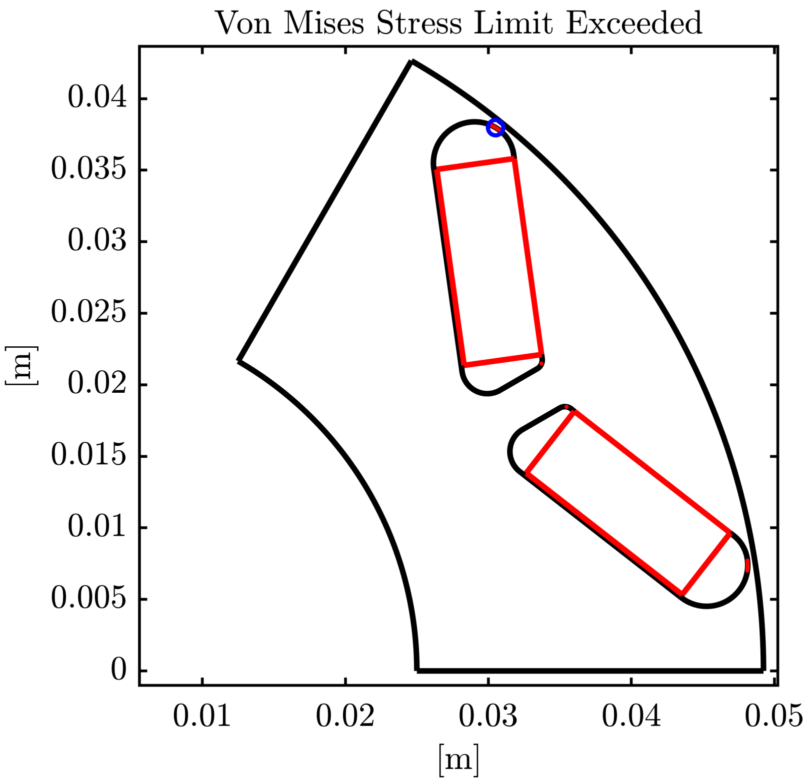

Figure 3.4.18: Exceeded stress areas of motor OPT4-379

3.4.3 Fifth optimization: Power Factor-Oriented Optimization

Unlike the previous optimization, for this last one the torque, the power factor and the Von Mises stress were set as the *Objectives and Penalization Limits*, as shown in Fig.3.4.19. The power factor was selected, instead of the torque ripple, because one of the principal aspects of the electrical motors is the ability to convert the electric power into a mechanical one. Since active and reactive power are the two power contributions, it is better to have an high power factor in order to increase the active contribution from which the mechanical power is generated. Therefore, this is another path that can be covered to obtain the best possible motor.

As for the previous optimizations, the Pareto front is reported in Fig.3.4.20, as well as the post-processing graph from which it can be easier to understand the optimization results. The motors evidenced with a red circles are:

	T [Nm]	PF	stress [MPa]
OPT5-231	323	0.6925	423.02
OPT5-585	321.93	0.6653	393.81
OPT5-609	350	0.7108	481.44
OPT5-622	324.45	0.6715	449.92

Table 3.4.4: Selected motor of the fifth optimization

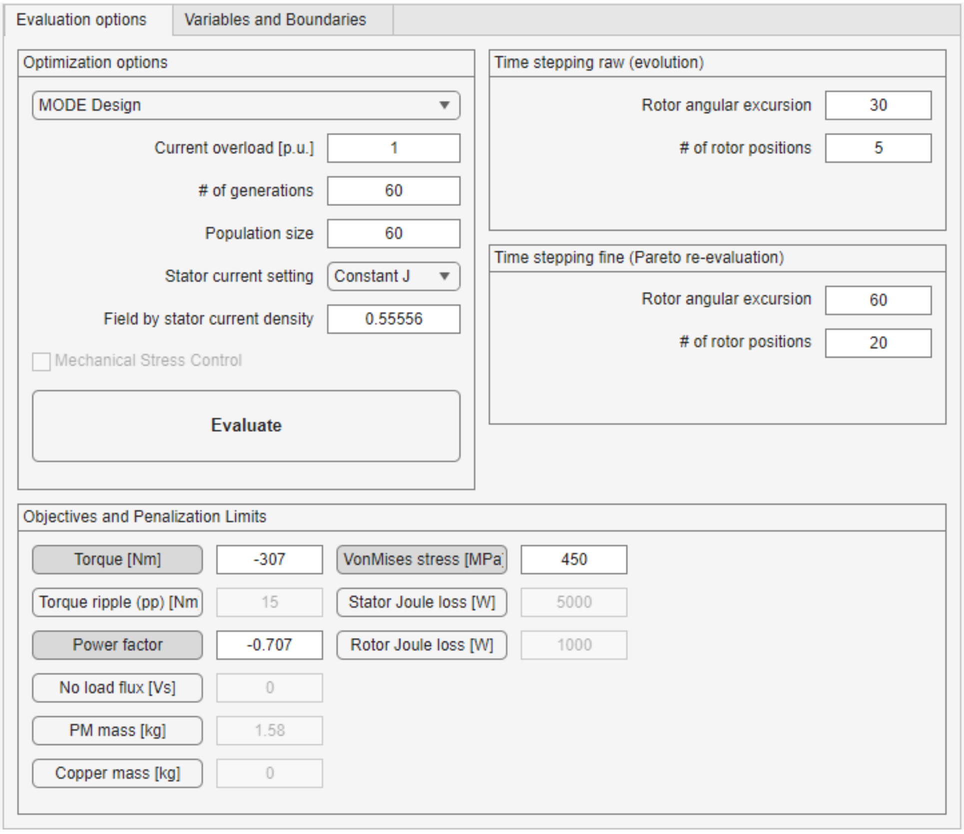

Optimization options

MODE Design

Current overload [p.u.] 1

# of generations 60

Population size 60

Stator current setting Constant J

Field by stator current density 0.55556

☐ Mechanical Stress Control

Time stepping raw (evolution)

Rotor angular excursion 30

# of rotor positions 5

Time stepping fine (Pareto re-evaluation)

Rotor angular excursion 60

# of rotor positions 20

Objectives and Penalization Limits

Torque [Nm] -307

Torque ripple (pp) [Nm 15

Power factor -0.707

No load flux [Vs] 0

PM mass [kg] 1.58

Copper mass [kg] 0

VonMises stress [MPa 450

Stator Joule loss [W] 5000

Rotor Joule loss [W] 1000

Figure 3.4.19: Objectives and penalization limits of the fifth optimization

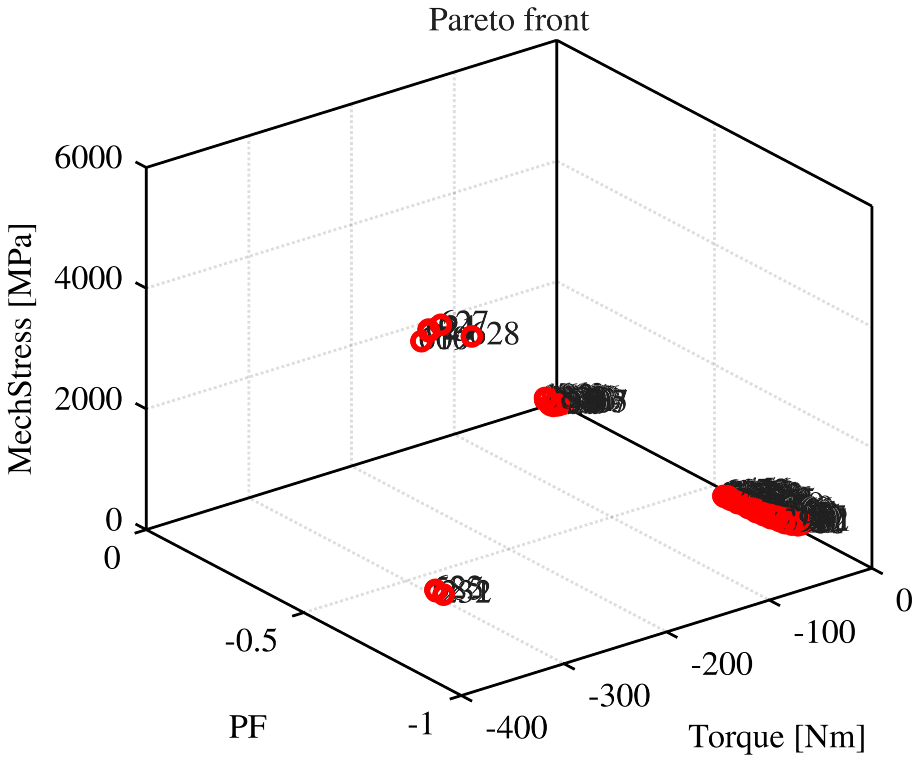
Pareto front

Figure 3.4.20: Pareto front of the fifth optimization

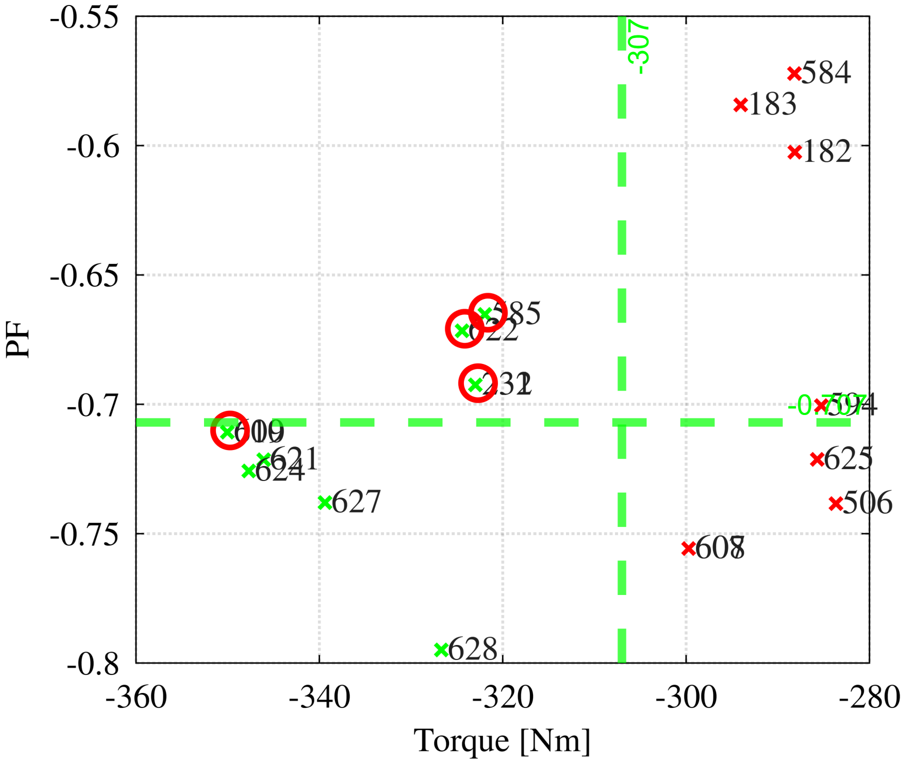

Figure 3.4.21: Torque-power factor chart

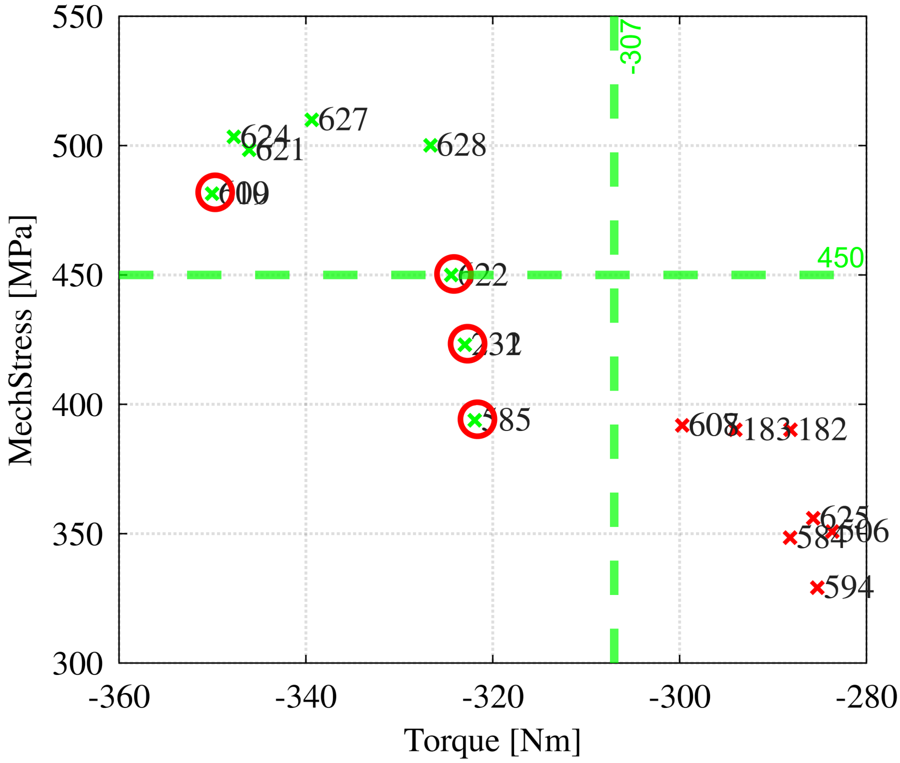

Figure 3.4.22: Torque-stress chart

As for the previous optimization, in addition to the motors that respect the target limits, also the motor OPT5-609 was considered because of its high torque value, which can be used to reduce the length of the motor. Since it is important to have a compact motor, the final motor selected is this last one, which has the highest torque and respects the PF target, even if the Von Mises stress exceeds the limit of 450 MPa . As said previously, this aspect can be improved with a further optimization, considering as variables the radial and tangential ribs. In the following figure the motor design is reported, followed by the motor specifications.

From Tab.3.4.5, as for the result of the previous optimization, the peak phase current exceeds the target limit. This aspect will be considered in the next section during the scaling of OPT5-609.

The torque and power characteristics are reported in Fig.3.4.24. Also in this case, the current levels were set at [0.83 1]. The first value is related to the current density that allows to match the torque target, while the to the current density target.

The last two figures, instead, represent the structural analysis, showing that the maximum stress value exceeds the limit, as already predicted in Fig.3.4.22.

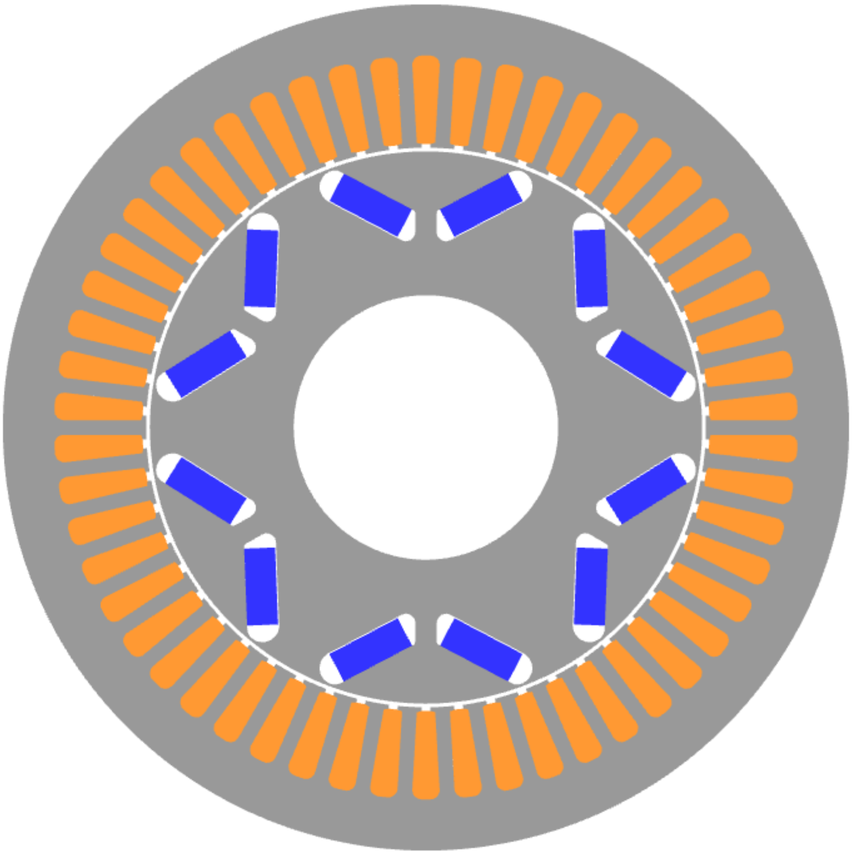

Figure 3.4.23: OPT5-609 motor design

Peak torque [Nm]	350
Peak power [kW]	254.6
Power at max speed [kW]	191.3
Base speed [rpm]	6722
Maximum speed [rpm]	25340
Peak current density [Arms/mm^2]	36
Peak phase current [Apk]	1049.5
DC-link voltage [V$_{DC}$]	400
Turns in series per phase	12
Thermal loading [kW/m^2]	130.6
Stator outer diameter [mm]	160
Rotor outer diameter [mm]	104.4
Air-gap length [mm]	0.7
Stack length [mm]	240

Table 3.4.5: OPT5-609 motor specifications

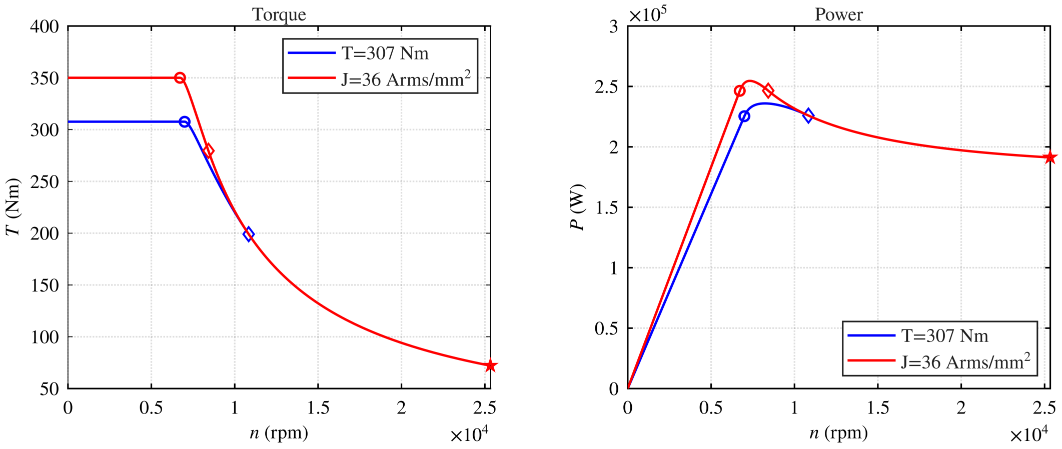

(a) (b)

Figure 3.4.24: OPT5-609 motor torque-speed (a) and power-speed (b) characteristics.

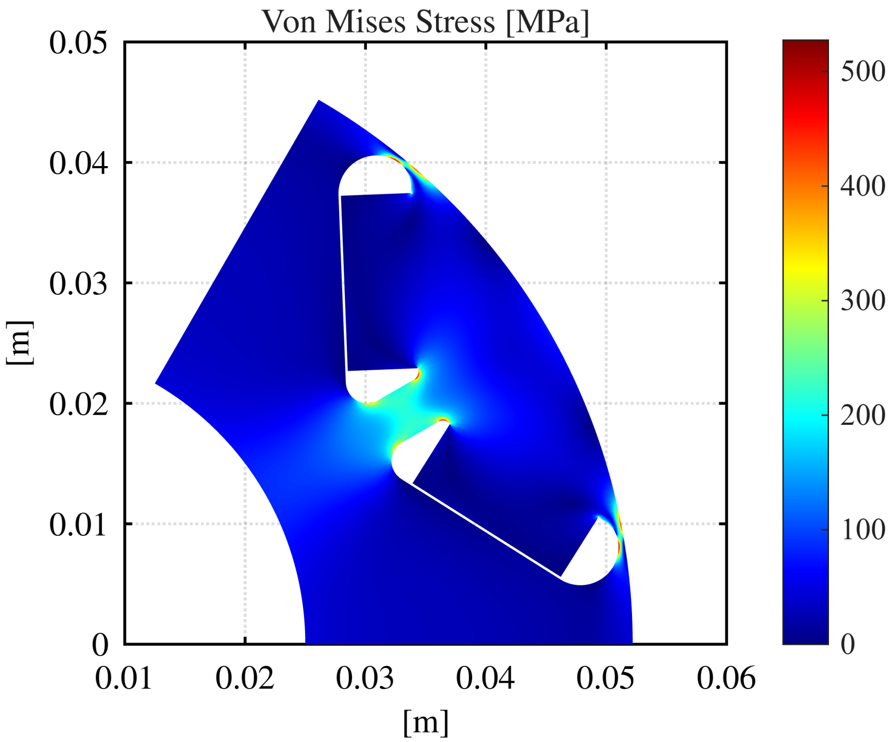

Figure 3.4.25: Von Mises stress graph of motor OPT5-609

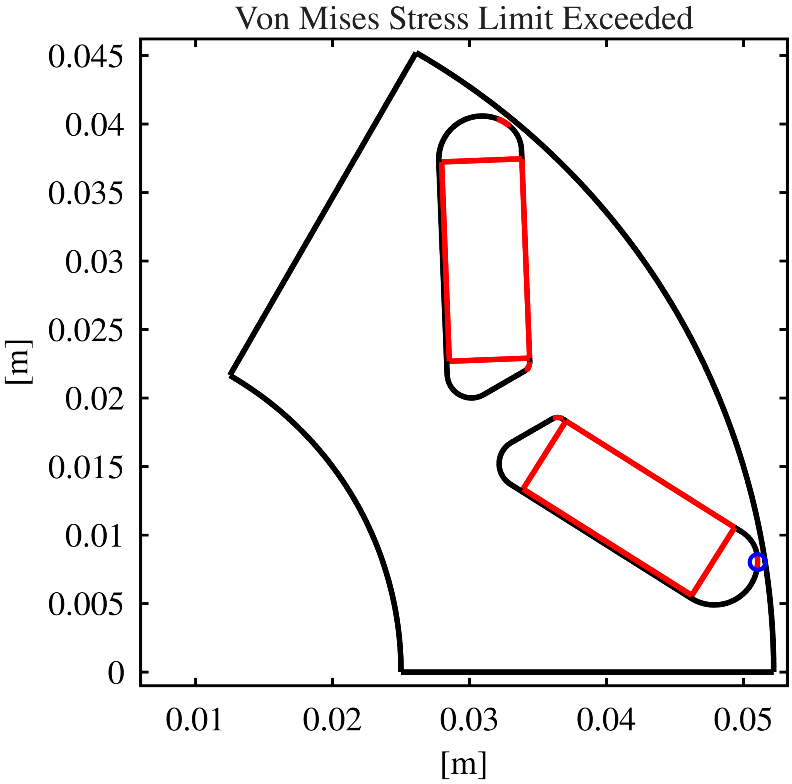

Figure 3.4.26: Exceeded stress area of motor OPT5-609

3.5 Final Scaling of Optimized Designs

As the output torque of the two optimized motors is higher than the target, a stack length reduction can be performed, reducing the motor active volume. The main goal of this process was to reduce the stack length, but also to understand the motor behavior considering the target peak phase current instead of those reported in Tabs.3.4.3-3.4.5. As in the previous scaling process, also in this case the *(L,N_s) Scaling Plane* of SyR-e MMM was used.

3.5.1 Scaling of the Fourth Optimization

The shortening process of OPT4-379 was performed considering that the scaling plane settings were imposed as follows:

- minimum and maximum axial length left to the values suggested
- minimum and maximum number of turns set to 6 and 16, respectively
- DC ling voltage imposed at 400 V
- peak phase current set to 800 A.

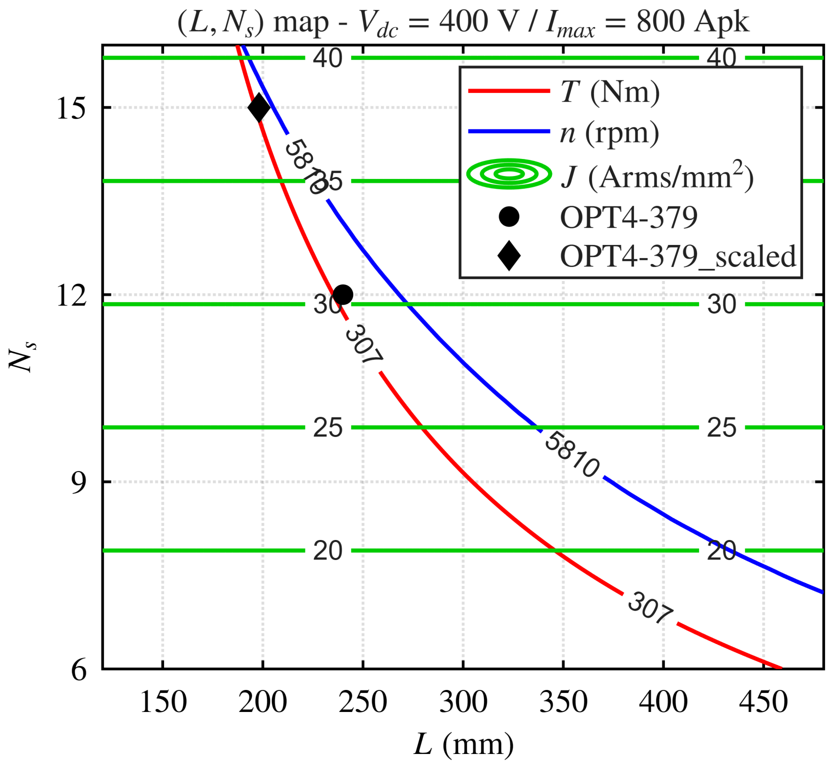

Figure 3.5.1: OPT4-379 motor scaling plane

After that, the plane of Fig.3.5.1 was investigated to understand how much the motor length could be reduced. As for the previous scaling process, also in this case the plane showing the torque, base speed and thermal loading was manipulated by substituting the last parameter with the current density.

Also in this case, the area above the target curve and below the speed curve is the area that respects the torque and base speed targets. For this reason the point (198, 15) was selected as the new motor. In this case, in addition to having changed the length of the motor, the number of turns was also modified and set to 15, in order to obtain a motor as compact as possible even at the slight expense of the current density, which slightly exceeds the target value.

Then the new motor configuration was saved, from which the new torque and power characteristics were obtained and reported below in the table, from which it is clear that, except for a little and acceptable increase in the current density, all the other electromagnetic parameters are respected. The motor length is reduced from 240 *mm* to 198 *mm*, obtaining a more compact motor.

Peak torque [Nm]	310
Peak power [kW]	204.2
Power at max speed [kW]	152.4
Base speed [rpm]	6027
Maximum speed [rpm]	25340
Peak current density [Arms/mm^2]	38
Peak phase current [Apk]	800
DC-link voltage [V$_{DC}$]	400
Turns in series per phase	15
Thermal loading [kW/m^2]	138.5
Stator outer diameter [mm]	160
Rotor outer diameter [mm]	104.4
Air-gap lenght [mm]	0.7
Stack length [mm]	198

Table 3.5.1: OPT4-379_scaled motor specifications

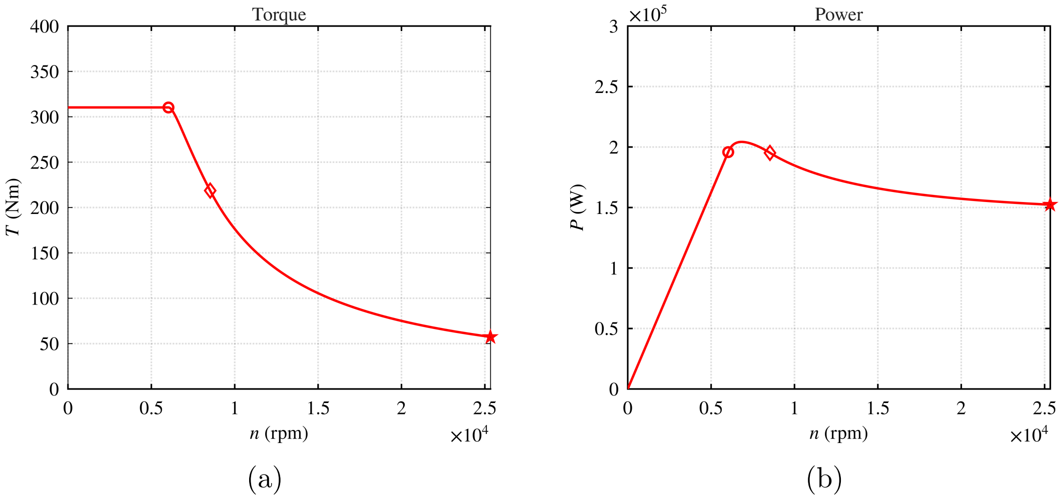

Figure 3.5.2: OPT4-379_scaled motor torque-speed (a) and power-speed (b) characteristics.

3.5.2 Scaling of the Fifth Optimization

The same procedure was also performed for the OPT5-609 motor. As for the result of the fourth optimization, the number of turns was increased to 15, while the stack length selected was 218 mm. In this case, the motor respects all the electromagnetic targets, including the current density . However, compared to the previous result, this motor is less compact.

Peak torque [Nm]	308
Peak power [kW]	202.5
Power at max speed [kW]	153.5
Base speed [rpm]	6035
Maximum speed [rpm]	25340
Peak current density [Arms/mm^2]	34.3
Peak phase current [Apk]	800
DC-link voltage [V$_{DC}$]	400
Turns in series per phase	15
Thermal loading [kW/m^2]	122.2
Stator outer diameter [mm]	160
Rotor outer diameter [mm]	104.4
Air-gap lenght [mm]	0.7
Stack length [mm]	218

Table 3.5.2: OPT5-609_scaled motor specifications

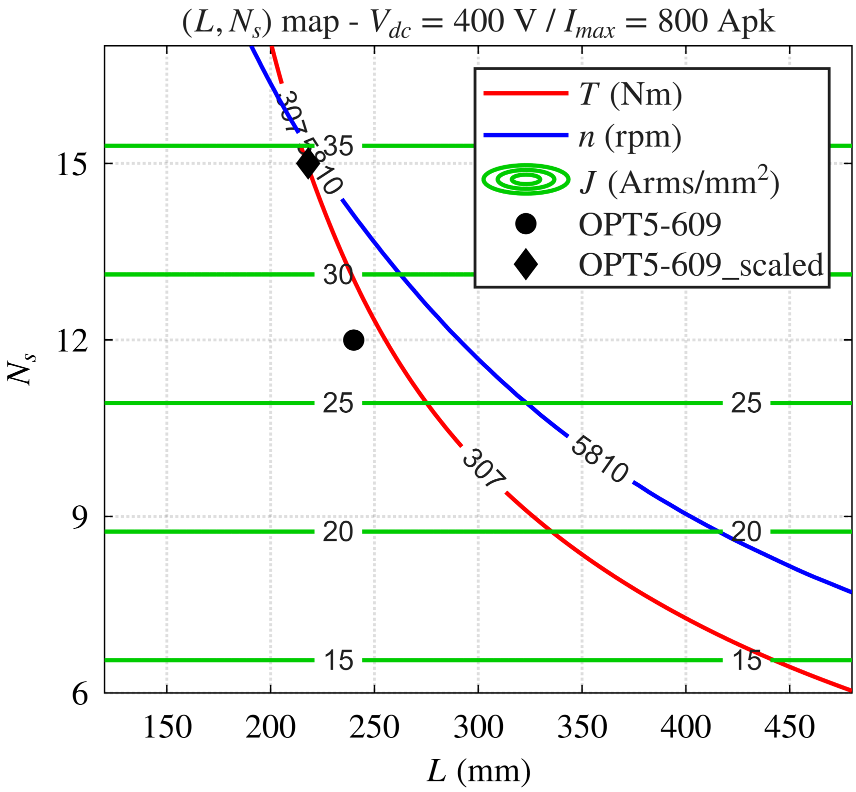

Figure 3.5.3: OPT5-609_scaled motor scaling plane

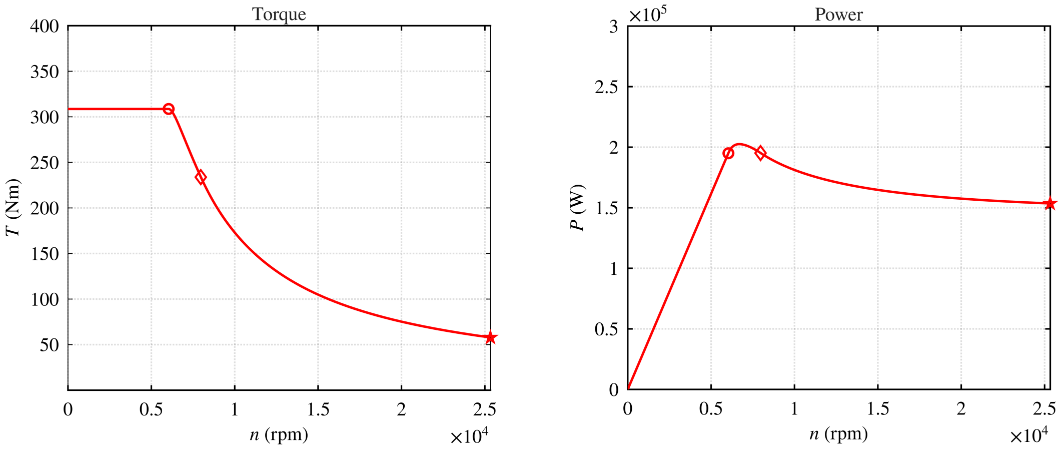

(a)

(b)

Figure 3.5.4: OPT5-609_scaled motor torque-speed (a) and power-speed (b) characteristics.

Chapter 4

Optimization Results and Motor Comparison

In this chapter, the resulting motors of the entire optimization process will be compared from the performance and structural aspects, in order to find the best option. Therefore, the first part will be more focused on the electromagnetic parameters, while the second more on the volumes.

4.1 Performance Evaluation

Before starting with the performance evaluation of the resulting motors, a table summarizing the targets and resulting motors specification is reported below.

	Targets	OPT4-379_scaled	OPT5-609_scaled
Peak torque [Nm]	307	310	308
Peak power [kW]	187	204.2	202.5
Power at max speed [kW]	137	152.4	153.5
Base speed [rpm]	5810	6027	6035
Maximum speed [rpm]	25340	25340	
Peak current density [Arms/mm^2]	36	38	34.3
Peak phase current [Apk]	800	800	
DC-link voltage [V$_{DC}$]	400	400	
Turns in series per phase	-	15	
Thermal loading [kW/m^2]	-	138.5	122.2

Table 4.1.1: Targets and resulting motors specifications

As can be noticed, the electromagnetic data of the final motors are very similar, in particular the peak torque and power, the power at maximum speed and also the base speed and all of them respects the minimum target reported in the first column. Therefore, already from this table it can be affirmed that the torque and power characteristics of the two motors are almost superimposable.

In order to verify this fact, Fig.4.1.1 reporting the torque and power characteristics are presented below.

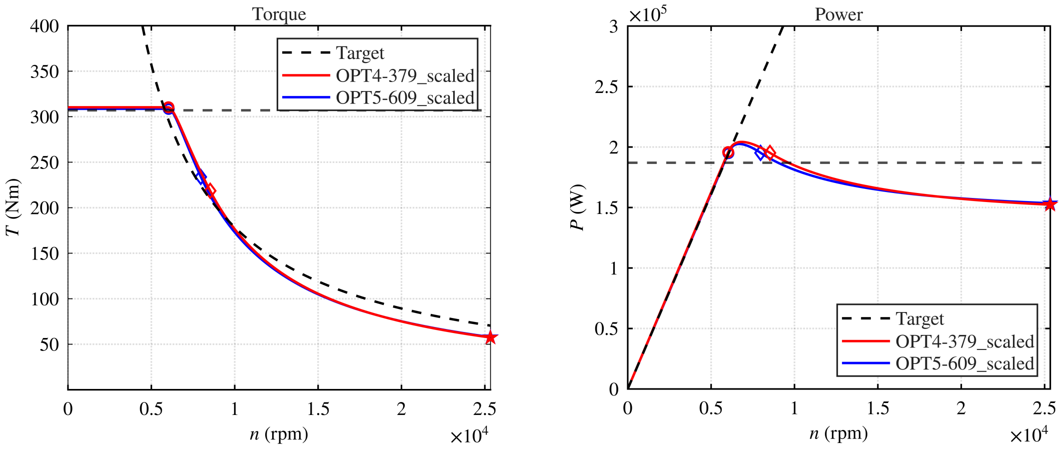

(a) (b)

Figure 4.1.1: OPT5-609_scaled motor torque-speed (a) and power-speed (b) characteristics.

From the torque-speed characteristic the two curves are practically superimposable and both of them respects the torque target, represented with a black dot horizontal line. The black dot curve, instead, represents the torque characteristic at constant power, in particular the target power, showing that the torque of both motors nearby 1000 *rpm* is lower than the one needed for having the peak power. This is also confirmed by the power-speed characteristic which shows that, in the aforementioned area, the power is lower than the target value. The main aspect of this second chart is that for both motors the peak power is higher than the target with a good margin. The reason of this is because the peak torques are maintained at their peak values until a speed of around 6000 *rpm* is reached.

The efficiency maps, obtained using the *Torque-Speed* tab of SyR-e MMM, are then reported. For both maps, the *Torque-Speed Performance Map & Efficiency Map* sub-tab settings were set as follows:

- torque and speed minimum limit left to 0
- torque and speed maximum limits set to 400 *Nm* and 25340 *rpm*
- number of points imposed both to 150 at the scope of having smooth curves
- winding temperature set to 120°C
- iron loss and PM loss set to YES, while skin effect to NO
- mech. loss poly, iron loss factor and PM loss factor left to the default value
- control strategy set to MTPA.

From the two efficiency maps it can be observed that for both of them the maximum efficiency reaches a good value of 97% and that the also in this case the two characteristics are very similar. The most remarkable difference is related to the maximum efficiency area. For OPT4-379_scaled motor this area is bigger compared to that of the other motor. In particular, the the left area is more extended, but overall the two motors have very similar efficiency.

Therefore, it is important to notice that even if the two optimization processes had different *Objective and Penalization Limits* selected, the algorithm converged toward a similar result and this is also evident by looking at the design of the motors presented in Figs.3.4.15-3.4.23. This is important to point out because this means that starting from the same starting point, you can arrive at more or less the same result by following different paths, thus guaranteeing greater flexibility of action to the designer.

The main differences regarding the motors specifications are related to the current density the thermal loading. The first is proportionally inverse to the slot area, while the second to the outer surface of the motor. Regarding the slot areas, OPT5-609_scaled motor has the tooth length equal to 17.43 *mm* and the slot width at 3.49 *mm*, while for OPT4-379_scaled motor these two values are 17.73 *mm* and 3.49 *mm*. Therefore, OPT5-609_scaled motor has larger slots compared to OPT4-379_scaled and this is the reason why, considering the same current, the current density of the first is lower than that of the second.

A similar argument applies to the thermal load. Since OPT4-379_scaled is shorter than OPT5-609_scaled, and since the efficiency maps confirm that the losses are very similar, the thermal loading factor of the shorter motor will be greater than that of the longer one.

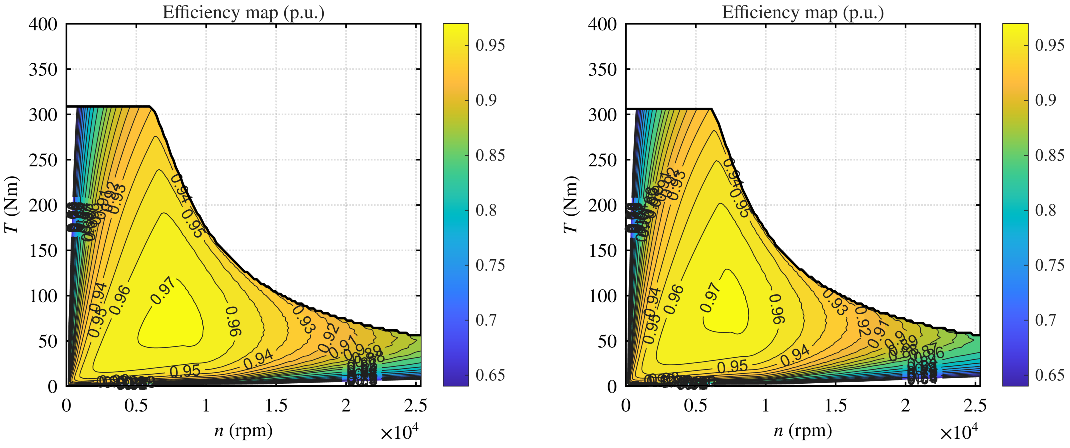

(a) (b)

Figure 4.1.2: Efficiency maps of motor OPT4-379_scaled (a) and OPT5-609_scaled (b).

4.2 Structural Evaluation

In order to have a better understanding of the two structure of the motors, a table reporting the stator and rotor dimensions, the motor length, volume and weight is reported below.

	syreDefaultMotor	OPT4-379_scaled	OPT5-609_scaled
Peak power [kW]	187	204.2	202.5
Power at max speed [kW]	137	152.4	153.5
Base speed [rpm]	4150	6027	6035
Maximum speed [rpm]	18100	25340	25340
Stator outer diameter [mm]	225	160	160
Rotor outer diameter [mm]	149.9	98.5	104.4
Stack length [mm]	134	198	218
Active volume [L]	5.33	3.98	4.38
Stator core mass [kg]	16.8	13.1	12.2
Winding core mass [kg]	4.6	3.5	4.2
Rotor core mass [kg]	11.9	6.7	8.7
PM mass [kg]	1.6	1.4	1.7
Total mass [kg]	35.0	24.8	26.8
Power density [kW/kg]	5.34	8.23	7.56

Table 4.2.1: Structural specifications of the resulting motors

Looking at the dimensions of the two motors, it is simple to understand why OPT4-379_scaled has a lower active volume compared to OPT5-609_scaled, but also the reason for the lower thermal loading factor. The second motor is longer by 20 *cm* compared to the first, meaning a 10% more than the first.

Considering the different masses of the motors, it can be observed that the stator core of the first motor is higher than that of the second and this is perfectly coherent with the dimensions reported above. The two motors have the same outer radial dimensions, but since the first motor has a lower rotor outer diameter, this means that its stator is bigger than that of the second, and so the mass.

For what concerns the winding core mass, also in this case, it is reasonable that for the second motor this value is higher due to a larger axial dimension, which increases the active length area, but also due to a larger rotor outer diameter, which increases the end winding length. All this is also true because the number of turns and the conductors of the two motors are the same.

The penultimate row of the table also shows the masses of the permanent magnets. For the first motor, this value is lower, again due to its shorter axial length. Furthermore, a slight increase in their width for the second motor must also be considered. Therefore, since the magnets for OPT5-609_scaled are longer and wider, their weight is greater. Both motors, however, are lighter than the Tesla motor and can achieve higher powers.

Therefore, the resulting motors can reach higher maximum speeds, higher peak powers and powers at maximum speed having lower volumes and being lighter, reaching also a higher power density as shown in the lat line of the table.

Chapter 5

Conclusions and Future Steps

This thesis addressed the optimization of an Interior Permanent Magnet (IPM) machine with the primary objective of increasing its maximum operating speed while preserving the required electromagnetic performance and ensuring mechanical integrity. The work was conducted starting from a reference motor configuration, which served as the baseline for the entire design process.

The study highlighted the importance of adopting a combined electromagnetic and structural design approach, particularly for high-speed electric machines, where performance improvements are inherently coupled with mechanical constraints. Several optimization procedures were carried out using the SyR-e environment, enabling the systematic exploration of the design space through finite element analysis (FEA) and multi-objective optimization techniques.

Different optimization strategies were investigated, initially focusing on rotor-only design variables and subsequently extending the analysis to both stator and rotor parameters. The obtained results demonstrated that modifications limited to the rotor geometry can lead to significant variations in machine behavior, although not always sufficient to satisfy all performance targets. The introduction of scaling procedures and successive optimization steps proved essential for refining the design and achieving more balanced solutions.

The final phase of the study led to the identification of two motor configurations exhibiting comparable electromagnetic performance while differing in their structural and geometrical characteristics. On one hand, a more compact and lighter motor was obtained, whose current density slightly exceeded the desired limit but satisfied the remaining electromagnetic requirements. On the other hand, a motor fully compliant with all imposed targets was achieved, although characterized by larger dimensions and increased weight.

The comparison between these solutions emphasized the presence of inherent trade-offs in electric machine design. The preference for one configuration over the other depends on the specific design priorities, which may favor compactness and reduced mass or stricter adherence to performance limits.

Despite the satisfactory electromagnetic results, both motor configurations require further improvement from a structural standpoint, as the Von Mises stress exceeded the prescribed limit. This aspect underlines the critical role of mechanical constraints in high-speed machine design and suggests that more specific analysis must be performed to ensure structural robustness.

Another key consideration emerging from this work concerns material utilization. In the context of developing more sustainable electric machines, minimizing the volume of critical materials such as copper and permanent magnets represents an important objective. However, this requirement introduces a fundamental compromise between sustainability and performance. Reduced material usage typically leads to lower power density and larger machine dimensions, whereas increased material exploitation enables more compact and efficient designs.

Therefore, sustainability should not be evaluated exclusively at the component level but rather within the broader framework of the entire production chain, including material extraction, manufacturing processes, and end-of-life management.

Overall, this thesis demonstrates that the design of high-speed IPM machines requires a careful balance between electromagnetic performance, structural reliability, geometrical constraints, and material utilization. The adopted optimization framework provides a structured methodology that can be extended to future studies and applied to different machine topologies or design objectives.

A relevant extension of the present work would involve the integration of thermal analysis within the optimization framework. Thermal behavior plays a crucial role in electric machine design, as temperature directly affects losses, efficiency, insulation lifetime, and the admissible current density. Including thermal constraints would therefore enable a more realistic evaluation of machine performance and operating limits.

Such an approach could improve the overall reliability of the design process, allowing the identification of solutions that simultaneously satisfy electromagnetic, structural, and thermal requirements.

However, the introduction of thermal modeling would inevitably increase the computational cost of the optimization procedure. The additional simulations required would lead to longer calculation times, particularly when combined with finite element analyses. Consequently, a trade-off arises between the accuracy and completeness of the design evaluation and the overall computational efficiency of the optimization.

Bibliography

[1] IEA (2025). *Global EV Outlook 2025*. Licence: CC BY 4.0. Paris: IEA. URL: `https://www.iea.org/reports/global-ev-outlook-2025`.

[2] MotorXP-PM. *Performance Analysis of the Tesla Model 3 Electric Motor using MotorXP-PM*. Tech. Rep., June 2020. URL: `https://motorxp.com/wp-content/uploads/mxp_analysis_TeslaModel3.pdf`.

[3] Ma Fangwu et al. "Design and Optimization of IPM Motor Considering Flux Weakening Capability and Vibration for Electric Vehicle Applications". In: *Sustainability 10.5* (2018), pp. 1–15. DOI: `10.3390/su10051533`. URL: `www.mdpi.com/journal/sustainability`.

[4] Gator Lamination. *Motor Stator Laminations*. URL: `https://www.gatorlamination.com/stator-and-rotor-lamination/`.

[5] *SyR-e*. DOI: `10.5281/zenodo.13944455`. URL: `https://github.com/SyR-e/`.

[6] S. Ferrari. *SyR-e User Manual*. Power Electronics InnovationCenter (PEIC), May 2025. URL: `https://github.com/SyR-e/syre_public/blob/main/Readme/syreManual.pdf`.

[7] David Meeker. *Finite Element Method Magnetics (FEMM)*. Version 4.2. 2023. URL: `http://www.femm.info`.

[8] S. Ferrari et al. "A Multiphysics Dataset Generation Procedure for the Data-Driven Modeling of Traction Electric Motors". In: *IEEE Access* vol. 13 (2025), pp. 54534–54546. DOI: `10.1109/ACCESS.2025.3554147`.

[9] Neri. F. and V. Tirronen. "Recent advances in differential evolution: a survey and experimental analysis". In: *Artif Intell Rev* vol. 33 (Feb. 2010), pp. 61–106.

[10] F. Cupertino, G. Pellegrino, and C. Gerada. "Design of Synchronous Reluctance Motors With Multiobjective Optimization Algorithms". In: *IEEE TRANSACTIONS ON INDUSTRY APPLICATIONS* vol. 50 (NO. 6 Nov. 2014), pp. 3617–3627.

[11] K. Deb et al. "A fast and elitist multiobjective genetic algorithm: NSGA-II". In: *IEEE Transactions on Evolutionary Computation* vol. 6 (no. 2 Apr. 2002), pp. 182–197.

Acknowledgements

Dopo due anni rieccoci di nuovo nel momento dei ringraziamenti che a differenza della scorsa volta, fortunatamente, non sarà davanti all'intera aula magna o almeno si spera.

Un grazie immenso va alla mia famiglia, che durante tutti questi anni mi ha sempre sostenuto. Mamma e papà, vi ringrazio per tutti i sacrifici che avete fatto durante questi anni e in generale per tutto quel che avete fatto per cercare di fare felici me e Paolino. Avete sempre messo noi davanti a tutto cercando di non farci mai mancare niente, anche nei momenti in cui eravamo più in difficoltà. Se ho imparato ad apprezzare anche solo i gesti più piccoli, di cui spesso non ci accorgiamo perché li diamo sempre per scontati, lo devo a voi. Un grazie anche a te Paolino, che sai sempre come farmi innervosire, anche solo con uno sguardo o una parola sbagliata nel momento sbagliato. Ormai i litigi tra di noi non si contano più da parecchio tempo, ma sei comunque la persona a cui voglio più bene. Abbiamo una rella relazione tossica.

Ringrazio, in generale, tutti i parenti che durante questi anni mi hanno fatto sentire il loro affetto. La nostra è una famiglia bella larga e molto variegata, ma molto, ed è proprio questo che la rende particolare e bella così com'è.

Grazie ai miei amici più stretti, il GDG. Abbiamo passato anni e anni assieme, ma non riesco mai a stancarmi di voi. Ogni vacanza fatta con voi è stata indimenticabile, da Imperia dove abbiamo passato notti magiche sul molo a parlare, bere, cantare e gelare alla Puglia, dalle vacanze fatte in Francia, Portogallo, Spagna a quella più recente in Marocco. Ognuna di loro porta con se ricordi indelebili, ma mai come la vacanza in Sardegna. Maledetta Sardegna. Mai decisione di non prendere parte ad una vacanza mi fu più fatale. Vi ringrazio comunque per non avermelo fatto pesare negli anni. Oltre a ciò non posso dimenticare le infinite uscite sotto il grattacielo, al Comala o in Santa Giulia, alle mille cene, pranzi e feste fatte sul terrazzo di Franci, ai momenti riflessivi passati sul balcone di Ciasa o su qualche panchina. Potrei continuare per ore ad elencare quello che abbiamo passato insieme in tutti questi anni, ma voglio ringraziarvi per esserci sempre stati. Vi voglio bene.

Sono grato, inoltre, di aver conosciuto dei compagni di università splendidi. Grazie a voi questi 5 anni al poli sono volati in pochissimo tempo. In tutti questi anni ci siamo divertiti parecchio tra corsi di cui ci chiedevamo l'utilità e professori particolari, a tratti speciali, e lezioni noiosissime ed altre per cui era praticamente impossibile rimanenere svegli, specie dopo aver pranzato, dagli esami passati per miracolo agli aperitivi da Aldo's, dalle feste all'Onoasi alle serate all'Imbarchino. Vi ringrazio per aver reso tutto più bello e meno stressante e spero che questo legame possa mantenersi anche in futuro.

Ringazio tutti i miei compagni di calcio, passati e presenti, per aver passato insieme stagioni intere tra ritiri estivi, allenamenti e partite. Ovunque sono andato mi sono sempre sentito come in una famiglia. In ogni spogliatoio ho passato momenti bellissimi, tra vittorie e risate, e momenti più difficili, dai litigi agli infortuni. Ogni squadra mi ha lasciato qualcosa che mi ha fatto crescere come giocatore, ma soprattutto come persona e spero in futuro di continuare a divertirmi come in passato.

Concludo ringraziando tutti/e quelli/e con cui ho passato dei bei momenti, da quelli meno recenti a quelli più recenti, sperando di condividerne altri assieme.